PREPARATION AND STUDY OF NICKEL BASED MAGNETIC THIN FILMS

BY

ABU JAFAR SALEH AHMED KHANDAKER

A THESIS SUBMITTED TO THE DEPARTMENT OF PHYSICS, BANGLADESH UNIVERSITY OF ENGINEERING AND TECHNOLOGY IN PARTIAL FULFILMENT OF THE REQUIREMENT FOR THE DEGREE OF DOCTOR OF PHILOSOPHY

বাংলাদেশ প্রকৌশল বিশ্ববিদ্যালয়
97638
তাং 27.5.03
লাইব্রেরী, ঢাকা

BANGLADESH UNIVERSITY OF ENGINEERING AND TECHNOLOGY
DHAKA, BANGLADESH

DECEMBER 2002

#97638#

BANGLADESH UNIVERSITY OF ENGINEERING AND TECHNOLOGY
DEPARTMENT OF PHYSICS

Certification of Thesis work

*The thesis titled "**Preparation and Study of Nickel Based Magnetic Thin Films**" submitted by **Mr. Abu Jafar Saleh Ahmed Khandaker**, Roll No. Ph.D.01F, Regd No.. 86069, Session 1990-91-92 has been accepted as satisfactory in partial fulfillment of the requirement for the degree of Doctor of Philosophy on 21 January 2003.*

BOARD OF EXAMINERS

1. ***Dr. M Ali Asgar (Supervisor)***
Professor
Department of Physics, BUET, Dhaka
— *Chairman*

2. ***Dr. Gias uddin Ahmad***
Professor
Department of Physics, BUET, Dhaka
— *Member*

3. ***Dr. Mominul Huq***
Professor
Department of Physics, BUET, Dhaka
— *Member*

4. ***Dr. A. B. M. Siddique Hossain***
Professor
Department of EEE, BUET, Dhaka
— *Member*

5. ***Dr. M. M. Shahidul Hassan***
Professor
Department of EEE, BUET, Dhaka
— *Member*

6. ***Dr. Nazma Zaman***
Professor & Head
Department of Physics, BUET, Dhaka
— *Member*
[Ex-Officio]

7. ***Professor M. Sayeedur Rahman Khan***
Department of Applied Physics & Electronics
Rajshahi University, Rajshahi
— *Member (External)*

8. ***Professor S. P. Sen Gupta***
Head, Material Science Department
IACS, Jadovpur, Kolkata 700032
— *Member (External)*

Dr. S.P. SEN GUPTA
Ph. D., F. Inst. P. (London), F.A.Sc. T
Professor of Physics
Department of Materials Science
Indian Association for the Cultivation of Science
Jadavpur, Calcutta-700 032, India

CANDIDATES DECLARATION

It is hereby declared that this thesis or any part of it has not been submitted elsewhere for the award of any degree or diploma.

Signature of the Candidate

*(**Abu Jafar Saleh Ahmed Khandaker**)*
Session 1990-91-92
Roll No. Ph.D. 01F

To my parents

CONTENTS

Acknowledgements *iv*
Abstract *vi*
Abbreviations and Symbols *viii*
Figure Captions *xi*

Chapter 1: Introduction

1.1 Introduction *1*
1.2.0 Review of Earlier Works *3*
1.2.1 Curie Temperature *3*
1.2.2 Field Induced Anisotropy *4*
1.2.3 Transport Properties *5*
1.2.4 Magnetization *6*
1.3 Application of Magnetic Thin Films *8*

Chapter - 2: Instrumentation and Sample Preparation

2.1 General Introduction *9*
2.2 Preparation of Alloys *10*
2.3.1 Substrate Shaping *10*
2.3.2 Substrate Cleaning *11*
2.4 Necessary condition for the preparation of thin film *11*
2.5 Preparation Technique *12*
2.6 Experimental Details: Apparatus *17*
2.7 Important Controlling Factors *20*
2.8 Fabrication of an Electromagnet *21*
2.9 Preparation of Masks *24*
2.10 Load Attachment *24*

Chapter - 3: Theoretical Aspects

3.1.0 Nucleation and Growth *27*
3.1.1 General Concepts *27*
3.1.2 Nucleation and Initial Growth *29*
3.1.3 Coalescence Growth *29*
3.1.4 Aggregations *30*
3.2.0 Magnetic Anisotropy *31*

3.2.1	*Origin of Uniaxial Anisotropy*	*31*
3.2.2	*Theories of Magnetic Anisotropy*	*31*
3.2.3	*Pair Model of Magnetic Anisotropy*	*33*
3.2.4	*Single- Ion Model of Magnetic Anisotropy*	*38*
3.2.5	*Theoretical Consideration of Magnetic Anisotropy in Thin Films*	*42*
3.3.0	*Transport Properties of Magnetic Thin Films; Electrical Resistivity*	*50*
3.3.1	*The Fuch's Model*	*50*
3.3.2	*Mayadas of Shatzkes Model*	*53*
3.3.3	*Islandization and Macroscopic Roughness*	*54*
3.3.4	*Soffer Model of Surface Scattering*	*54*
3.4.0	*Magnetization of Thin Films*	*55*

Chapter - 4: Experimental Details

4.1	*Thickness Measurement*	*63*
4.2	*XRD*	*65*
4.3.0	*SEM*	*69*
4.3.1	*Principle of SEM*	*69*
4.3.2	*Magnetic Specimens*	*72*
4.4.	*SIMS*	*73*
4.5.0	*Experimental setup for Anisotropy Measurement*	*74*
4.5.1	*Principle of Torque Magnetometer (TM)*	*74*
4.5.2	*Mathematical formulation for Torque Analysis*	*74*
4.5.3	*Design and Working Principle of TM*	*78*
4.5.4	*Experimental Details*	*81*
4.5.5	*Sample Suspension*	*82*
4.5.6	*High Temperature Oven*	*83*
4.5.7	*Calibration of TM*	*85*
4.6.0	*Resistivity Measurement*	*88*
4.6.1	*Theory of Electrical Resistivity*	*88*
4.6.2	*The Vander Pauw's Technique*	*89*
4.6.3	*Experimental Setup*	*91*
4.7.0	*Experimental Setup for Magnetization Measurement*	*92*
4.7.1	*Principle of VSM*	*92*
4.7.2	*Mechanical Design of VSM*	*93*
4.7.3	*Electronic Circuit of VSM*	*96*
4.7.3.1	*Sensitivity Limits*	*98*
4.7.3.2	*Stability Tests Differential Measurements*	*98*

4.7.3.3	*Vibration Amplitude*	*99*
4.7.3.4	*Image Effects*	*99*
4.7.3.5	*Vibration Frequency*	*99*
4.7.3.6	*Vibration Problems*	*99*
4.7.4.0.	*Calibration of VSM*	*100*
4.7.4.1.	*Calibration Data*	*103*

Chapter - 5: Results and Discussion

5.1	*XRD*	*104*
5.2	*SEM*	*104*
5.3	*SIMS*	*110*
5.4.0	*Induced Anisotropy Energy (K_u)*	*110*
5.4.1	*Fourier Analysis of Torque Curve*	*110*
5.4.2	*Stress Induced Anisotropy of Ni-Co Films*	*111*
5.4.3	*Temperature Dependence of K_u*	*121*
5.5.0	*Transport Properties*	*122*
5.5.1	*Resistivity Measurements*	*122*
5.6	*Specific Magnetization Measurements*	*128*
5.6.1	*Specific Magnetization at room temperature*	*128*

Chapter 6 Conclusion *130*

Chapter 7 Reference *133*

Appendix Data and Tables

Acknowledgement

The successful completion of any research work requires a team effort and as such many individuals and organization have contributed to my thesis project.

First of all I would like to express my heartfelt respect and everlasting gratefulness to my supervisor Prof. M. Ali Asgar, Department of Physics, BUET, Dhaka, for his constant guidance, indispensable supervision, valuable discussions and inspirations during the completion of this thesis.

I am thankful to Prof. Nazma Zaman, Head, Department of Physics, BUET, Dhaka for her helf and inspiration in carrying out my research work.

I am grateful to my honorable teachers Prof. Gias uddin Ahmad, Prof. Tafazzal Hossain, Prof. Mominul Huq, Prof. Md. Abu Hashan Bhuiyan and Prof. Jiban Podder of Physics Department, BUET for their inspiration, encouragement, suggestions and other helps.

I shall remain ever grateful to Dr. Md. Feroz Alam Khan, Associate Professor, Department of Physics, BUET, for his co-operation and help in my laboratory works and for providing helpful suggestions.

I have my gratitude to Mrs. Dil Afroze and Mrs. Fahima Khanam, Associate Professor; Dr. Md. Mostak Hossain, Dr. Md. Nazrul Islam and Dr. A. K. M. Akther Hossain, Assistant Professor; Mrs. Afia Begum and Mr. Md. Rafi Uddin Lecturer of Physics Department, BUET, for their help, cooperations and well wishes.

I am also grateful to Prof. A. B. M. Siddique Hossain, Department of EEE, BUET, a member of the doctoral committee, for his evaluation of my research work and valuable suggestions that he has given from time to time.

I am indebted to my friends Dr. M. A. Rashid, Dr. Faruk Uz Zaman Chowdhury of BIT, Chittagong, Dr. S. S. Shikder, BIT, Khulna, Mr. A. K. Mallik, S.S.O., INST, AERE, Savar and other Ph.D. and M.Phil students of Physics Department, BUET.

I am really grateful to Mr. Shajedul Hossain Sarker (Shaheen) Instrument Engineer, STRC, Dhaka University, Dhaka. I am able to brought the coating unit into working condition with his active cooperation and suggestions.

I am also indebted to Mr. M. A. Mazid CSO, (Retd), AECD, Dhaka for his valuable suggestion and helps. I am also grateful to Dr. Md. Amanullah chowdhury, CSO, Dr. M. A. Hakim, P.E. and Mrs. Shireen Akter P.S.O. of AECD Dhaka for their help and cooperation.

I am grateful to Prof. S. P. Sengupta, Material Science Division, Indian Association for the Cultivation of Science, Jadabpur, Kolkata, India for allowing me to use the experimental facilities of his laboratory for XRD and SEM.

I indebted to Prof. P. Chakraborty, Surface Physics Department, Shaha Institute of Nuclear Physics, Bidhan Nagar, Kolkata, India for his help in SIMS analysis.

I am particularly grateful to Prof. Dr. K. A. Khan, Department of Applied Physics, Rajshahi University allowing me to the M. R. Sarker thin film laboratory of Rajshahi University.

I am thankful to all the staff and officer of machine shop and central workshop of BUET for their cooperation and help in repairing and making spares for the different machines.

I wish to thanks Mr. Md. Liaquat Ali for skillfully typing this thesis and to Mr. Haroun for drafting the figures. I am also grateful to all the staff of the Department of Physics, BUET, Dhaka for their help and cooperation.

I am particularly gratefully to my wife Milia Afroze (Shapna), my sister in law Mrs. Hosne Akter Hossain and Dr. Farida Begum, for their interest, inspiration through out the period of my working on this thesis.

Finally, I would like to express my gratefulness to the BUET authority for allowing me to carryout my research work in this renowned institution and also to the UGC for awarding me the joiner fellowship.

I am grateful to the Ministry of Education, Govt. of People's Republic of Bangladesh for kindly give me the permission and for granting deputation for higher studies.

Abstract

Thin films of nickel and nickel based alloys with composition $Ni_{100-x}Co_x$ *[* x *= 5, 10, 15 and 20] with and without external field have been prepared by evaporation technique using Edward 306E. High vacuum was maintained during the deposition, the pressure being of the order* 10^{-6} *Torr just before the beginning of the evaporation. For the preparation of samples with induced anisotropy, samples of pure Ni and Ni-Co alloys were deposited onto quartz substrate with an applied field of 500* O_e*. A special electromagnet, used within the vacuum chamber, was designed and fabricated locally. The thickness of the samples were controlled by varying the time of evaporation, the heating current and the amount of powder contained in the tungsten basket. The effect of the variables on thickness was controlled empirically by trial and error and the thicknesses was determined by Tolansky interference method. For characterization of the samples; small angle X-ray diffraction, scanning electron microscopy and secondary ion mass spectroscopy have been carried out. X-ray diffraction shows that the deposited cluster have the fcc structure with the replacement of nickel atoms by cobalt atoms in the case of Ni-Co alloys, the cluster size being about 10Å. The composition is found to be homogeneous and identical with that of the starting alloys as found from SIMS. The ferromagnetic phase transition temperature of the samples with varied thickness and compositions have been determined by resistivity anomaly, which shows that the transition*

temperature decreases with decreasing thickness. The magnetic anisotropy of the samples are determined by using a specially designed torque magnetometer, where proportional integrating and differentiating circuit is used with a sensitivity of 10^{-10} Nm. The transition temperatures are also measured from the temperature dependence of the magnetic anisotropy which agree quite well within the experimental error, when the difference in the methods of measurements in the two systems are taken into account. Since the samples were too thin for the sensitivity of our vibrating sample magnetometer, only sample with highest thickness could be studied which shows saturation magnetization to be 92.84 emu/gm at room temperature for $Ni_{95}Co_5$. The thickness dependence of transition temperature, as determined by resistivity anomaly, shows that in the limit of two dimensions, where thickness should be vanishingly small, ferromagnetic ordering most likely cease to exist.

Abbreviations and symbols used in this thesis

A	Area
Å	Angstrom
a	fringe width
b	Fringe shift
Co	cobalt
D	Dimension
dc	Direct current
d	distance, film thickness
E	Electric field
EA	Easy axis
E_a	Total anisotropy energy
E_u	Total anisotropy energy density
E_x	Exchange energy
f, F	Frequency
Fe	Iron
Gd	Gadlium
H_c	Coercive force
H	Magnetic field
h	Plank constant
$\mathfrak{R}$	Hamiltonian
I	Current, Intensity
J	Exchange integral, Current density, Joule
k_B	Boltz-mann's constant
K	Kelvin
k	Wave number
K_1	1st order anisotropy constant
K_2	2nd order anisotropy constant

K_u	Stress induced anisotropy energy
KG	Kilo Gauss
KV	Kilo Volt
l	Mean free path
L	Orbital angular momentum
M	Magnetization, Induced magnetic field
$M_s(0)$	Saturation magnetization at 0 K
$M_s(T)$	Saturation magnetization at T K
Mo	Molybdenum, Molecular weigh
Ni	Nickel
Nm	Newton meter
No	Avogadro number
<n>	Spin wave probability
O_e	Orested
OD	Outer diameter
p	Probability, Pressure
PID	Proportional Integrating Differentiating
R	Distance, Universal gas constant
Rg	Reflection coefficient (grain boundary)
rad	Radian
s	Second
S	Electron spin angular momentum
SEM	Scanning electron microscope
SIMS	Secondary ion mass spectrometer
t	Thickness
T	Temperature
T_c	Curie temperature
Torr	Unit of pressure (1 mm of Hg)
Ta	Tantalum
TM	Torque magnetometer
VSM	Vibrating sample magnetometer

V	volume
w	Interaction energy between coupling atoms
W	Tungsten
XRD	X-ray diffraction
y	Distance
Z	Partition function
μ_B	Bohr magnetron
ω	Angular velocity
λ	Spin orbit parameter, Weiss constant, Wave length
α_i's	Direction cosines with magnetization
σ	Conductivity
σ_F	Conductivity of film
σ_∞	Conductivity of bulk specimen
δ	Film thickness
ρ	Resistivity
Ω	Ohm
σ	Specific magnetization
σ_s	Specific magnetization (saturation).

Figure Captions

Fig. No. 2.1(a) Photograph of coating unit (Edward 306E)

Fig. No. 2.1(b) A typical oil-diffusion-pump evaporation station used in SSP laboratory Physics Dept., BUET. The notations stand for A, quartz iodine lamp heater; B, substrate; C, deposition monitor; D, substrate mask; E, shutter; F, vapors from evaporation source; G, adapter collar between the bell jar and the pump base plate flange; H, air-inlet valve; I, base plate flange; J, Pirani gauge; K, roughing valve; L, Liquid nitrogen trap; M, cooled chevron baffles; N, diffusion pump; O, cooling coils; P and Q, backing valves; R, Pirani gauge; S, fore-pump with air-inlet valve T; U, diffusion-pump heater; V, filament holders; W, multiple feed through; X, Penning gauge; Y, Meissner trap; Z, baffle valve.

Fig. No. 2.2(a): Sketch of electromagnet

Fig. No. 2.2 (b): Photograph of the electromagnet

Fig. No. 2.3: Different types of mask (a) for the measurement of thickness, resistivity and X-ray diffroctogram, (b) for the measurement of anisotropy energy and saturation magnetization.

Fig. No. 3.1: Schematic of coalescence process.

Fig. No.3.2: Spatial distribution of dε and dγ orbits.

Fig. No. 3.3: Energy levels of dε and dγ electrons in (a) octahedral and (b) tetrahedral sites.

Fig. No 3.4: Logarithmic plot of $(\rho - \rho_\infty)/\rho_\infty$ for several of the theoretical models of thin film resistivity: the approximation of Fuchs model for $\rho = 0$; ....., the full Fuchs expression for $\rho=0$; -o - o - o -, the full soffer expression for r = 1; oooo, the full soffer expression for r = 0.2, —ooo—, the full soffer expressioon for $r_1 = 1$, $r_2 = 0.2$; - - - - , the full Soffer - Mayadas - Shatzkes expassion with $r_1 = r_2 = 0.2$, $R_g = 0.25$ and w = d.

Fig. No 3.5: Normalized magnetization vs normalized temperature for sc square films of varying thickness the integers on the curves denotes film thickness in number of atoms layers (after Klein Smith[3.41]).

Fig. No. 4.1: The schematic diagram of multiple-beam inter-ferrometer.

Fig. No 4.2 X-ray diffraction pattern of as deposited $Ni_{95}Co_5$ film of thickness 1134Å and $P = 8 \times 10^{-6}$ torr.

Fig. No. 4.3: The schematic diagram of scanning electron microscope.

Fig. No 4.4: Cross section of the upper part of the torque magnetometer.

Fig. No 4.5: Schematic diagram of the high temperature oven.

Fig. No 4.6: Torque curve for a single crystal of nickel disc in (100) plane at room temperature (25^0C).

Fig. No. 4.7: Photograph of torque magnetometer.

Fig. No 4.8(a): Vander Pauw's specimen; corner contacts made to an epitaxial layer of thickness, δ, on a square substrate; triangular or square contacts with side dimension, β, are shown on a square specimen of side dimension *l*.

Fig. No 4.8(b): Vander Pauw's specimen: schematic.

Fig. No 4.9: Mechanical construction of the vibrating sample magnetometer.

Fig. No 4.10: Schematic diagram of electronic system in the vibrating sample magnetometer.

Fig. No 4.11: Calibration curve of magnetic field vs, decade transformer readings (VSM).

Fig. No 5.1(a): Intensity vs 2θ graph of $Ni_{95}Co_5$ thin film with very slow angular rotation (0.004^0 per sec)

Fig. No 5.1(b): Radial distribution function (RDF) vs, inter-atomic distance (r) in angstroms Å.

Fig. No 5.2.1: Scanning electron micro graphs of $Ni_{90}Co_{10}$ at different magnifications (a) 1000, (b) 2000, (c) 3000 and (d) 4000

Fig. No 5.2.2: Scanning electron micro graphs of $Ni_{85}Co_{15}$ at different magnifications (a) 1000, (b) 2000, (c) 3000 and (d) 4000.

Fig. No 5.2.3: Scanning electron micro graphs of $Ni_{80}Co_{20}$ at different magnifications (a) 750, (b) 2000, (c) 3000 and (d) 4000

Fig. No 5.4.1(a): Torque curves $Ni_{95}Co_5$ sample deposited in presence of field 200 O_e.

Fig. No 5.4.1(b): Torque curves $Ni_{95}Co_5$ sample deposited without any external field.

Fig. No 5.4.2: Fourier co-efficients vs inverse magnetic field.

Fig. No 5.4.3(a): Temperature dependence curve of anisotropy energy for $Ni_{80}Co_{20}$.

Fig. No 5.4.3(b): Temperature dependence curve of anisotropy energy for $Ni_{85}Co_{15}$.

Fig. No 5.4.3(c): Temperature dependence curve of anisotropy energy for $Ni_{90}Co_{10}$.

Fig. No 5.4.3(d): Temperature dependence curve of anisotropy energy for $Ni_{95}Co_{05}$.

Fig. No 5.5.2(a): Variation of resistivity with temperature for different thickness of the films with composition $Ni_{80}Co_{20}$.

Fig. No 5.5.2(b): Variation of resistivity with temperature for different thickness of the films with composition $Ni_{85}Co_{15}$.

Fig. No 5.5.2(c): Variation of resistivity with temperature for different thickness of the films with composition $Ni_{90}Co_{10}$.

Fig. No 5.5.2(d): Variation of resistivity with temperature for different thickness of the films with composition $Ni_{95}Co_{05}$.

Fig. No 5.6.1: Specific magnetization vs magnetic field of thin film with composition $Ni_{95}Co_{05}$.

CHAPTER 1
INTRODUCTION

1.1 Introduction
1.2.0 Review of Earlier Works
1.2.1 Curie Temperature
1.2.2 Field Induced Anisotropy
1.2.3 Transport Properties
1.2.4 Magnetization
1.3 Application of Magnetic Thin Films

লাইব্রেরী, ঢাকা

1.1 Introduction

Research on thin ferromagnetic films has proved rewarding from two stand points. First, the study of this specialized branch of magnetism has deepened knowledge of the fundamental nature of magnetism in general. Second, because ferromagnetic properties are highly structure sensitive, the ferromagnetic behavior of films can provide insight into structure and properties of all thin films. Many subtle variations in the physical structure of ferromagnetic films, although clearly manifested in ferromagnetic behavior, prove to be very difficult for quantitative magnetic measurements.

The behavior of magnetic thin films is quite different from that of bulk materials for two essential reasons. First, in contrast to the interior electron spin, the surface spins are usually in an environment of lower symmetry due to the fact that they have neighbors only on one side. Second, the arrangement of the atoms of the first few layers on the substrate side of a thin film is influenced by the nature of the substrate and the temperature maintained during deposition of the film. Magnetic thin films are of special theoretical interest because, the magnetization of thin films as low dimensional material differs noticeably from that of a bulk one[1.1].

Since the problem of thin film magnetization involves the basic question of whether or not a two dimensional lattice is ferromagnetic, an experimental study of magnetic thin films have been taken up by many workers[1.1-1.5] to address this question. However, the results of different experiments do not agree quantitatively because of their non identical preparation conditions, varying degrees of vacuum used during deposition and the influence of substrate temperature on magnetic ordering.

Klein and Smith, in their theory of thin films calculated the quantum mechanical Hamiltonian in terms of Heisenberg exchange energy of the atomic spins, magnetic dipole-dipole interaction energy between electrons of different atoms and the Zeeman energy of interaction between the magnetic moments of each atom and the external magnetic field and by taking approximation applicable to the thin films. They evaluated saturation magnetization $M_S(T)$ by numerical methods for films of varying thickness. However, the theory so far developed for simple cubic lattice can not be strictly applicable to magnetic thin films of alloys of interest. In recognizing the inadequacies of the theory of Klein and Smith, Neel's[1.6] theory of magnetic sub-lattice was applied where equivalent particles situated at identical environment were considered. In contrast to ferrimagnet case, however, which was originally considered by Neel, the sub-lattices do not interlace in this case, but gradually pass from one to the other. Using this Neel's modified model the most interesting results regarding the magnetization of thin films is excepted by making multi-layer thin film using Ni, Co and Fe[1.7].

The other interesting aspect of the magnetic thin film is to measure the induced magnetic anisotropy due to the applied field during its deposition. The influence of substrate temperature and the pressure during deposition on the magnetic properties of thin films is also of interest.

The practical importance of magnetic thin films arise from the various possible applications of low dimensional magnetic materials. Thus at present magnetic thin films are considered to be a good candidate for computer memory and logic element. Real interest in magnetic thin film started when Blois[1.8] deposited films of permalloy in a magnetic field which showed rectangular hysteresis loop. Such

film can be used as bi-stable memory elements. Dietrich and Probster[1.9] found that such films were capable of reversing magnetization in about 10^{-9} second. Thus giving rise to the possibility of producing magnetic bubbles and of increasing switching time by a factor of 100 in comparison to that of ferrite cores. However, persistence technical problems like stability and mobility of magnetic bubbles are prevented in thin films by replacing ferrite areas as memory device[1.10~1.11].

1.2 Review of earlier works:

In a qualitative sense, the intrinsic properties are; Curie temperature, induced anisotropy, magnetization and transport properties, glass transition temperature, magnetostriction, and the extrinsic properties are coercive force, reminance to saturation ratio, permeability, relative quality factor and the loss factor as a function of frequency.

1.2.1 Observations around Curie Temperature

Around Curie temperature (T_c) at which there is thermal excitations, structural relaxation's and stress relief need to be considered carefully. The relaxation of local atomic configurations perturb both the magnetic and chemical environment and as such, the moment distribution change is observed by J. W. Cable[1.12]. Consequently, as temperature is raised towards T_c, substantial irreversible change in moment distribution and reordering of paramagnetic inclusions is expected. Thus, although the samples can preserve the amorphous state, they are structurally different, on a local scale as compared to the as quenched system. Therefore T_c has

বাংলা প্রকৌশল বিশ্ববিদ্যালয়
97638
তাং 27/5/03
লাইব্রেরী, ঢাকা

to be considered as spin order disorder transition temperature of a relaxed system that preserves the amorphous state as explained by E. Figueroa et al[1.13] and R. Malmhall et al.[1.14].

Generally it is claimed that thin films are amorphous in nature. Because x-ray diffraction pattern of very thin films are not shows the crystal structure. However we consider that pure metals or there alloys with out glass forming material can not remain in the amorphous state at room temperature. At present we do not have the experimental facilities to resolve this controversy.

Present work involves the measurement of resistivity as a function of temperature and determination of the Curie temperature from the resistivity anomaly, also for different thickness of the films. The magnetic anisotropy as a function of temperature is studied for films of different composition and for different field applied during the preparation of the samples.

1.2.2 Field induced anisotropy

When a static magnetic field is applied parallel to the substrate during deposition of a Ni-based (Ni-Co) thin magnetic film, an easy axis is developed in the direction of the field giving rise to a uniaxial anisotropy[1.15]. One of the most intriguing and interesting aspects of magnetic thin films is the origin of this uniaxial magnetic anisotropy.

The contributing source of this anisotropy is at least five fold (i) Co-pair formation in a nickel lattice, (ii) preferential imperfection orientation (iii)

magnetostriction due to induced stress (iv) local variation of the magnetocrystalline due to anisotropy and (v) vapor beam angle incident effect.

Some of the films, when subjected to magnetic anneal either at room temperature or elevated temperatures for a sufficient length of time change their direction of easy magnetization acquired during deposition to that of the subsequent annealing field. The origin of this "rotatable anisotropy" is of considerable interest. A careful study of its characteristics may help to decide which of the five mechanism is mainly responsible for the uniaxial anisotropy in thin film.

Several methods may be used for the measurement of this anisotropy. The most common techniques employed are the torque magnetometer the hystersis lopper and ferromagnetic resonance spectrometer. We used a torque magnetometer and shall discuss the techniques along with a description of the apparatus. The measurements involves compositional dependence of stress induced anisotropy and temperature dependence of the induced anisotropy upto ferromagnetic transition temperature (T_c).

1.2.3 Transport Properties

Electron transport properties of two dimensional solids have inspired much curiosity and motivated extensive investigations ever since the first known work on thin film of Ag and Pt by Moser in 1891. A comprehensive account of the work done before 1955 is given by Mayer[1.16]. Brief topical reviews on the development in the recent years in this field and the results on electrical conduction, galveno-magnetic effect and thermal transport of thin film has been investigated by many workers[1.17~1.18].

A contribution to electrical resistance of ferromagnetic materials (Ni, Co, Fe, Gd, etc.) may be provided by the scattering of electrons in the magnetic domain walls where the spins are disordered spins. Since, in thin ferromagnetic films, the ratio of disordered spins pinned at the surface to the free spins in the bulk is a function of thickness, the conductivity shells exhibits a size effect. Results of Schüler[1.19] on Gd film above and below T_c verified the spin contribution.

1.2.4 Magnetization

One of the central problems in bulk ferromagnetism is the determination of the magnetization as a function of temperature. In low temperature region (i.e. at temperature T that are low compare to the Curie temperature T_c) $\mathbf{T<T_c}$ of ferromagnet the temperature dependence of the magnetization M can be computed by the use of non interacting spin wave theory leading to the well-known Bloch[1.20] power law ($\mathbf{M\sim T^{3/2}}$). When the dynamic interaction between spin waves is included, Dyson[1.21] found by series expansion in power of T valid at low temperature. Opechowski[1.22] has obtained an expression for **M(T)** valid at vary high temperatures by series expansion in **(1/T).** The functional behavior of magnetization at intermediate temperature is much more difficult to calculate. However, an approximate expression for this temperature range including the interesting region near T_c has also recently given by Callen[1.23] using Green's function method.

In the case of the magnetization in thin films, regorous theoretical calculation to date is based upon the results of spin wave theory, which is only applicable to temperature low compared to Curie point. However, an attempt to extend the valid

temperature range by means of Weiss[1.24] molecular field theory has also been made.

The literature on the saturation magnetization of a material at 0 K is one of the basic properties of specific magnetization's are usually expressed as average moment in unit area A m^2/kg. The room temperature saturation magnetization measurements of thin film are one of the important field of research. For this, we have installed a Vibrating Sample Magnetometer (VSM). The techniques to measure the temperature dependence of magnetization of thin film will be developed in near future.

The theoretical behavior of magnetization as a function of temperature of permalloy thin film was studied by Klein and Smith[1.25]. It was seen that the normalized magnetization $[M_s(T)/M_s(0)]$ abruptly falls with temperature (K_BT/J) and it varies with film thickness.

The study of the relative magnetization as a function of temperature in the region near T_c is interest with.

The temperature dependence of magnetization is found to obey the usual law

$$M_s(T) = M_o(T)\ [1-BT^{3/2}-CT^{5/2}].$$

This dependence has been observed over an usually wide range of temperature in nickel based magnetic thin film. Our measurements involve the determination of specific magnetization, curie temperature and temperature dependence magnetic anisotropy of nickel based magnetic thin films.

1.3 Application of Magnetic Thin Films

The main application of magnetic thin films at present is their use as computer memory and logic elements. In addition, they are used as variable inductance, coupling elements in parametric circuits in the megacycle frequency range and in millimeter wave isolators[1.26].

When Ni-Co alloy films are deposited onto a glass substrate with a static magnetic field applied in a given direction during deposition, an easy axis develop in this direction. The film remains anisotropic even after the static field is removed subsequent to the deposition process. This induced uniaxial anisotropy may be represented by $K_1 \, Sin^2\theta$, where K_1 is the first order anisotropy constant and θ is the angle between the magnetization and the easy axis. Thus two direction of minimum energy ($\theta = 0, \pi$) exist; these bistable states may be used to represent the "0" and "1" states in a linear system. Thus, if a film is already in a state of "0", application of a field to align the magnetization in the zero-state direction will not alter the state of the system. On the other hand, if the film is originally in state "1", magnetization will be reversed in this process giving an output signal. Because of its small physical size and easiness of flux reversal, a memory using thin films has great promise in high speed computer circuitry. Since the hysteresis loops of thin films are highly rectangular, no film reversal occurs for reversing fields less than the coercive force (H_c). Thus a small H_c is required to minimize the film drive. In addition to their use as memories, film can also function as logic elements.

As a variable reactance element in a parametron, a film could be used to generate the first sub-harmonic frequency (F/2).

CHAPTER 2

INSTRUMENTATION AND SAMPLE PREPARATION

2.1 General Introduction
2.2 Preparation of Alloys
2.3.1 Substrate Shaping
2.3.2 Substrate Cleaning
2.4 Necessary condition for the preparation of thin film
2.5 Preparation Technique
2.6 Experimental Details, Apparatus
2.7 Important Controlling Factors
2.8 Fabrication of an Electromagnet
2.9 Preparation of Masks
2.10 Load Attachment

2.1 General Introduction

There are various methods and related technology for preparing thin solid films for research, development and production purposes.

The deposition technique for solid thin films may be broadly classified under three headings :

1) Physical technique
2) Chemical technique and
3) Physico-Chemical technique

Each of the techniques named above are divided into various methods for solid thin film deposition.

1) Physical technique :
   (a) Thermal evaporation
   (b) Cathodic sputtering and
   (c) Ion-assisted technique
2) Chemical technique :
   (a) Chemical vapor deposition
   (b) Pyrolysis method and
   (c) Deposition from solution
3) Physico-Chemical technique :
   (a) Glow-discharge deposition and
   (b) Plasma polymerization

Among all, the thermal evaporation process is most suitable the easiest one. It is nothing but a cocking process. Solid materials are evaporated at high temperature and are deposited on to a cooler substrate. The condensation of vapor on to a

cooler substrate results in solid thin films. Suitable types of mask can be used to get desirable shape of thin films.

2.2 Preparation of Alloys

Pure nickel (99.95%) and pure cobalt (99.95%) in fine powder from were collected (E'mark). The density (8.9gm/cc) of both magnetic materials are nearly the same. Preparation of powder alloys is rather easy. Both the metals are weighed in an electronic balance with high accuracy (10^{-5}gm), added together in a clean, dried bottle and shake it for several thousand time. The mixture of $Ni_{100-x}Co_x$ [x = 5,10,15,20] with appropriate proportions of two metals are made. We choose two metals of same density and almost same evaporation temperature. Below 10^{-4} Torr the evaporation temperatures for Ni and Co are 1535°C and 1530°C respectively[2.1]. Thin film samples $Ni_{100-x}Co_x$ alloy are made by vapor deposition technique (thermal evaporation) from the two metal power mixing.

2.3.1 Substrate Shaping

We use thin glass substrate and quartz substrate for the deposition of thin magnetic films. For the measurements of uniaxial anisotropy by a torque magnetometer and magnetization by VSM the shape of the samples (thin film) choosen was perfect circular discs of about 5mm dia. Making such type of substrate is a very tough job. Because the disc should be perfectly circular otherwise shape anisotropy will contribute much more than the crystal anisotropy. Glass substrates were made perfectly round. For this purpose, its sides are polished very carefully with fine emery papers of special grade. Other samples are made by using suitable mask of various types.

2.3.2 Substrate and its Cleaning

The support of thin film is termed as substrate. Generally, glass (Pyrex), quartz, plastic, ceramic substrates are commonly used as substrate material. The nature and surface finish of the substrate are extremely important. Ordinary microscope soda-glass substrates are usually employed. For our work we used quartz as substrate materials.

The cleanliness of the substrate surface exerts a decisive influence on film growth and adhesion. A thoroughly cleaned substrate is a prerequisite for the preparation of films and the choice of cleaning techniques depend on the nature of the substrate and the degree of the cleanliness required. The following procedure are used in our laboratory and is found satisfactory for substrate cleaning. The gross contaminants are removed by dipping the substrate in a solution of $K_2Cr_2O_7$ and H_2SO_4 for a week or more. Then the substrates are removed from the solution and rinsed thoroughly in de-ionized water and subjected to vapor degreasing using acetone. Before use, the cleaned substrate are dried by blowing hot air[2.3].

2.4 Necessary Conditions for the Preparation of Magnetic Thin Films

Solid materials vaporize when heated to sufficiently high temperature. The condensation of vapor on to a cooler substrate yields thin solid films. The deposition by the thermal evaporation method is very convenient and is at present most widely used.

Because of the collision with ambient gas atoms, a fraction of the vapor atoms, proportional to $e^{-d/l}$ will be scattered and hence randomized in direction in a distance 'd' during their transfer through the gas. Here *'l'* is the mean free path of the gas atoms which for air molecules at 25°C and pressures 10^{-4} torr and 10^{-6} torr are about 45cm and 4500cm respectively. So pressure lower than 10^{-5} torr are necessary to ensure straight line path for most of the emitted vapor atoms, for substrate to sources distance (10~50cm) in our vacuum evaporator. Thus, the distance between source to target (substrate) was a small in comparison to the mean free path of the ambient gas atoms (air).

2.5 Preparation Techniques

Thin films may be prepared by various methods stated in the section 2.1. The vapor deposition method is one of the most widely used method for the preparation of thin solid films. In this method the materials are evaporated in vacuum and the resulting vapor stream is allowed to impinge upon a substrate usually made of glass or quartz. The vapor deposition method involves the melting of the material to be deposited in a vacuum and allowing the resulting vapor beam to strike a substrate, thus forming a film.

Thermal evaporation may be achieved directly or indirectly by a variety of physical methods (a) resistive heating (b) flash evaporation (e) arc evaporation (d) exploding wire technique (e) laser evaporation. In our experiments we use the resistive heating technique.

The resistive heating method consists of heating the material with a resistively heated filament or boat or basket, generally made of refractory materials such as tungsten (W), molibdenium (Mo) and tantalum (Ta) with or without ceramic coatings. Crucibles of quartz, graphite, alumina, beryllia and zirconia are used with direct heating. The choice of the support material is primarily determined by the evaporation temperature and resistance to alloying and /or chemical reaction evaporent. In our case, the magnetic materials such as Fe, Ni, Co are highly reactive materials. However by choosing materials suitable for the evaporation of magnetic materials, it is not so difficult to get pure films[2.2]. In our case the heating materials are tungsten filaments and tungsten buskets.

The vacuum system and lead arrangements used in the deposition of thin magnetic films are usually of conventional design[2.4] with pressure ranging from 2×10^{-5} down to 5×10^{-6} torr before the evaporation begins. Because of the tendency of molten iron, nickel and cobalt to alloy with tantalum, molybdenum and other refractory metals commonly used for crucibles; it is necessary to use aluminium crucibles and high frequency induction heating. However, we use tungsten basket for this purpose to get films of magnetic materials. Tungsten do not make alloy with molten Ni, Co, or Fe.

In our laboratory we used the coating unit (**Edward 306E**) which works under the conditions stated above. The photograph of the coating unit and the schematic diagram of thin film vacuum deposition system are shown in figures 2.1a and 2.1b respectively.

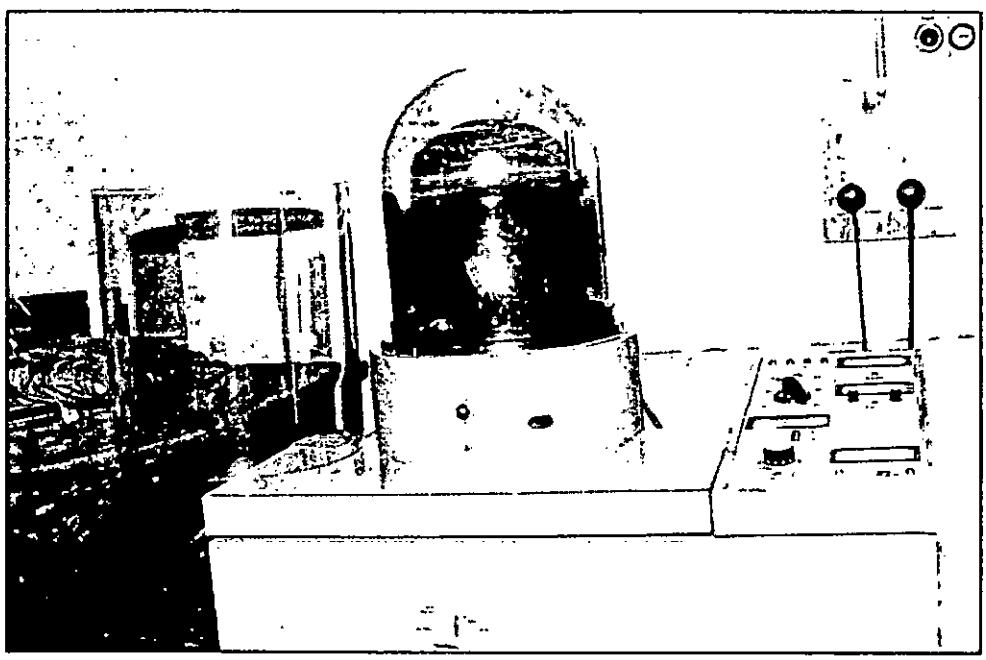

Figure-2.1a: Photograph of the coating unit (Edward 306E)

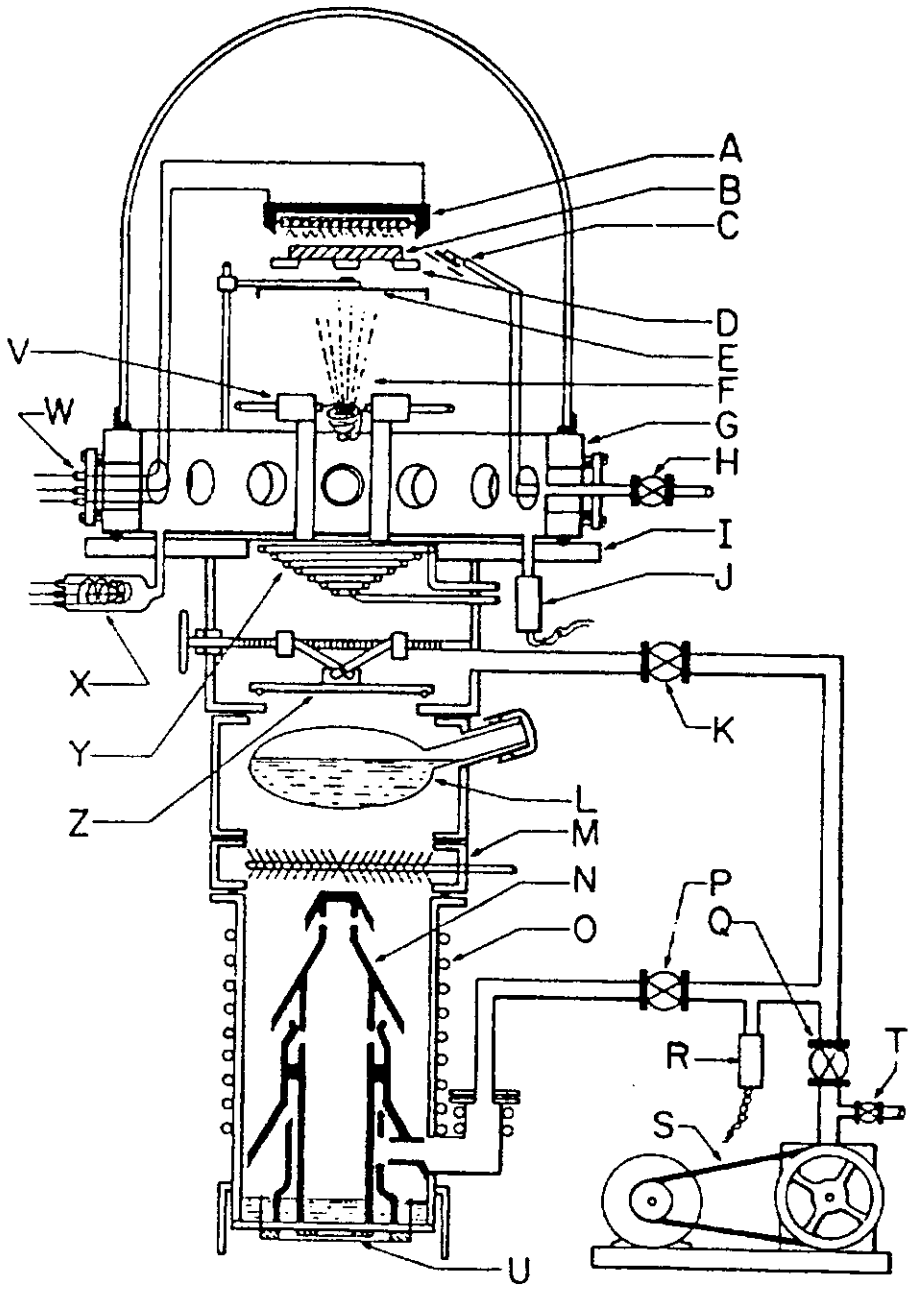

Fig. No. 2.1(b) A typical oil-diffusion-pump evaporation station used in SSP laboratory Physics Dept., BUET. The notations stand for A, quartz iodine lamp heater; B, substrate; C, deposition monitor; D, substrate mask; E, shutter; F, vapors from evaporation source; G, adapter collar between the bell jar and the pump base plate flange; H, air-inlet valve; I, base plate flange; J, Pirani gauge; K, roughing valve; L, Liquid nitrogen trap; M, cooled chevron baffles; N, diffusion pump; O, cooling coils; P and Q, backing valves; R, Pirani gauge; S, fore-pump with air-inlet valve T; U, diffusion-pump heater; V, filament holders; W, multiple feed through; X, Penning gauge; Y, Meissner trap; Z, baffle valve.

The Edward 306E coating unit is a typical diffusion pump (high speed oil pump) bell-jar system. The figure 2.1(b) shows schematically the various components and accessories essential for a reasonable system. The list is by no means comprehensive but should give an idea of the requirement of an evaporator. A high speed oil diffusion pump system (~1000 litre/sec) is relatively simple and it allows repaid 1 hour cycling form atomsphere to 10^{-5} Torr for a bell-jar of reasonable size. By careful baking and degassing of the evaporator component, pressure of 10^{-6} Torr are obtained in several hours which is the desired vacuum. The vapor pressure of the diffusion pump fluid (DC 704) is 10^{-8} Torr at 15^0C. With this one can reach upto ~10^{-6} Torr, which is necessary for preparing the desired samples.

Since the mean free-path of the evaporating atoms is large compared with the dimension of the system and therefore the size of the aperture of the oven, conditions of molecular streaming occur on a plane surface at a distance 'y' from the oven. The intensity 'I' or the number of atoms arriving per unit area of the surface per unit time in a direction θ measured from the source surface is given by

$$I = \frac{N_o}{\sqrt{2\pi M_o RT}} \cdot \frac{A}{\pi y^4} \cos^4 \theta \qquad (2.1)$$

where A is the area of orifice, N_o is the Avogadro number. R is the Universal gas constant. M_o is the molecular weight of evaporating substance. It has been experimentally found that the variations in film structure on varying the rate of evaporation result mainly from the variation of beam intensity and not for thermal velocity variations. The melting temperature of Ni, Co, Fe (~10^{-4} torr) are 1525°C 1530°C and 1455°C respectively[2.1], so that the source heating element must be able to produce 1800°C.

It has been observed that before evaporation the surface of the filament or the basket are contaminated by metallic oxides which is removed by burning the filament in vacuum[2.6].

2.6 Experimental Details : Apparatus

The preparation of thin films by the deposition technique describe in the section 2.5 requires a verity of ancillary techniques, equipment and jigs. An outlines of a brief "Know how" on this importance aspects of thin film technology are given here. Vacuum technology has under gone major development primarily as a result of the demand of thin film technology for better vacuum. Details reviews on evaporation's are given by Holland[2.7] and Caswell[2.8]. The various types of pumps, their ultimate pressure, and the various type of gauges employed to measure pressure are summarized in K. L. Chopra[2.2].

The practical steps taken to prepare the films

1. Basically two types of evaporators are used in thin film preparation at below ultra high vacuum range ($<10^{-8}$ Torr). (a) a diffusion pump (high speed oil pump) bell-jar system and (b) a getter-ion pump bell jar system. Typical representatives of these, used in our laboratory is shown in figures 2.1a and 2.1b with the various components and accessories essential for a reasonable system. With this we can easily reach upto a sufficient low pressure ($\sim 10^{-6}$ torr) with in three hours.

2. The ultimate pressure in an evaporator depends not only on the pumps employed but also on the rate of desorption of the evaporator hardware and

degassing of the evaporant. These rates are sufficiently high for a commonly employed system to warrant the use of pumps with speeds not less than 200 liter/sec. For ultra high vacuum polish stainless steel and aluminum are used for their lowest desorption rates. Pyrex glass bell jar is suitable for vacuum above 10^{-7} torr. For ultra high vacuum system glass bell jar is not desirable due to some serious faults and contamination.

Among the various elastomers used for gasket and 'O' rings, the fluoroelastomers called Viton A, has the lowest permeability for the principal atmospheric gases and disorption rate after degassing at 150°C. It decomposes at temperature above 150°C, however liberating mainly HF. Thus a breakable system should have 'O'-ring seals made of metals (Cu, Al, Au). In our system almost 'O'-rings are organic vacuum seals. The liquid nitrogen trap is a simple thimble design which requires a minimum of one collision with a cold surface in order for an oil molecule to pass the trap. The liquid nitrogen trap in the roughing line serves to minimize diffusion of forepump oil into the bell-jar chamber during roughing operation and also maintain the fore-pressure of the diffusion pump at approximately 10^{-4} torr. The high vacuum portion of the system is constructed of either hard glass or welded stainless steel sections. Readings of pressures are usually made by Pirani gauge and Penning gauge located in pump line. Since evaporators are dynamic systems these readings during deposition may differ by a factor of 5 from reading obtained in panning gauge located in the bell jar.

The substrate may be baked by a radiant tungsten heater prior to deposition and holding there at elevated temperature during deposition. A liquid nitrogen trap in a bell jar may be constracted from copper tubing through which liquid nitrogen can be circulated continuously[2.7]. This trap increases the possible vacuum available

significantly. With this a commercially available conventional evaporator, pressure in the order of 10^{-7} torr may be achieved[2.8].

Oil vapors reach a vacuum system from the rotary pump during roughing cycle, and from the diffusion pump by back streaming, and also as a result of the high vapor pressure of light hydrocarbons even at low temperatures. Optically dense, cryogenic chevron buffles are absolutely essential even though they don't completely eliminate the oil vapors. Traps with a molecular sieve (e.g., Zeolite) preferably cooled by liquid nitrogen an also essential between the rotary pump and the vacuum system. The vapor pressure of diffusion pump fluids (DC 704 or 705) is ~10^{-8} to 10^{-10} torr at 15°C, so that a monolayer of oil will be adsorbed under equilibrium condition in 10^2 to 10^4 sec. if every molecule strikes on the first impact. Oil vapors or hydrocarbons present in an ion pump system will decompose in the glow discharge to deposit a polymer film.

During deposition, considerable change in the partial pressure of residual gases may occur because of desorption from the evaporant, interaction of the gases with the hot filament and the depositing film, chemical reactivity of the glow discharge process, etc.

The amount of residual gases in an average evaporator is large enough to be of concern if good quality films are required. The use of a liquid nitrogen trap (Messier trap) at 77K can play a paramount role in reducing the influence of water vapors. A liquid helium cryogenic pump is of-course, the solution for drastically reducing the residual pressure of all constituents.

2.7 Important Controlling Factors

The mechanism of formation of the thin films on crystalline or amorphous substrate is of great interest. An appreciable number of facts has been accumulated experimentally, it has not been possible to formulate a comprehensive theory of epitaxy that would explain all the experimental observations. Many scientist work on this and give theory on nucleation solid surfaces. There are essentially three steps necessary in the calculation on nucleation rate on crystalline surface. The growth of deposits on amorphous substrates is more complicated. However, it may be concluded that in any case, the principal contribution of the initial surface to the effectiveness of condensation occurs when the condensed layer is not more than a few atom layers in thickness.

It is necessary to interpose a mechanically controlled shutter between evaporant source and the substrate for the reason of controlling deposition. Different types of shutter are used for concern preparation of thin films size, shape, and uniformity.

For non uniform deposition, substrate size is too large in comparison to the vapor source and for uniform coating or the preparation of uniform thin films the distance between evaporant to the substrate should be short (10~15cm) and also substrate size should be small in comparison to the evaporator. For large size substrate it may be rotated during deposition. A rotating substrate also reduces structural effect that may arise because of the large angle of incidence of vapor.

By laying a suitable mask over the substrate during deposition, films in some pattern of shape can be obtained. For the measurement of different magnetic properties of thin films the size and shape of films are different. So different masks

are used for different purpose, e.g. to measure the uniaxial anisotropy contents by a torque magnetometer we need a circular sample of 5mm diameter. So mask should be about 5mm diameter and of perfect circular shape.

To get good and uniform films we have to be careful in all steps. The pressure in the bell jar where the evaporator, substrate, shutter, masks, radiant heater circuit etc. should be of the order of 10^{-6} Torr. Above this range the contamination will be predominant. Source to substrate distance should be small in comparison to the mean free path of residual gas molecules.

2.8 Fabrication of a Special Type of Electromagnet

The magnetic properties of thin films of ferromagnetic materials are determined by the magnitude of the magnetic anisotropies present in the film. These anisotropies can originate in any of several different mechanisms which depend upon the film structure. However, the net anisotropy resulting from the presence of uniaxial anisotropies from two different mechanisms [e.g. field **(M)** induced and oblique incidence] with non linear easy axis **(EA)** which leads to another uniaxial anisotropy of a predictable magnitude with an **EA** in a predictable direction[2.9~,2.10]. In ferromagnetic films several types of anisotropy may occur: (i) shape anisotropy (ii) magnetocrystalline anisotropy (iii) strain magnetostriction anisotropy and (iv) **M**-induced uniaxial anisotropy. We are interested in field induced uniaxial anisotropy. For the preparation of such samples a magnetic field is applied to the substrate plane during deposition. For applying a uniform and variable field during deposition we designed and fabricated an electro-magnet as shown in figure 2.2a and 2.2b.

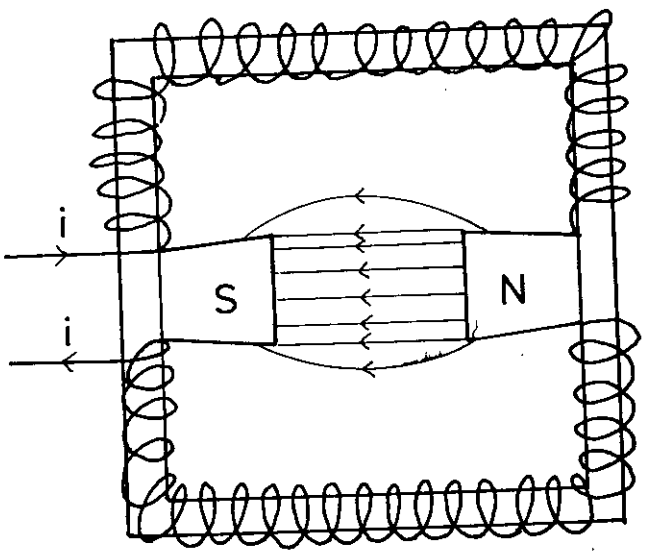

Fig. 2.2(a) : Sketch of Electromagnet.

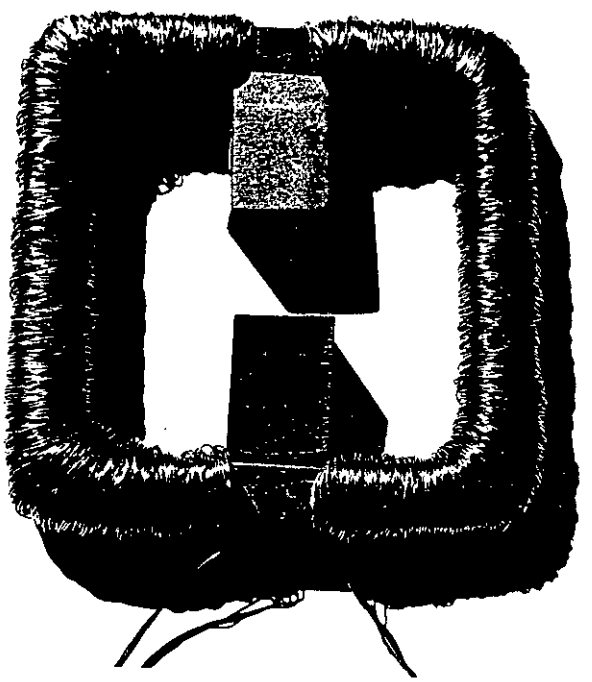

Fig. No. 2.2 (b): Photograph of the electromagnet

2.9 Preparation of Masks

The direct deposition of thin film pattern require a suitable shaped aperture, commonly referred to as a mask. This may be a thin metal sheet, a graphite plate or a glass plate with the desired pattern cut or attached to it. The mask is placed in the proximity to the substrate, thereby allowing condensation of the evaporant only in the exposed substrate areas. The masks are prepared in such a way, that the edges of the mask are very smooth so that it is helpful for determining the film thickness accurately. For better accuracy, we also use the sharp edge of razor blade (unused) as mask inner boundaries.

In our case we use aluminum foil to prepare masks. First the foils are cut in a shape and size it to match those of the substrate holders. Then the apertures are made with the help of precision files. The masks that are used in our laboratory are shown in figure-2.3a amd 2.3b.

2.10 Lead Attachment

Electrical connections to thin films for measurements or interconnections within thin film circuits can be obtained in a variety of ways which are discussed by several authors[2.11~2.12]. But in general two methods are used for attaching lead to thin films, namely, solid phase bonding and alloy bonding. The solid phase bonds are formed by thermal compression and ultrasonic means, where as the alloy bonds are formed by soldering. Wiener[2.13] used metallic indium as soldering material to make electrical contacts (Ohmic). Belser[2.14] has found that by using pure metallic indium as soldering material, without a flux, adherence to thin metallic films may be radially obtained without destruction of the films.

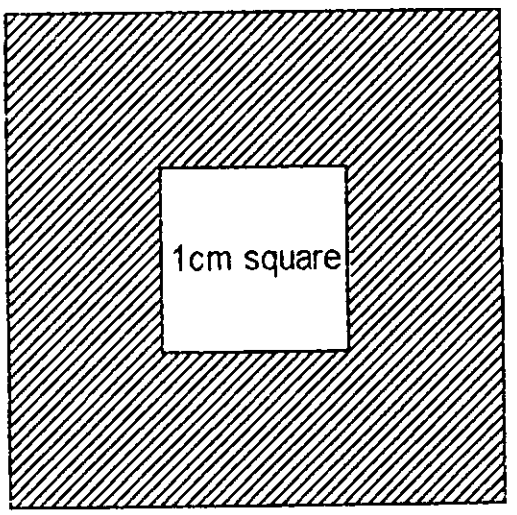

(a)

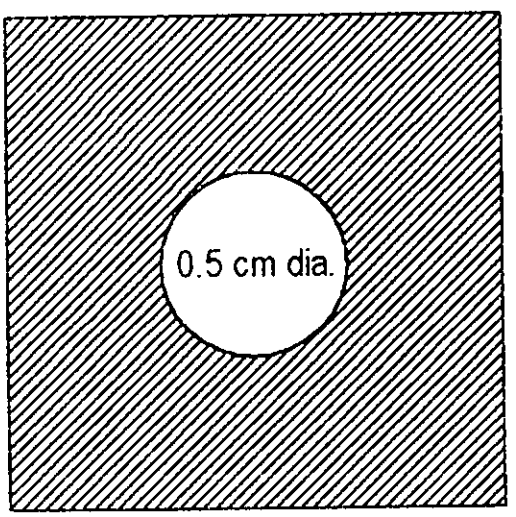

(b)

Fig.2.3 Different types of masks; (a) for the measurement of thicness, resistivity and X-ray diffractogram; (b) for the measurement of anisotropy energy and saturation magnetization.

For electrical measurements, lead attachment is a very important factor. Soldering is the most commonly used process in joining leads to the thin films. Indium dot is first soldered on the corner of the film using a low power (20 Watt) fine tip soldering iron, one end of a fine copper whisker is then wetted by indium and then placed in contact with the indium dot and soldered by fine tip soldering iron. The technique mentioned above we adapt in our laboratory for the measurement of electrical resistivity at temperature ranges (30~250°C). For the measurement of resistivity at high temperature (250~450°C) silver paint in used as lead attachment material though it takes time and is very tough.

CHAPTER 3
THEORETICAL ASPECTS

3.1.0 Nucleation and Growth
3.1.1 General Concepts
3.1.2 Nucleation and Initial Growth
3.1.3 Coalescence Growth
3.1.4 Aggregations
3.2.0 Magnetic Anisotropy
3.2.1 Origin of Uniaxial Anisotropy
3.2.2 Theories of Magnetic Anisotropy
3.2.3 Pair Model of Magnetic Anisotropy
3.2.4 Single- Ion Model of Magnetic Anisotropy
3.2.5 Theoretical Consideration of Magnetic Anisotropy in Thin Films
3.2.0 Transport Properties of Magnetic Thin Films; Electrical Resistivity
3.2.1 The Fuch's Model
3.2.2 Mayadas of Shatzkes Model
3.2.3 Islandization and Macroscopic Roughness
3.2.4 Soffer Model of Surface Scattering
3.3.0 Magnetization of Thin Films

3.1 Nucleation and Growth of Films

Thin films are most commonly prepared by condensation of atoms from the vapor phase of a material. At the earliest stage of observation, atomistic condensation takes place in the form of three dimensional nuclei which then grow to form a continuous film by diffusion controlled processes. The novel structural behavior and properties of film can largely be ascribed to this growth process, which is therefore of basic importance of the science and technology of thin films.

3.1.1 General Concepts

Nucleation is the birth state of a film, is essentially a problem of solid-vapor phase transition. As a film is deposited onto a substrate, its structure evolves in a way which is dependent on the substrate and film materials.

The initial process of formation of a critical nucleus is of great importance for its subsequent growth. In heterogeneous model of nucleation, binding forces between substrate and the deposit are of central importance [3.1]. Some workers[3.1-3.4] use the theory of homogeneous nucleation which is historically based on nucleation of droplets in a saturated vapors. In homogeneous nucleation, particles are spontaneously formed. The presence of a substrate surface slightly modifies the model. In order to form stable particles on the surface, an activation barrier of nucleation must be overcome. Initially formed stable critical clusters are of a few angstrom in size.

Calculation on the size of initially critical cluster which is stable usually of a few angstrom. The initial condensation process must be treated in terms of atomistic nucleation[3.2-3.3]. Here macroscopic thermodynamic concepts (surface energy and contact angle between the substrate and the contact island) are avoided, only inter

atomic forces and metal substrate binding forces are consigned. The atomistic nucleation theory is greatly developed in recent years. The growth of a film can be described by either of the three different models characterized by initial condensation process[3.4].

i) **Island growth**: when the condensation material is much more bound to than to substrate.
ii) **Layer growth**: when the deposit is most strongly bound to the substrate
iii) **Intermediate growth**: when initially a layer is formed but the subsequent growth is island growth.

In general terms the nucleation and growth is characterized on the following sequence[3.5~3.9].

(a) The initial stage is described by atomistic nucleation theory. Here the critical nucleus, which continuous only a few atoms is formed.
(b) There is a low temperature and high temperature region of growth.
(c) Stable cluster coalesce, reduce the density of clusters and there occurs a saturation density (typically at a few mono-layers).
(d) The coalescence growth which now follows results in a decrease of cluster density.
(e) Further deposition completes the discontinuous stage in large scale coalescence when a semi-continuous film is formed.
(f) There is a continuous film when substrate surface is completely covered.

3.1.2 Nucleation and initial growth

In homogeneous nucleus the initial stage of film growth from vapor is essentially a vapor-solid phase transformation. The condensation of the vapor is determined by its interaction with the surface. An adatom (absorbed vapor atom) on a surface loses its velocity component normal to the surface with in a short time[3.10]. The adatom has a finite stay time on the surface. During this time the atom can be thermally equilibrated and absorbed on the surface, absorbed within substrate material or it can be disorbed from the surface. When an atom is absorbed to a critical nucleus, a stable nucleus is formed[3.2~3.3].

The nucleation and growth have been described by rate equations; mainly three processes contribute to the growth.

i) Single atom arrives directly from vapor

ii) Single atom arrives to the nucleus by diffusion on the surface and

iii) Clusters diffuse on the surface where a binary collision followed by liquid like coalescence results in an island.

3.1.3 Coalescence growth

Coalescence takes place when two particles merge into one at a temperature 200-400^{0}C. A schematic of coalescence process is shown in figure 3.1. The coalescence occurs in less than 0.1s for the small nuclei and is characterized by decreased in total projected area of the nuclei on the substrate. There are two different kinds of coalescence:

(a) Coalescence by growth of Islands: If two growing particles touch one another they can coalesce into one. By this process a portion of the substrate surface is exposed, upon which secondary nucleation can occur.

(b) Coalescence due to diffusion of islands on the substrate: When the mobile islands meet each other they can coalesce.

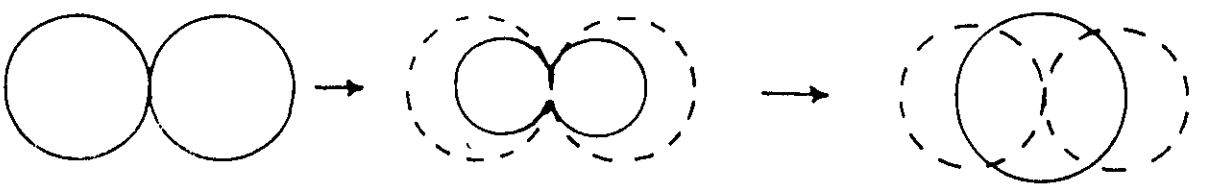

Fig. No. 3.1: Schematic of coalescence process.

3.1.4 **Aggregations**

Aggregation is a process which occurs below the coalescence temperatures, i.e. then particles touch and strike each other. In this case aggregates of complex shape are produced. In gas evaporated particles, aggregation occurs when the vapor of the evaporated material is cooled sufficiently by the inert gas. This type of aggregation is observed in for example, particles prepared from certain colloidal solution[3.11].

3.2.0 Magnetic Anisotropy

3.2.1: Origin of Uniaxial anisotropy

Ferromagnetic single crystal have easy and hard directions of magnetization, it is an experimental fact. The difference between the energies required to magnetize the crystal in the hard and easy direction is known as the anisotropy energy. The theory that have been proposed to explain the magnetic anisotropy of thin ferromagnetic films are basically the extension of the ideas proposed for the origin of anisotropy in crystalline and disordered solids. For single crystal ferromagnetic metals, such as Ni, Co, Fe and their alloys prepared in presence of a magnetic field, their anisotropy has cubic symmetry. The classical dipole-dipole coupling does not contribute to the cubic anisotropy, when the spins are all parallel, there is some contribution in the second approximation of quantum mechanical perturbation theory in which complete parallelism is not assumed. The main source of contribution to the cubic anisotropy obtained from second order perturbation theory is due not to the classical dipole-dipole interaction but due to interactions that are purely quantum mechanical in origin. These are "pseudodipole" and "pseudoquadrapole" couplings. The pseudoquadrapole interaction is 50 times larger in magnitude than the ordinary dipole-dipole interaction. The quantum mechanical origin of this couplings is due to the combined effects of spin orbit interaction and the partial quenching of the orbital angular momentum by inhomogeneous crystalline electric fields and by orbital exchange interaction with neighboring atoms[3.12].

3.2.2 Theories of magnetic anisotropy

In order to understand the origin of magnetic anisotropy in amorphous solids, we will first look at the theories developed for magnetic anisotropy of crystalline

solids based on the localized electron model. Akulov[3.13] is the pioneer to drive the first theoretical expression for the temperature dependence of magnetic anisotropy constant K_i. Using a simple classical argument and assuming a system of independent spins, Akulov assumed that each spin had a free energy of the form

$$K_1 = (\alpha^2_1\alpha^2_2 + \alpha^2_2\alpha^2_3 + \alpha^2_3\alpha^2_1) \qquad 3.1$$

where the direction cosines α_1 refer to a particular spin. A simple statistical calculation gives the relationship between K_i and the spontaneous magnetization M.

$$\frac{K_1(T)}{K_1(0)} = \left[\frac{M(T)}{M(0)}\right]^{10} \qquad 3.2$$

The number 10 arises from the structural combination of the direction cosines in the usual expression for the anisotropy energy, a combination dictated solely by the asymmetry of the crystal. The power law holds well for many insulators and rare-earth metals, for which the localized electron model is particularly applicable. But agreement with the experimental data for nickel and iron is not satisfactory; for example, in nickel the temperature variation of K_1 exhibits a dependence of the 50th power of the magnetization[3.14].

In further classical treatment of magnetic anisotropy Zener[3.15], generalized the 10th power law to an $\frac{n}{2}(n+1)$ law assuming a system of independent spins. Zener showed that, if the anisotropy energy E_a is written in terms of spherical harmonics,

$$E_a = \sum_n k_n(T) Y_n^m(\alpha) \qquad 3.3$$

then $$\frac{k_n(T)}{k_n(0)} = \left[\frac{M(T)}{M(0)}\right]^{\frac{n}{2}(n+1)}$$

Here the $k_n(T)$ are linear combinations of the $K_i(T)$, and in particular

$$k_2(T) = K_1(T) + \frac{1}{11} K_2(T) + \ldots\ldots\ldots\ldots \text{and } k_3(T) = K_2(T) \qquad 3.4$$

The two assumptions basic to Zener's derivation are:

(i) the existence of regions of sort range order of spins around each atom, inside which the anisotropy constants are temperature independent. Thus the only effect of raising the temperature is to introduce small perturbations in the direction of the local magnetization.

(ii) the distribution of spins within each region is random so that the local anisotropy energy may be averaged over all directions.

3.2.3 Pair model of Magnetic Anisotropy

Magnetic anisotropy describes the circumstance that the energy of a system changes with a rotation of magnetization. The relation between the change in energy of a system with the change in energy of atomic pairs is called the pair model of anisotropy. Van Vleck[3.16] first developed this theory. The most important interaction between the atomic magnetic moments is the exchange interaction. This energy is only dependent on the angle between the neighboring atomic moments, independently of their orientation relative to their bond direction. In a view to explain magnetic anisotropy we may assume that the pair energy is dependent on the direction of the magnetic moment, ϕ, as measured from the bond

direction. In general, we express the pair energy by expanding it in Legendre polynomials,

$$w(\cos\Phi)=g+I\left(\cos^2\Phi-\frac{1}{3}\right)+q\left(\cos^4\Phi-\frac{6}{7}\cos^2\Phi+\frac{3}{35}\right)+\ldots\ldots\ldots\ldots \quad 3.5$$

The first term is independent of ϕ; hence the exchange energy is to be included in this term. The second terms is called the dipole-dipole interaction.

If the pair energy were due exclusively to magnetic dipolar interaction, it should follow that

$$I=-\frac{3M^2}{4\pi\mu_o r^3} \quad 3.6$$

The actual value of I can be evaluated from the uniaxial crystal anisotropy. In most cases the estimated value is 10^2 to 10^3 times larger than that given by equation (3.6). The origin of this strong interaction is believed to be the combined effect of spin-orbit interaction and exchange or coulomb interaction between the neighboring orbits. That is, if there are small amounts of orbital magnetic moment remaining unquenched by the crystalline field, a part of the orbit will rotate with a rotation of the spin magnetic moment because of a magnetic interaction between the two, and the rotation of the orbit will, in turn, change the overlap of the wave function between the two atoms, giving rise to a change in the electrostatic or exchange energy. This type of interaction is termed as the anisotropic exchange. It should be noted here that the dipolar term of equation. (3.5) does not contribute to the interaction energy E_a, since the spins are perfectly parallel. The dipole terms between the atomic pairs with different bond directions cancel out as long as their distribution maintains cubic symmetry. If, however, the crystal has a lower symmetry than the cubic crystal, as in a hexagonal crystal, the dipole-dipole interaction gives rise to magnetic anisotropy.

Van Vleck pointed out that the dipole-dipole interaction does give rise to cubic anisotropy since the perfect parallelism of the spin system is distributed by the dipolar interaction itself. Thus if I<0 and all the spins are parallel, the dipole-dipole interaction gives rise to a large pair energy for $\Phi = \pi/2$. In such a case, a more stable configuration of the spin pair will be an anti-parallel alignment. Some of the spins will therefore take the anti parallel direction in an equilibrium state.

According to Van Vleck's calculation, the cubic anisotropy constants for an f.c.c. system due to dipole-dipole interaction are

$$K_1 = \frac{9NI^2}{8SMH_m} \; at \; T = 0^0 K \qquad 3.7$$

where S is the total spin quantum number, M the atomic magnetic moment, and H_m the molecular field. In the classical picture, K_1 should vanish by letting $S \rightarrow \infty$.

Now, since $NMH_m \approx 10^9$ J/m^3 and $NI \approx 10^7$ J/m^3, the order of magnitude of magnitude of K_1 due to dipole-dipole interaction is

$$K_1 \approx \frac{(NI)^2}{NMH_m} \approx \frac{(10^7)^2}{10^9} \approx 10^5 J/m^3$$

This is sufficient to explain the magnitude of the observed anisotropy energy.

Judging from the origin of anisotropy, it would be practical to suppose that the anisotropy constant decreases with increasing temperature and disappears at the Curie point. Actually this does happen, and the temperature dependence is more drastic than that of spontaneous magnetization. Zener treated this problem in a simple way and explained the temperature dependence fairly well. He assumed that the pair energy is given by equation (3.5) even for the thermally perturbed spin system, since the neighboring spins maintain approximately the parallel

alignment upto the Curie point, where, because of the strong exchange interaction, parallel spin clusters prevail in the spin system. Carr followed this method to calculate the crystal anisotropy constant for iron, nickel and cobalt[3.17].

Let (α_1,α_2, α_3) denote the direction cosines of the average magnetization, and (β_1, β_2, β_3) the direction cosines of the local magnetization. Since we assume local parallelism i the spin system, the anisotropy energy should be given by the average of the local anisotropy energies, so that

$$E_a(T)=K_1(O)\langle\beta_1^2\beta_2^2+\beta_2^2\beta_3^2+\beta_3^2\beta_1^2\rangle \qquad 3.8$$

where $K_1(0)$ is the anisotropy constant at T = OK and $\langle\ \rangle$ denotes the average over all possible orientations of local magnetization. Using the polar co-ordinates (θ,Φ), where θ is the angle between the local spin and the average magnetization, and Φ the azimuthal angle around the magnetization direction, we have

$$E_a(T)=K_1(o)\frac{\int_o^{\pi}\left[\left(\frac{1}{2\pi}\right)\int_o^{2\pi}\left(\beta_1^2\beta_2^2+\beta_2^2\beta_3^2+\beta_2^3\beta_1^2\right)\right]n(\theta)d\theta d\Phi}{\int_o^{\pi}n(\theta)d\theta} \qquad 3.9$$

where $n(\theta)d\theta$ is the number of spins which point in the solid angle between θ and (θ + dθ). Since

$$\frac{1}{2\pi}\int_o^{2\pi}\left(\beta_1^2\beta_2^2+\beta_2^2\beta_3^2+\beta_3^2\beta_1^2\right)=\frac{1}{5}\left[1-P_4(\cos\theta)\right]+\left(\alpha_1^2\alpha_2^2+\alpha_2^2\alpha_3^2+\alpha_3^2\alpha_1^2\right) \qquad 3.10$$

where $P_4(\cos\theta)$ is the fourth order Legendre polynomial the equation (3.10) becomes

$$E_a(T)=K_1(0)\langle P_4(\cos\theta)\rangle\ \left(\alpha_1^2\alpha_2^2+\alpha_2^2\alpha_3^2+\alpha_3^2\alpha_1^2\right) \qquad 3.11$$

$$\text{where} \qquad \langle P_4(\cos\theta)\rangle = \frac{\int_o^{\pi} P_4(\cos\theta)\, n(\theta) d\theta}{\int_o^{\pi} n(\theta) d\theta} \qquad 3.12$$

This can be expressed in a polynomial series in

$$\frac{1}{\alpha} = \frac{kT}{MH_m}$$

where H_m is the molecular field

$$\langle P_4(\cos\theta)\rangle = 1 - \frac{10}{\alpha} + \frac{45}{\alpha^2} - \frac{120}{\alpha^3} + \ldots\ldots\ldots\ldots \qquad 3.13$$

On the other hand

$$M(T) = M(0)\left(\coth\alpha - \frac{1}{\alpha}\right) \approx M(0)\left(1 - \frac{1}{\alpha}\right) \qquad 3.14$$

So that

$$\left[\frac{M(T)}{M(0)}\right]^{10} = 1 - \frac{10}{\alpha} + \frac{45}{\alpha^2} - \frac{120}{\alpha^3} + \ldots\ldots\ldots\ldots \qquad 3.15$$

comparing equation. (3.13) and equation. (3.15) we get

$$\left[\frac{K_1(T)}{K_1(0)}\right] = \left[\frac{M(T)}{M(0)}\right]^{10} \qquad 3.16$$

equation. (3.16) holds good for the temperature dependence of K_1 of iron. Carr also explained the temperature dependence of K_1 for nickel and cobalt by taking into consideration the effect of thermal expansion of the crystal lattice. But, in constant to Zener's theory, Van Vleck obtained a much more gentle temperature dependence of magnetic anisotropy. Keffer[3.18] investigated this point and showed that the Zener's theory is valid at least at low temperature, while Van Vieck's theory is valid at high temperature.

3.2.4 Single Ion Model of Magnetic Anisotropy

The orbital state of magnetic ions plays an important role in determining the magnetic anisotropy. The orbital state of the magnetic ion is influenced by a given crystalline field and the resultant orbital state gives rise to magnetic anisotropy. This phenomenon is described by the single ion model of magnetic anisotropy. The model has been successful in interpreting the magnetic anisotropy of various anti-ferromagnetic and ferromagnetic crystals.

In free atomic states, every 3d electronic state has the same energy. In other words, their energy levels are degenerate. When the atom is placed in a cubic field, the orbital states of 3d electrons are split into two groups. One is the triply degenerate dε orbits, the spatial distributions of which are expressed by xy, yz or zx. The other is the doubly degenerate dγ orbits whose distributions are expressed by $2z^2 - x^2 - y^2$ and $x^2 - y^2$. Figure 3.2 explains that the dε orbits extends to ⟨110⟩ directions, while the dγ orbits extend along the co-ordinate axes. In octahedral sites, the surrounding anions are found on the three co-ordinate axis, so the dγ orbits, which extend towards the anions, have a much higher energy than dε orbits, because of the electrostatic repulsion between anions and orbits. For tetrahedral sites dγ orbits are more stable than dε orbits (Fig. 3.3).

Let us consider the case of the d electrons occupying the 3d energy levels. First let us assume that the magnetic ion has only 3d electron. Each electron will naturally occupy the available lowest energy level. Now as the three dε levels have the same energy, the lowest orbital state is triply degenerate (triplet). Such as orbital degeneracy plays an important role in determining the magnetic anisotropy.

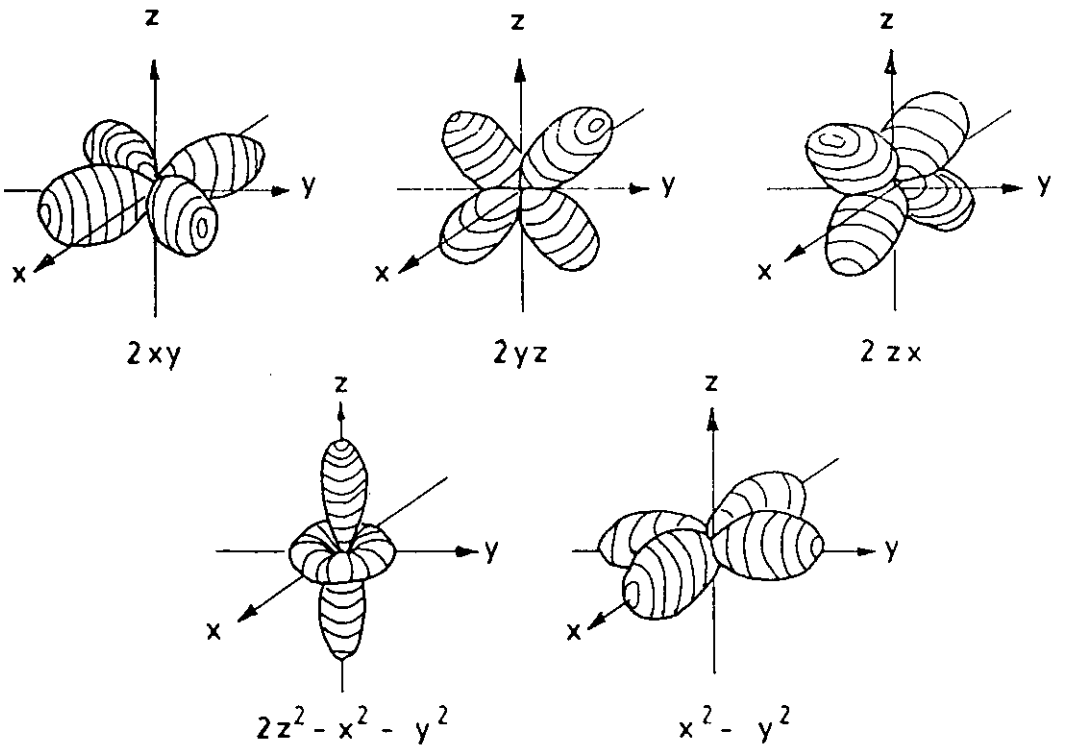

Fig. No.3.2: Spatial distribution of dε and dγ orbits.

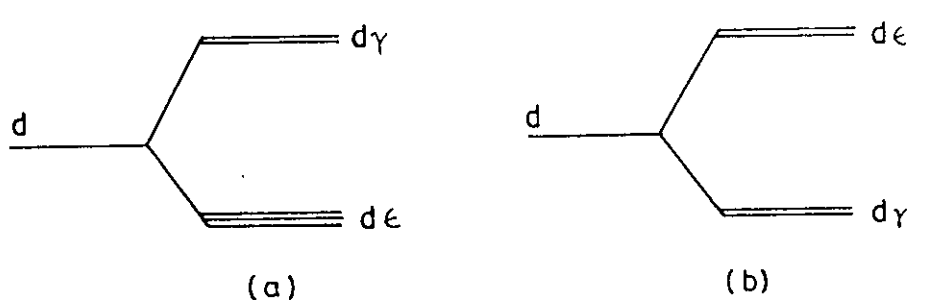

Fig. No. 3.3: Energy levels of dε and dγ electrons in (a) octahedral and (b) tetrahedral sites.

If there are additional 3d electrons, they should occupy exclusively the plus spin levels, because the exchange interaction between these 3d electrons is much larger than the energy separation between the dγ and dε levels. In the case of $(3d)^3$, the three electrons occupy the three dε levels, so that the ground state is non-degenerate (singlet). For $(3d)^5$, three electrons occupy the dε levels and remaining one occupies one of the two dγ levels, thus the state is doubly degenerate (doublet). In the case of $(3d)^5$, all electrons occupy plus spin levels, so that the ground state is a singlet. When there are more than five electrons, first five fill up the plus spin levels while the remaining electrons occupy the minus spin levels in the same way as for the plus spin levels.

As for the Fe^{2+} ion, the sixth electron should occupy the lowest singlet state, so that the ground state is non-degenerate. On the other hand, the Co^{2+} ion has seven electrons, so that the last one should occupy the doublet. In such case the orbit has the freedom to change its state in the plane which is normal to the trigonal axis, so that it has an angular momentum parallel to the trigonal axis. Now since the angular momentum is fixed in direction, it tends to align the spin magnetic moment parallel to the trigonal axis through the spin-orbit interaction. The energy of this interaction can be expressed as $-\lambda LS|\cos\theta|$, where λ is the spin-orbit parameter, L and S are the orbital and spin-angular momentum and θ is the angle between the magnetization and the trigonal axis. This model was first proposed by Slonczewski[3.19], who explained the magnetic annealing effect in Co ferrite by this model. He also explained the temperature dependence of the anisotropy constant of cobalt-substituted magnetite. In the normal, or non-magnetically annealed state, Co^{2+} ions should be distributed equally among the four kinds of octahedral sites each of which has its trigonal axis parallel to one of the four $\langle 111 \rangle$ directions, so that the cubic anisotropy can be obtained by averaging the anisotropy energy $-\lambda LS|\cos\theta_i|$ over four direction of trigonal axes.

If the ground orbital state is non-degenerate, we cannot expect any orbital angular momentum so long as the atom stays in the ground state; in other words, the orbital angular momentum is quenched by the crystalline field. In such a case we cannot expect an anisotropy as large as that of the Co^{2+} ion in an octahedral site. There are, however, various sources which result in a fairly small magnetic anisotropy, which is nevertheless sufficiently large to account for the observed values. Yosida and Tachiki[3.20] calculated the various types of anisotropy and applied their results to the Mn, Fe and Ni ferrites, which contain Mn^{2+}, Fe^{3+}, Fe^{2+} and Ni^{2+} ions. Firstly, they found that the magnetic dipole-dipole interaction is too weak to account for the observed magnitude of anisotropy. The main source of anisotropy is thought to be the distortion of the 3d shell from spherical symmetry. In a distorted 3d shell the inter-atomic dipole-dipole interaction between the spin magnetic moments may depend on the direction of magnetization; this is similar to the dependence of the magneto-static energy on the direction of magnetization in a fine elongated single domain particle, and gives rise to anisotropy energy.

The anisotropy is also induced through spin-orbit interaction. That is, some amount of orbital angular momentum can be induced by spin-orbit interaction by exciting additional orbital states. In a distorted 3d shell this excitation is dependent on the direction of magnetization, giving rise to anisotropy. Yosida and Tachiki showed that the anisotropy due to these mechanisms should vanish for S = ½, 1 and $^3/_2$, where S is the total spin angular momentum, and that anisotropy of this type cannot be expected for Ni^{2+} and Co^{2+} ions. Accordingly, the main source of the anisotropy of Mn, Fe and Ni ferrites is considered to be the Mn^{2+}, Fe^{3+} and Fe^{2+} ions. since Ni^{2+} ion has no effect on the magnetic anisotropy in Ni ferrite, the difference in anisotropy energy between Fe and Ni ferrites must be explained by the anisotropy due to Fe^{2+} ions. Yolsida and Tachiki also calculated the temperature dependence of the anisotropy constant for Mn ferrites and fitted the theory with experiment.

3.2.5 Theoretical consideration for Uniaxial Magnetic Anisotropy in Thin Films

For hexagonal and uniaxial single crystals, etc., the dipole-dipole interaction (classical or pseudo), due to the loss of cubic symmetry, no longer vanishes in the first approximation when all spins are assumed parallel. In this section, we shall discuss in particular the Neel-Taniguchi theory of induced uniaxial anisotropy in bulk Permalloy formed in the presence of magnetic field which is related to the prominence of the pseudodipole term in the noncubic crystals. Comparing the results of this theory to the experimental observations on the uniaxial anisotropy in thin films, we find that although this source of induced anisotropy is all important in bulk Permalloy, it is probably not the only mechanism which is responsible for the uniaxial anisotropy in Permalloy films. Therefore, subsequent to the discussion of the Neel-Taniguchi theory, we shall examine the possible contribution to the uniaxial anisotropy in thin films due to magnetostriction and imperfection orientation.

Neel-Taiguchi Theory

When a binary alloy such as Permalloy is heat treated in a magnetic field, a uniaxial anisotropy is developed therein. Neel[3.21] and Taniguch[3.22] have interpreted this as the creation of a short-range directional order. They consider an alloy of two components, *A* and *B*, and assume that the energy of the link between two neighboring atoms depends both on their natures, and on the angle between the line joining them and the spontaneous magnetization. During the annealing in a strong magnetic field, the diffusion of the atoms on the lattice leads to anisotropic distributions of the *A-A*, *A-B*, and *B-B* links, and this state can be conserved at room temperature by quenching. The same interaction energy between the nearest-neighbor links and the magnetization leads to a uniaxial

anisotropy. We shall first give the mathematical formulation of the theory and then compare the theoretical results with experiment.

Starting with the Van Vleck Hamiltonian of Equation

$$\Re = -g\mu_B H\sum_i S_{zi} + \sum_{i,j}{}' w_{i,j} \qquad 3.17$$

where H = H_{ex} + λM and w_{ij} is the interaction energy between atoms i and j;

we may find its eigen values. Then the partition function Z of the system can be obtained by expanding it in a power series of $(kT)^{-1}$.

$$\frac{Z}{Z_o} = 1 - \langle\sum_{i,j} w_{ij}\rangle / k_B T + \langle(\sum_{i,j} w_{ij})^2\rangle / 2k_B^2 T^2 \qquad 3.18$$

where,Z_o is partition function of the unperturbed system corresponding to the first term of Equation(3.17) and $\langle\sum_{i,j}{}' w_{ij}\rangle$ denotes the expectation value of $\sum_{i,j}{}' w_{ij}$ etc.

The free energy F of the system is then given by

$$F = -k_B T \ln Z = -k_B T \ln Z_o + \langle\sum_{i,j}{}' w_{ij}\rangle \langle(\sum_{i,j}{}' w_{ij})^2\rangle / 2k_B T + \ldots\ldots \qquad 3.19$$

which shows that the anisotropy can be found if $\langle\sum_{i,j}{}' w_{ij}\rangle$ etc., can be evaluated.

Since the pseudodipole interaction is expected to be dominant in a noncubic crystal even to the first approximation, we may neglect the pseudoquadrupole term in w_{ij}. Then, it follows that

$$w_{ij} = \sum_{q,q'=x,y,z} a_{ij}^{qq'} S_{qi} S_{q'j} \qquad 3.20$$

where $a^{qq}{}_{ij}$ $(= a^{qq}{}_{ij})$ is the qq′ component of the coupling constant a_{ij} referred to the coordinate system (x,y,z) so oriented that the field is always in the z direction. S_{qi}

and $S_{q/j}$ are, respectively, the q component of the spin of atom i and the q' component of the spin of atom j, and

$$\langle w_{ij} \rangle = \sum_{q,q'} a_{ij}^{qq'} \langle S_{qi} S_{q'j} \rangle = a_{ij}^{zz} B_1^2 \qquad 3.21$$

where $$B_1 = SB(\theta) = \frac{2S+1}{2} \coth\left(\frac{2S+1}{2}\theta\right) - \frac{1}{2}\coth\left(\frac{\theta}{2}\right) \qquad 3.22$$

and $\theta = g\mu_B H/k_B T$. Here S is the spin quantum number of all atoms, and $B(\theta)$ is the usual Brullioun function.

To study anisotropy, it is necessary to express the interaction energy w_{ij} in terms of constant A_{ij} for a system of axes (X,Y,Z) fixed relative to the crystal instead of fixed relative to the field, i.e.

$$w_{ij} = \sum_{q,q'=x,y,z} A_{ij}^{qq'} S_{qi} S_{q'j} \qquad 3.23$$

The transformation relation between the a_{ij}*s and the* A_{ij}*'s* is

$$a_{ij}^{qq'} = \sum_{p,p'=x,y,z} \lambda_{qp} \lambda_{q'p'} A_{ij}^{pp'} \qquad 3.24$$

$$A_{ij}^{pp'} = C_{ij}(\delta_{pp'} - 3n_{ij}^{P} n_{ij}^{P}) \qquad 3.25$$

where C_{ij} is the coupling constant, $\delta_{pp}{}'$ the Kronecker delta, and $n^{p}{}_{ij}$ the cosine of the angle between the direction of the atom pair (i,j) and that of the p axis. From Equation (3.21) we have

$$\langle \sum_{i,j}{}' \omega ij \rangle = \frac{N}{2} B_1^2 \sum_j a_{ij}^{zz} \qquad 3.26$$

where the summation $\sum_{i,j}{}'$ has been replaced by $\frac{N}{2}\sum_{j}$ and N is the number of atoms per unit volume, since all atoms are identical for the cubic lattice of concern here. Using Eqs. (3.24) and (3.25), Ea. (3.26) becomes

In Equation (3.27) α_1, α_2 and α_3 have been used in place of λ_{zx}, λ_{zy} and λ_{zz}.

$$\langle\sum_{j}\omega_{i,l}=\frac{n}{2}B_1^2(\alpha_1^2\sum_{j}A_{ij}^{xx}+a_2^2\sum_{j}A_{ij}^{yy}+a_3^2\sum_{j}A_{ij}^{zz}$$
$$+2\alpha_1\alpha_2\sum_{j}A_{ij}^{xy}+2\alpha_2\alpha_3\sum_{j}A_{ij}^{yz}+2\alpha_3\alpha_1\sum_{j}A_{ij}^{zx} \qquad 3.27$$

In cubic crystals, sums like $\sum A_{ij}^{xy}$ in which a letter in the superscript appears only once vanish while.

$$\sum_{j}A_{ij}^{xx}=\sum_{j}A_{ij}^{yy}=\sum_{j}A_{ij}^{zz}=\frac{1}{3}\sum_{j}\left(A_{ij}^{xx}+A_{ij}^{yy}+A_{ij}^{zz}\right)=\Omega_o \qquad 3.28$$

For this case Equation (3.27) simply becomes

$$\sum_{i,j}{}'w_{ij}\rangle=\frac{N}{2}B_1^2\Omega_o \qquad 3.29$$

which is independent of the direction of the magnetization. Thus the dipole-dipole coupling, to the first order, does not contribute to the magnetic anisotropy in cubic crystal composed of only one kind of atom[3.23]. The situation is quite different, however, for cubic solid solutions of the substitutional type as we shall now elaborate in what follows.

Consider a cubic solid solution of the substitutional type, composed of two kinds of atoms *A* and *B*. The energy of the pseudodipole due to the interplay between spin-oribit coupling and orbital valence, unlike the ordinary magnetic diapole-

dipole interaction, decreases more rapidly than the inverse three power of the distance between atom pairs[3.12]. Thus, without great loss of generality, we may consider the pseudodipole interaction as existing between nearest neighbors only. Furthermore, one can assume for simplicity that the spin quantum numbers are the same for the constituent atoms and only the coupling constant C_{ij}'s in Equation. (3.25) differ for different kinds of nearest neighbor atom pairs. We then let C_{AA}, C_{BB} and C_{AB} to be the coupling constants of nearest neighbor atom pairs *A-A*, *B-B* and *A-B*. In the absence of anisotropic interaction among atoms, such as that associated with super-lattice formation or precipitation other than that of magnetic origin, we may suppose that if the concentration of *B* atoms is an the total number of nearest-neighbor atoms is z, the nearest-neighbor atoms around a given atom are nz of B atoms and (1-n)z of A atoms. Since, within the framework of the nearest-neighbor approximation, only the distribution of B atoms in the neighbors of a given B atom may be responsible for the induced anisotropy, we may replace $(N/2)\sum_j$ in the previous equations by $(N/2)n\sum'_j$ where $\sum'_j$ denotes the summation over all nearest-neighbors of a given B atom.

The diffusion of atoms during magnetic anneal takes place at high temperatures below the Curie point. An increase by unity i the number of *B-B* atom pairs in one of the nearest-neighbor directions through any interchange between A and B atoms results in an increase by unity in the number of A-A atom pairs and a decrease by two in the number of A-B atom pirs in the same direction. It follows that the change in the energy of the pseudodipole coupling due to an interchange between an A and a B atom at a temperature T' may be expressed as $CB^2_1(T')(1\text{-}3\cos^2\phi)$ with the help of Eqs. (3.21), (3.22) and (3.23), where $C = C_{AA} + C_{BB} - 2C_{AB}$ and ϕ is the angle between the direction of the spontaneous magnetization and the direction of the B-B atom pair considered. Therefore, the

probability that an B-B atom pair takes the direction specified by the angle ϕ in the equilibrium state, $\omega(\phi)$, is given approximately by

$$\omega(\phi) = \frac{1}{z} e^{-CB_1^2(T')(1-3\cos^2\phi)/k_BT} \qquad 3.30$$

since the pseudodipole coupling is very much smaller than the thermal agitation energy so that the deviation from isotropic distribution is very small. Accordingly, the equilibrium distribution of solute atom pairs becomes slightly anisotropic below the Curie temperature. Then, the result of our calculation for the cubic anisotropy for pure metals obtained above, which may also be applicable for solid solutions having the isotropic distribution of solute atom pairs, does not hold in this case. In contrast to the negative result expressed by Equation (3.29) with regard to the first order contribution of the pseudodipole interaction to the cubic anisotropy of a crystal of identical atoms, the first-order pseudodipole interaction in this case gives rise to an anisotropy of form, according to Equation (3.27) and discussion above:

$$F = F_o + \alpha_1^2\Omega^{xx} + \alpha_2^2\Omega^{yy} + \alpha_3^2\Omega^{zz} + 2\alpha_1\alpha_2\Omega^{xy} + 2\alpha_2\alpha_3\Omega^{yz} + 2\alpha_3\alpha_1\Omega^{zx} \qquad 3.31$$

where the isotropic term F_o is equal to - k_BT In Z_o and

$$\Omega^{PP'} = \frac{N}{2} nB_1^2(T) \sum_j{}' A_{ij}^{PP'} \qquad 3.32$$

The anisotropy induced during magnetic anneal can now be calculated using Eqs. (3.31). For the specific case where the induced anisotropy is in the X-Y plane induced by an annealing field in this plane, F may be written as

$$F = F_o - \Omega_1 \cos^2\theta + \Omega_2 \cos\theta \sin\theta \qquad 3.33$$

where

$$\Omega_1 = \Omega^{yy} - \Omega^{xx}$$

$$\Omega_2 = 2\Omega^{xy} \qquad 3.34$$

and θ is the angle between the magnetization vector and the direction of the annealing field. For the induced anisotropy in which the *X-Y* plane corresponds to the (110) or (001) plane and where the *X* axis coincides with the [111], [110] or [001] direction, eqs. (3.33) and (3.34) become

$$F = F_o - \Omega_1 \cos^2\theta \qquad 3.35$$

$$\Omega_1 = \frac{A' N n^2 C^2 B_1^2(T) B_1^2(T')}{k_B T} \qquad 3.36$$

and the value of A' is as given in Table for various crystal lattices. Thus, the anisotropy in this case is uniaxial with its easy axis of magnetization lying along the direction of the annealing field and with its anisotropy constant given by equation (3.36). Since the magnetic dipole-dipole coupling is too small to account for the observed magnetostriction, another form of dipole-dipole interaction, probably of spin-orbit coupling origin, is introduced as parameter. In the more explicit form, the energy of interaction $w(r, \phi)$ between two atoms is given by

$$w(r, \phi) = g_1(r)P_2(\cos\phi) + g_2(r)P_4(\cos\phi) + \ldots\ldots\ldots\ldots\ldots\ldots 3.37$$

where P_2, P_4 are Legendre polynomials. The coefficient of $P_2(\cos\phi)$, namely $g_1(r)$, is the sum of a term due to ordinary magnetic dipole-dipole coupling between atoms of moment μ and other terms, probably due to spin-orbit coupling. Since the spin-orbit interaction decreases more rapidly than $1/r^3$ at large distance, it is sufficient to take only nearest neighbors into account for the spin-orbit term in Ea. (3.37). Letting the distance between two atoms be $r = r_o + \delta r$ where r_o is the average separation, we find from equation (3.37) that

$$w=\left(-\frac{3\mu^2}{r^3}+L+M\delta r\right)\left(\cos^2\phi-\frac{1}{3}\right) +(Q+S\delta r)\left(\cos^4\phi-\frac{30}{35}\cos^2\phi+\frac{3}{35}\right) \quad 3.38$$

where L, M, Q and S are coefficients dependent on r_o. since $\delta r \ll r_o$, we can retain only first order terms in δr in Equation (3.38). The anisotropy constant K_1 is obtained by multiplying the mean value of w by the number $nN_o/2V$ of liaisons contained within 1 cm^{-3} where n = 12, 8 and 6 for the fcc, bcc, and sc lattices. N_a is Avogadro's number and V is the atomic volume.

Thus, we find

$$E_a = K_1(\beta_1^2\beta_2^2+\beta_2^2\beta_3^2+\beta_3^2\beta_1^2) \quad 3.39$$

with $K_1 = cN_aQ/V$, where c is a numerical coefficient equal to zero for an isotropic substance and equal to 1, $^{16}/_9$, and 2 for the face-centered, body centered, and single cubic lattices.

Thus, following a similar calculation as that used in deriving Equation (3.33) from Equation (3.30), we find that the anisotropy energy density E_u bound to the "orientation superstructure" is given by

$$E_u=\frac{nc_a^2L'L_oQ}{2VRT'} \quad 3.40$$

where $L_o = L$ when $T = T_o$, and where Q is given as a function of the direction cosines β_1, β_2, β_3 of the field H_1 and γ_1, γ_2, γ_3 of the direction of the magnetization by

$$Q=\frac{1}{9}-S_{22}+(S_{22}-S_4)(\beta_1^2\gamma_1^2+\beta_2^2\gamma_2^2+\beta_3^2\gamma_3^2) -4S_{22}(\beta_1\beta_2\gamma_1\gamma_2+\beta_2\beta_3\gamma_2\gamma_3+\beta_3\beta_1\gamma_3\gamma_1) \quad 3.41$$

The quantities S_4 and S_{22} are the mean values of α_i^4 and of $\alpha_j^2\ \alpha_j^2$, for the n possible interaction directions, where $\alpha_1, \alpha_2, \alpha_3$ are the direction cosines of the interaction directions with respect to the quaternary axes. For the isotropic polycrystalline substance, $S_4 = {}^1/_5$ and $S_{22} = {}^1/_{15}$, while in a fcc lattice, $S_4 = {}^1/_6$ and $S_{22} = {}^1/_{12}$.

Equation (3.41) valid for small values of c_a can be extended, to a first approximation, to the entire sample by replacing c^2_a by $c^2_a c^2_b$. In an isotropic substance, E_u then becomes

$$E_u = \frac{nc_a^2 c_b^2 L_o L'}{15VRT'} \cos^2\theta \qquad 3.42$$

where θ is the angle that the magnetization makes with the annealing field H_1 subsequent to quenching at temperature T_o.

3.3.0 Transport Properties of Magnetic Thin Films: Electrical Resistivity

A brief account of the theories which have been developed in recent and past years to interpret the data on resistivity of thin metallic films have been dealt in this section.

3.3.1 The Fuchs Model

The Fuchs model[3.24] of resistivity is very well known and consequently only needs brief review. Using a Boltzmann model for the behavior of the free electrons with a mean free path λ_∞ in the bulk material within a metal slab of thickness 'd' in which the electrons have a probability 'p' (the specularity parameter) or being specularily reflected from the surface, the analysis yields.

$$\frac{\sigma_F}{\sigma_\infty}=\frac{\rho_\infty}{\rho_F}=1-\frac{3}{2K}\int_o^1 du(u-u^3)\frac{(1-p)\left\{1-\exp\left(-\frac{k}{u}\right)\right\}}{1-p\exp\left(-\frac{k}{u}\right)} \qquad 3.43$$

where k = d/λ_∞ and ρ_F,σ_F are slab resistivity and conductivity respectively while λ_∞, σ_∞ are their bulk values. This expression reduces to

$$\frac{\sigma_\infty}{\sigma_\infty}=\frac{\rho_F}{\rho_\infty}\sim 1+\frac{3}{8k}(1-p)$$

i.e.

$$\rho_F\sim\rho_\infty+\frac{3}{8}\frac{\rho_\infty\lambda_\infty}{Kd}(1-p) \qquad 3.44$$

This expression (with p = o), illustrated by the straight line in figure 3.4 and it leads to the '1/d' dependence which had been predicted by earlier simpler theories which Fuchs model with its use of the Boltzmann equation superseded. However, this theory still has four basic limitations [3.25]. (i) it assumes a simple free electron model of the metal, (ii) it assumes (essentially implied by the first assumption) that the resistivity scattering time is isotopic over the Fermi surface, (iii) it models the surface scattering of electrons by supposing that, regardless of their angle of incidence to the surface, all electrons have the same probability 'p' of being reflected specularity and (iv) it assumes that the metal films is essentially a plane parallel sided slab with only microscopic roughness at the two boundary surfaces.

Examination of any physical situation in which surface scattering plays some significant role reveals that there are much more appropriate models involving the scattering or radiation of wavelength λ' from a rough surface. In general, the

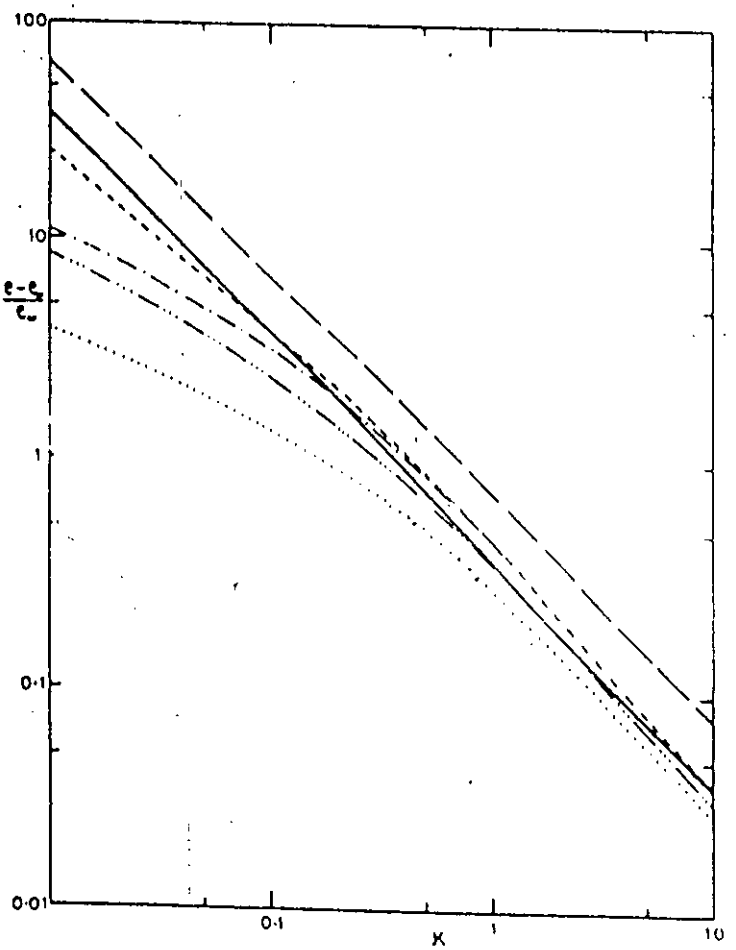

Fig. No 3.4: Logarithmic plot of $(\rho - \rho_\infty)/\rho_\infty$ for several of the theoretical models of thin film resistivity: the approximation of Fuchs model for $\rho = 0$; ....., the full Fuchs expression for $\rho=0$; -•-•-•-, the full soffer expression for $r = 1$; ••••, the full soffer expression for $r = 0.2$, —•••—, the full soffer expressioon for $r_1 = 1$, $r_2 = 0.2$; - - - -, the full Soffer - Mayadas - Shatzkes expassion with $r_1 = r_2 = 0.2$, $R_g = 0.25$ and $w = d$.

nature of the scattering will depend on the ratio of λ' to the surface roughness, a measure of this surface roughness being the r.m.s. deviation 'h' of the surface from the mean level. If $h>>\lambda'$ then the surface may be characterized as very rough and the radiation will be mainly diffusely scattered. By contrast, if $h<\lambda'$ then the radiation will scatter specularly to an extent which depends on the angle of incidence. This raises a very serious equation over the applicability of Fuchs model to all but the roughest films, for which the Fuchs specularity 'p' will be effectively zero. Finally, experimental observation reveals that thin films are 'holey' or almost islandized and even when they are continuous they have a large number of grain boundaries defects and dislocations. Thus it is almost certain that no metal films have ever been produced which can be expected to have a resistivity which varies with thickness and mean free path (temperature) in the fashion predicted by Fuchs model.

3.3.2 Mayadas and Shatzkes model.

Mayadas et al [3.26] and Maydas and Shatzkes[3.27] have modelled the effects of grain boundary scattering in thin films. Their theory again assumes free-electron behavior and models the grain boundaries and randomly placed partially reflecting surfaces perpendicular to the film. Combining Fuchs theory with this model of grain boundary scattering, Mayadas et al found that the contribution to the resistivity from grain boundary scattering is given by

3.45

R_g being the grain boundary reflection coefficient and ω being the mean grain growth.

It is found experimentally that often the grain size varies roughly linearly with film thickness[3.28] and consequently this grain boundary scattering gives a resistivity which varies inversely with the film thickness. All the surface scattering theories lead to a markedly temperature dependent contribution from the surface scattering (the so-called deviation from Mathiessen's rule) whereas grain boundary scattering theories give no such temperature dependence. Therefore, it appears to be, necessary only to measure over a substantial temperature range for various thickness to be able to establish the relative magnitudes of grain boundary and surface scattering.

3.3.3 Islandization and Macroscopic roughness

Namba[3.29-3.30] was the first to produce the islandization or macroscopic roughness of the film. This simple model represented the variation in film thickness due to islandization as one dimensional size wave in the direction of current. Hoffmass and Vancea[3.31] employed this model to fit their data on thin film resistivity.

3.3.4 Soffer's Model of Suface scattering:

Soffer[3.32] has proposed a model of surface scattering within which he introduced an angularly dependent specularity parameter p(θ), where

$$p(\theta)=\exp\left\{-\left(\frac{4\pi h}{\lambda_e}\right)^2\cos^2\theta\right\} \qquad 3.46$$

where λ_e is the electron wave length, 'h' is the r.m.s. surface roughness and θ is the angle of incidence of the electron relative to the surface normal. Using this p(θ)

Soffer predicted variations in ρ with thickness 'd' which, except for a absurdly high levels of roughness, did not give the '1/d' dependence commonly expected. This is in contrast with Fuchs model which apart from a small correction gives such a dependence for the surface caused resistivity. Watanabe and coworkers[3.33] utilized for close approximations[3.34] in their excellent studies of gas adsorption of thin films prior to its use by Sambles and coworkers[3.35-3.36] for gold, aluminum and silver films.

At present the most useful and physically reasonable model of surface scattering in thin samples is that due to Soffer.

3.4 Magnetization of thin films

General theory of magnetization

In order for an assembly of spins to be aligned spontaneously, there must exist some very strong forces between them. An estimate of the order of magnitude of the equivalent field may be obtained by observing that the thermal agitation energy is nearly equal to the Zeeman energy of a magnetic moment in this field at the order disorder transition point.

Thus,

$$H \cong \frac{k_B T_c}{\mu_B} = 4.5 \times 10^6 \, Oe \qquad 3.47$$

for $T_c = 300^0$K. Here k_B is the Boltzmann's constant and μ_B the Bohr magnetron, is the magnetic moment of an electron spin. The origin of this enormous field is of obvious importance in the theory of magnetism.

Weiss, in his phenomenological theory of magnetism, assumes that there exists a very large field, which, like the Lorentz field, is proportional to the magnetization[3.37]. In this way, he derived an expression for the magnetization which is in good agreement with experiment. The physical origin of this Weiss molecular field, however, remained unclear until 1928 when Heisenberg pointed out that it is related to the quantum mechanical exchange integral. It can be shown that semi classically[3.38].

$$E_{ex} = -2J\boldsymbol{S}_i.\boldsymbol{S}_j \qquad 3.48$$

where E_{ex} is the exchange energy between atoms i and j bearing vector spins S_i and S_j respectively, while J, known as the exchange integral, has no classical analogue. J expresses the difference in coulomb interaction energy of the system when the spins are parallel or anti-parallel. If the exchange integral J is positive, parallel alignment of spins or ferromagnetism results. On the other hand, if J is negative, anti-parallel spins or anti-ferromagnetism results. In general J is negative, favoring the non-ferromagnetic state. However, for certain elements such as Fe, Co, and Ni, the ratio between the radius of the 3d orbit and the inter-atomic separation is within the proper range for ferromagnetism to occur.

The magnetization of a magnetic material is defined as the magnetic moment per unit volume and is in general a decreasing function of temperature. The decrease of the magnetization as temperature is increased is interpreted as departure from saturation due to the excitation of spin waves[3.39]. The probability<n> that a particular spin wave of energy $\hbar\omega$ will be occupied at a given temperature T is given by

$$\langle n\rangle = \frac{1}{e^{\hbar\omega / k_B T} - 1} \qquad 3.49$$

for a system at thermal equilibrium at temperature T. Here k_B is Boltzmann's constant, $\hbar$ is Planck's constant h divided by 2π, and ω is the frequency of the spin wave. The difference between the saturation magnetization at OK, $M_s(0)$, and that at temperature T, $M_s(T)$, is given by

$$M_s(0)-M_s(T)=\frac{2\mu_B}{V} \qquad 3.50$$

where $\mu_B = e\hbar/2mc$ is the magnetic moment of a free electron, V is the volume of the specimen and k is the spin-wave wave vector. The factor of 2 appears in figure (3.50), because a spin reversal corresponds to a change of $2\mu_B$. For a three dimensional lattice, the umber of energy states per unit volume with wave number less than k is $(1/2\pi)^3(4\pi/3)k^3$. This result follows from the fact that the number of normal modes per unit volume is $4\pi/3\lambda^3$ and $\lambda = 2\pi/k$. Thus, we find from Eqs. (3.49) and (3.50) that

$$M_s(0)-M_s(T)=\frac{8\pi\mu_B}{(2\pi)^3}\int_o^\infty \frac{k^2dk}{e^{\hbar\omega/k_nT}-1} \qquad 3.51$$

Now, the energy of a spin wave of frequency ω, according to spin-wave theory is given by

$$\hbar\omega=(2S)\,J\,(ka)^2\,\hbar\gamma\,\frac{2A}{M_s(T)}k^2 \qquad 3.52$$

where A the exchange constant, a the lattice constant, γ the gyro-magnetic ratio, and S the spin 2S = 1 for S = ½ and letting K = ka, Equation (3.51) may be transformed to

$$M_s(0)-M_s(T)=\frac{8\pi M_s(0)}{(2\pi)^3}\int_o^\infty \frac{K^2dK}{e^{JK2/k_BT}-1} \qquad 3.53$$

where we have identified μ_B/a^3 as the saturation magnetic moment per unit volume at 0K or $M_s(0)$, since there are 2S spins per atom. Integrating Equation (3.53), we readily find for a simple cubic crystal,

$$M_{s3}(T)=M_s(0)\left[1-0.1174\left(\frac{k_BT}{J}\right)^{3/2}\right] \qquad 3.54$$

This is Bloch's 3/2 power law. for bcc and fcc crystals, the constant 0.1174 should be replaced by 0.0587 and 0.0294, respectively.

Thin Films

Similarly, for a two dimensional lattice,

$$M_{s2}(T)=M_s(0)\left[1-\frac{2(2\pi)}{(2\pi)^2}\int_o^\infty \frac{KdK}{e^{JK^2J/k_BT}-1}\right] \qquad 3.55$$

This integral diverges at the lower limit, a result which is interpreted to mean that the plane lattice has no spontaneous magnetization. For this case, the basic assumption of the Bloch theory that the magnetization is close to the saturation value, is invalid. Therefore, in order to examine the behavior of the magnetization as a function of temperature for thin films, we must take into account the discrete nature of the lattice.

Theory of Klein and Smith

To begin with, let us consider a three dimensional ferro-magnet in a magnetic field. The quantum mechanical Hamiltonian is given by

$$\begin{aligned}\Re=&-\frac{1}{2}\sum_{i,j=1}^{N}2J_{ij}(R_{ij})S_i.S_j\\&+\frac{1}{2}\sum_{i,j=1}^{N}\frac{4\mu_B^2}{R_{ij}^5}(R_{ij}^2S_iS_j-3S_i.R_{ij}S_j.R_{ij})-\sum_{i=1}^{1}2\mu_BS_i^{(z)}H\end{aligned} \qquad 3.56$$

Here N is the total number of atoms while the sums over i and j each run from 1 to N, summands with i = j being omitted. R_{ij} = [R_i - R_j] is the distance between the centers of gravity of the i^{th} and j^{th} atoms, J_{ij} the exchange integral between these

atoms, S_i the spin-angular momentum operator of the atom at R_i in units of $\hbar$ and H the z directed magnetic field.

Diagonalizing the Hamiltonian (3.56), neglecting the dipole-dipole terms (2nd term) we obtain its eigen values E as[3.40].

$$E = C + \frac{1}{2}\sum_{\lambda} A_{\lambda} N_{\lambda} \qquad 3.57$$

where N = 0, 1, 2, ... and

$$C + \sum_{i,j} J_{ij} S^2 - 2\mu_B SNH \qquad 3.58$$

and $$A_{\lambda} = \sum_{\lambda} 2SJ_h(R_h)(1 - e^{iK_{\lambda}.R_h}) + 2\mu_B H \qquad 3.59$$

where $R_h = R_i - R_j$ and K_λ is the reduced wave vector. The usual periodicity conditions require its components to take the values $K^1{}_\lambda = 2\pi n_i/G_i$ where i. = x, y, z and G_i is the linear dimension of the specimen in the i^{th} direction in units of the lattice constant. Thus, n_i assumes integral values between $-½G_i$ and $½G_i - 1$.

The spontaneous magnetization M_s as a function of temperature T can now be obtained from the partition function Z by the relation

$$M_s(T) = \frac{k_B T}{V}\frac{\partial}{\partial H} \ln Z \qquad 3.60$$

where V is the volume of the sample. According to Equation (3.57) and (3.59), Z is Given by

$$Z = \sum_{E} e^{-E/k_B T} = e^{-C/k_B T} \prod_{\lambda} (1 - e^{A/k_B T})^{-1} \qquad 3.61$$

For an sc lattice of atoms with spin ½, the spontaneous magnetization is given by

$$Ms(T)=\frac{N\mu_B}{V}\left\{1-\frac{2}{N}\sum_{n_x,n_y,n_z}\left\{\exp\left[\frac{2J}{k_BT}\sum_{i=x,y,z}\left(1-\cos\frac{2\pi n_i}{G_i}\right)\right]-1\right\}^{-1}\right\} \qquad 3.62$$

Since N is the total number of atoms in the crystal, $N\mu_B/V$ is equal to the saturation magnetization at 0K, $M_s(0)$.

Consider now a thin film with its surface normal in the z direction. G_x and G_y, taken equal to G for convenience, are still very large numbers. On the other hand, since the film is thin in the z dimension, G_z need not be a large number, and is in any event much smaller than G. Therefore, we can integrate over n_x and n_y but not over n_z. We then obtain from Equation (3.62)[3.41].

$$Ms(T)=\frac{N\mu_B}{V}\left\{1-\frac{2G^2(2\pi)}{N(2\pi)^2}\sum_{n_z=0}^{G_z-1}\int_{2\pi/G}^{\infty}\frac{KdK}{e^{(J/k_BT)/(K^2+2-2\cos(2\pi n_z/G_z)}}\right\} \qquad 3.63$$

Klein and Smith have set the lower limit on the integral of Equation (3.63) non zero because they observed that the state with $n_x = n_y = n_z = 0$, corresponding to the classical picture of all spins being parallel with the spin system aligned in an arbitrary direction, makes an infinite contribution to the magnetization as given by Equation (3.62).

The upper limit in Equation (3.63) is set equal to infinity without appreciable error because the important contributions to the integral come from the region of small K when $J/k_BT \gg 1$, a necessary condition for the applicability of the Bloch theory. The integrand of Equation (3.63) can now be evaluated with the following result:

$$Ms(T)=\frac{N\mu_B}{V}\left\{1-\frac{k_BT}{J}\frac{1}{2\pi G_z}\sum_{n_z=0}^{G_z-1}(-)\ln\left[1-\left(1-\frac{J}{k_BT}\frac{4\pi^2}{G^2}\right)\times e^{-f(n_z)}\right]\right\} \qquad 3.64$$

where

$$f(n_z)=\frac{2J}{k\,T}\left(1-\cos\frac{2\pi n_z}{G}\right) \qquad 3.65$$

Since G is very large, we have retained only the first order term in the series for

$$e^{(J/k_BT)(4\pi^2/G^2)}$$

Klein and Smith[3.41] have carried out the summation in equation (3.64) by numerical methods for films varying in thickness from 1 to 128 atom layers with representative results shown in figure 3.1. Here T_B is the characteristic temperature determined by setting $M_{s3}(T)$ equal to zero in equation (3.54), giving $T_B = 3.9J/k_B$. For $M_s(T)/M_s(0)$ less than about 0.75, the results of spin wave theory are no longer strictly valid and the curves below this value have been drawn dotted for emphasizing this point. The plot of $G_z = \propto$ is merely a plot of equation (3.54).

It is seen from Fig. 3.1 that for films thinner than about 60 atom layers, there is a significant deviation of the magnetization from the three dimensional value at a given temperature. Furthermore, for these sufficiently thin films $M_s(T)$ falls off more sharply with temperature than $T^{3/2}$ given by the Bloch law.

Permalloy, the nickel-iron alloy, is either bcc or fcc depending upon the relative composition of nickel and iron. Thus, the theory developed above for simple cubic lattices could not be strictly applicable to these alloys of interest to magnetic thin films. Glass and Klein[3.42], however, have studied theoretically the magnetization behavior of thin films for both the body centered and the face centered lattices. The calculation involved is quite analogous to that for the simple cubic case discussed above.

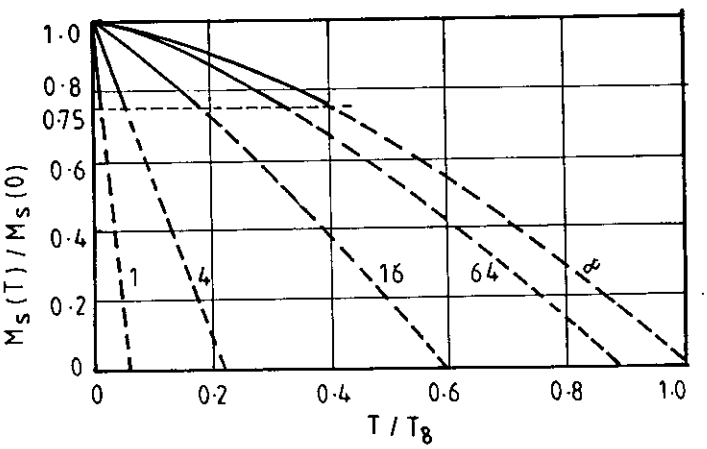

Fig. No 3.5: Normalized magnetization vs normalized temperature for sc square films of varying thickness the integers on the curves denotes film thickness in number of atoms layers (after Klein Smith[3.41]).

CHAPTER 4
EXPERIMENTAL DETAILS

4.1 Thickness Measurement
4.2 XRD
4.3.0 SEM
4.3.1 Principle of SEM
4.3.2 Magnetic Specimens
4.4 SIMS
4.5.0 Experimental setup for Anisotropy Measurement
4.5.1 Principle of Torque Magnetometer (TM)
4.5.2 Mathematical formulation for Torque Analysis
4.5.3 Design and Working Principle of TM
4.5.4 Experimental Details
4.5.5 Sample Suspension
4.5.6 High Temperature Oven
4.5.7 Calibration of TM
4.6.0 Resistivity Measurement
4.6.1 Theory of Electrical Resistivity
4.6.2 The Vander Pauw's Technique
4.6.3 Experimental Setup
4.7.0 Experimental Setup for Magnetization Measurement
4.7.1 Principle of VSM
4.7.2 Mechanical Design of VSM
4.7.3 Electronic Circuit of VSM
4.7.3.1 Sensitivity Limits
4.7.3.2 Stability Tests Differential Measurements
4.7.3.3 Vibration Amplitude
4.7.3.4 Image Effects
4.7.3.5 Vibration Frequency
4.7.3.6 Vibration Problems
4.7.4.0 Calibration of VSM
4.7.4.1 Calibration Data

-97638

4.1 Thickness measurement

Thickness is the single most significant film parameter. It may be measured either by in-situ monitoring of the rate of deposition, or after the film is taken out of deposition chamber. Techniques of the first type often called as monitor method generally allow both monitoring and controlling of the deposition rate and film thickness other techniques are also used for thickness measurement. Any physical quantity related to film thickness can in principle be used to measure the film thickness. The methods chosen on the basis of their convenience, simplicity and reliability. The monitor methods are of different types [1] Electrical methods : (a) Film resistance (b) capacitance monitors and (c) Ionization monitors [2] Microbalance monitors: (a) Microbalances (b) Quartz crystal monitors [3] Mechanical methods (stylus) (4) Radiation absorption and Radiation emission methods (5) Beam photometers. Other methods are also used to measure film thickness, one of this type is optical interference method, which may be of three types: (a) photometric method (b) spectrophotomatric method and (c) Interference fringes. In our laboratory we use the last one. A brief description of the method is given below.

Multiple-Beam Interferometry:

When two reflecting surface are brought into close proximity, interference fringes are produced, the measurement of which makes possible a direct determination of film thickness and surface topography with high accuracy. Wiener[4.1] was the first to use the interference fringes to measure the film thickness.

This method developed to a remarkable degree by Tolansky[4.2~4.3], utilize the resulting interference effects when two silvered surfaces are brought close together and are subjected to optical radiation. These interference techniques, which are of great value in studying surface topology in general, may be applied simply and directly to film thickness determination and these methods are accepted as one of the standard methods for a long time.

Two types of fringes are utilized for thickness measurements. The Feizeau fringes of equal thickness are obtained in an optical apparatus of the type shown in figure 4.1. The interferometer consists of two slightly inclined optical flats, one of them supporting the film, which forms a step on the substrate. When the second optical flat is brought in contact with the film surface, and the interferometer is illuminated with a parallel monochromatic beam at normal incidence. Broad fringes are seen arising from interference between the light beams reflected from the glass on the two sides of the air wedge. At points along the wedge where the path difference between those two beams are an integral number of wave lengths, bright fringes occur. Where the path difference is an odd number of half wave lengths, dark fringes occur. If the glass surfaces of the plate are coated with highly reflecting layers, one of which is partially transparent, then the reflecting fringe system consist of very fine dark lines against a bright back ground. The film whose thickness is to be measured is over coated with a silver layer to give a good reflecting surface and a half silvered microscope slide is laid on the top of the film whose thickness is to be determined. a wedge is formed by the two microscope slides and light multiply reflected between the two silvered surfaces forms an interference pattern with a discontinuity at the film edge. The thickness of the film 't' can then be determined by the following relation

$$t = \frac{\lambda}{2}.\frac{b}{a} \qquad 4.1$$

where λ is the wave length of monochromatic source and b/a is the fractional discontinuity identified in figure 4.1. In general monochromatic source is the sodium light, where average λ = 5893Å and in practice several half silvered slides of varying thickness and therefore of varying transmission are collected, as one of these is selected for maximum resolution. a resolution of about 20Å may be obtained in a careful measurement and about 100Å in a routine procedure. Accurate determination of fringe spacing are difficult and time consuming; but a method of image comparison which considerably improves the case and rapidity of measurement has been developed[4.4~4.5]. Other refinements of Tolansky method which uses a simple film thickness gauge utilizing a Newton's ring may be developed which involves no critical adjustment of wedges etc., and which reduces error in film thickness determination[4.6].

We setup an arrangement as described above (Tolansky method) for thickness measurements of solid thin films which is widely used and in many respect this method is also most accurate and satisfactory one.

4.2 X-ray Diffraction Study (XRD)

The structure of the Ni-based magnetic thin films were studied by X-ray diffraction. In X-ray diffraction measurement the film was first placed in the rectangular groove of a rectangular flat plate called the specimen holder, and this sample holder was placed inside the specimen chamber around which a goniometer rotates.

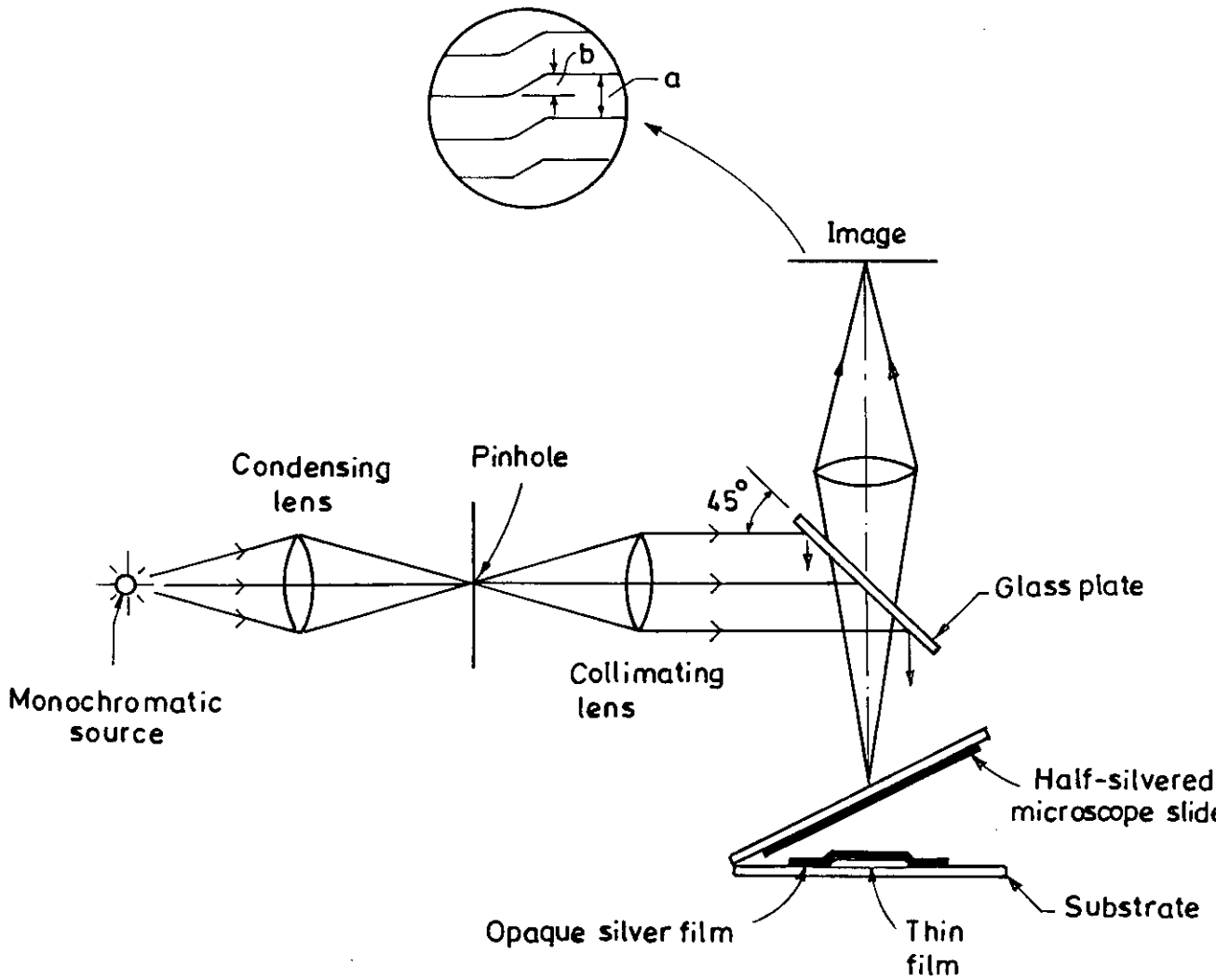

Fig. 4.1: The schematic diagram of multiple-beam interferometer.

A chiller was then switched on, which sends cold water (15°C) around the copper or iron target in order to cool the target material from which X-ray originates. After correct setting of power, the difractometer is switched on and the sample was exposed to X-ray. Different angles of incident starting from 5° to 100° (or above) were obtained by rotating the goniometer around the specimen chamber. The diffraction pattern was observed from a gauge on the diffractometer at different angles and different range which was fixed earlier. After the scan was completed, the goniometer was set at auto scan in the specified range at a rotational speed of two degree per minute. The charting unit was switched on and the diffractogram, which plotted intensity of radiation diffracted through sample at varying angles. In our case almost all samples are appeared to be amorphous (figure 4.2).

Although most workers[4.7-4.8] report that thin films prepared by coating units, as in our case, to be amorphous on the basis of normal X-ray diffraction pattern, in fact metals and alloys without glass forming materials cannot stay in amorphous state at normal temperature. This erroneous conclusion about the state of the thin films arises from the low dimensions of the films. We believe that X-ray diffraction pattern produced by very low Bragg's angle would demonstrate the crystalline nature of the films. X-ray diffraction pattern of $Ni_{95}Co_5$ was taken in Indian Association for the Cultivation of Science (IACS) laboratory with very slow angular rotation of 0.004^0 per second where we observed a hump around 25^0, which is reported in chapter 5.

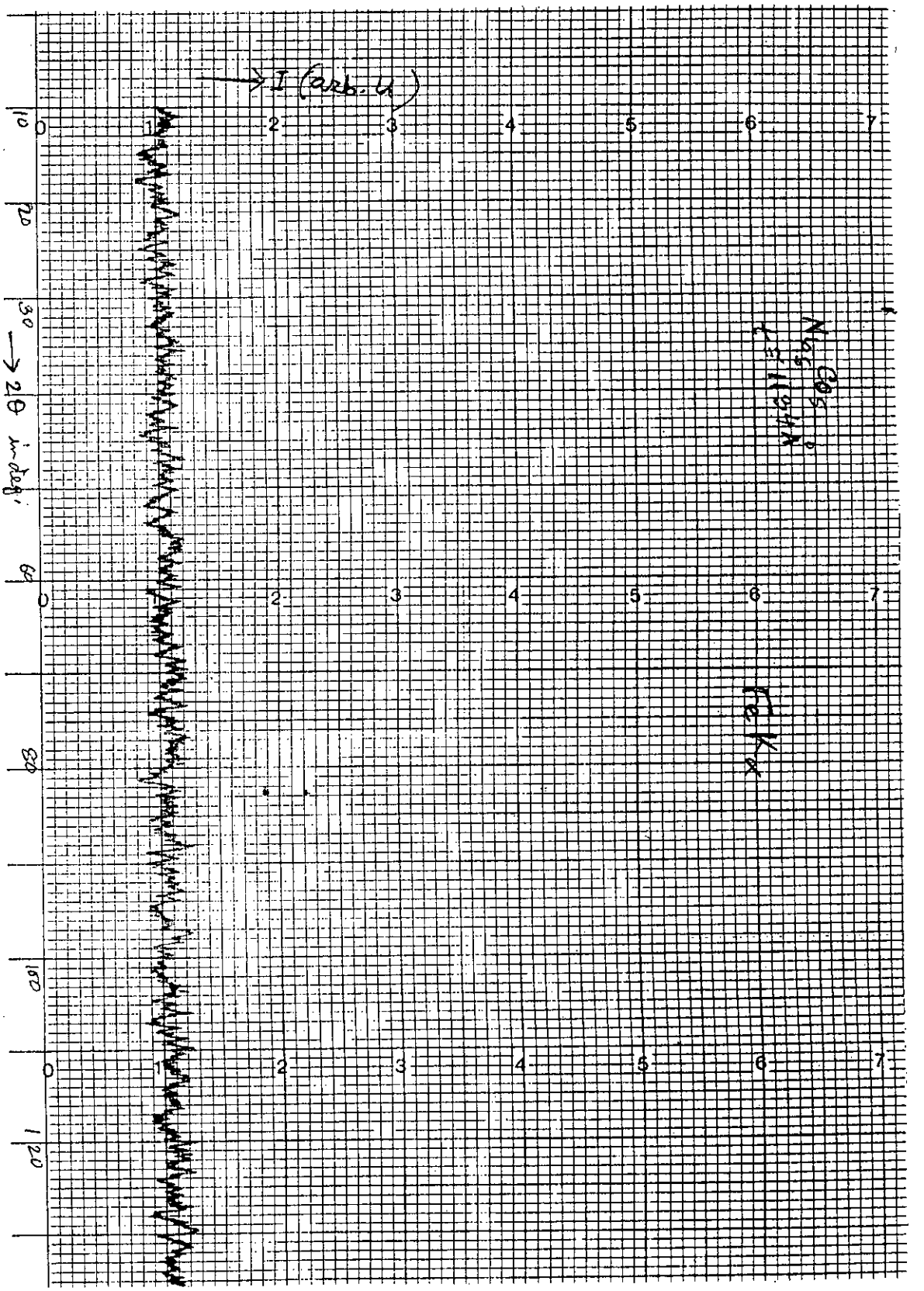

Fig. No 4.2 X-ray diffraction pattern of as deposited $Ni_{95}Co_5$ film of thickness 1134Å and P = 8×10^{-6} torr.

4.3.0 Scanning Electron Microscopy (SEM).

The SEM in one of the important techniques widely used to obtain surface morphological information of solid specimens[4.13]. This technique has also been used to determine the surface morphology and the granular size of powder particles[4.9] present. To examine the presence of powder particles[4.10-4.11] and their distributions uniformity and defects in thin films[4.12], this technique can also be applied to study the structural formation of thin magnetic films. In our work, we have studied the surface morphology of different Ni-based magnetic thin films prepared in our laboratory.

4.3.1 Principle of SEM

The basic principle of SEM is to scan a specimen with a finely focussed electron beam of the order of Kilovolt energy. An image is formed by scanning a cathode-ray tube in synchronism with the beam (figure 4.2) and by modulating the brightness of this tube with beam excited signal. In this way an image is built-up point-by-point which shows the variations in the generation and collection efficiency of the chosen signal at different point of the specimen.

In SEM, there is no need to refocus the signal carrying particles generated in the specimen as in transmission electron microscope (TEM). This makes it possible to examine rough, solid specimens with a minimum of specimen preparation. By using different conditions and specimens, it is possible to obtain images showing surface topography, average atomic number, surface potential distribution, magnetic domains, crystal orientation, crystal defects in solid specimen and also the structure formation in thin solid films.

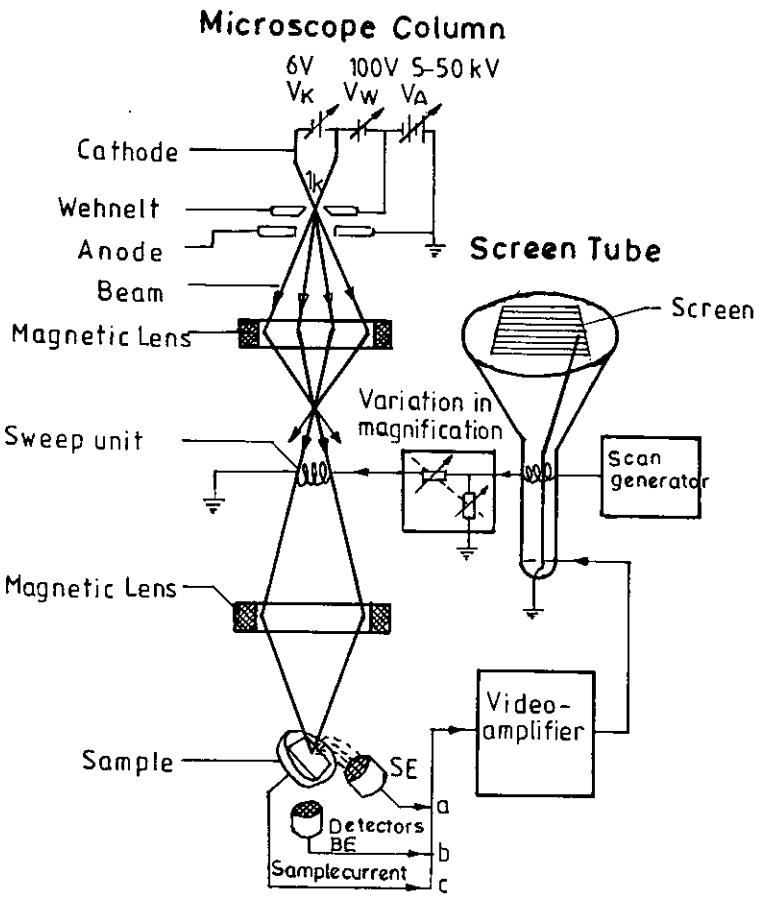

Fig. 4.3: The schematic diagram of scanning electron microscope.

The main elements of SEM are:

(a) Electron gun (heated cathode e.g. W-hairpin or LaB_6-tip,field emission cathode in high performance instruments)

(b) Electro-magnetic lenses for focussing electrons

(c) Sample chamber with specimen stage and detector, and

(d) Electronic systems to display image.

The electrons emitted from the electron gun are focussed on the object surface by means of Wehnelt cylinder and 2 to 3 electromagnetic lenses; the diameter of the focal spot (diameter of electron probe) which can at present be attained lies between 5 to 10nm. A sweep generator is controlled so that the electron beam scans the sample line by line synchronized with the electron beam in a cathode ray tube monitor.

The secondary electrons and/or back scattered electrons emitted from the sample are monitored by suitable detectors; in addition, the electron current taken up by the sample can be measured. The signals emerging from the detectors serve either singly or electronically mixed by a video-amplifier to modulate the intensity on the screen. The adjustment of the magnification depends on the size of the scanned sample surface. For a constant image size on the screen, the magnification is given by the ratio of the screen size and the size of the scanned surface area. The schematic diagram of a scanning electron microscope is shown in figure 4.3.

Small samples (upto several millimeter and same time even larger) can be investigated directly in the SEM if the sample material has a sufficiently electric conductivity to prevent charging produced by the bombardment with the electrons. If the sample is an insulator, the sample has to be coated with an extremely thin

layer of an electrically conducting material, like gold. This can be done by high vacuum evaporation unit by vertical vapor deposition.

4.3.2 Magnetic specimens:

Magnetic specimens can be studied in the SEM in two main ways. for sample cobalt, Yttrium ortho-ferrite and magneto-plumbite, the fringing field will modulate the trajectories of the secondary electrons between the specimen and the collector. This shows up as wide, diffused bands superimposed on the domain boundaries and is designated type-1 magnetic contrast.

Type - 2 magnetic contrast shows up in back scattered electron image of the materials such as silicon, iron and nickel, which have cubic symmetry and a sufficiently strong internal field. Depending on the experimental arrangement, this can show up either as domain contrast (in which the alternative domains appear as bright and dark) or wall contrast (in which the domains appear equally bright but domain wall appears as bright or dark narrow bands).

Type-2 magnetic contrast seldom exceeds 1% of the collected current and in many cases may be considerably smaller even than this. Therefore, it is generally necessary to prepare the sample with a flat, smooth surface and to orient this in the SEM so as to minimize competing image contrast.

Experimental details: Ni_{100-x} Co_x thin films were deposited on to quartz substrates by vapor deposition technique (Sec 2.5). Scanning electron micro-graphs of as deposited $Ni_{05}Co_5$, $Ni_{90}Co_{10}$ and $Ni_{85}Co_{15}$ films surface were taken using a scanning electron microscope. For this purpose we used the facilities of IACS laboratory Kolkata.

4.4 SIMS: Secondary ion mass spectroscopy

Secondary ion mass spectroscopy (SIMS) is a technique based on sputtering of material surfaces under primary ion bombardment. A fraction of the sputtered ions which largely originate from the top one or two atomic layers of the solid is extracted and passed into a mass spectrometer where they are separated according to their mass to charge ratio and subsequently detected. Because of the sputter yields of the individual species, coupled with their ionization probabilities can be quite high and the mass spectrometers can be built with high efficiencies, the SIMS technique can provide an extremely high degree of surface sensitivity. Using a particular mode like static SIMS, where a primary ion current is as low as 10^{-11} amp, the erosion rate of the surface can be kept as low as 1Å per hour and one can obtain the chemical information of the uppermost atomic layer of the target. The other mode like dynamic SIMS, where the primary ion current is much higher, can be employed for the depth profiling of any chemical species within the target matrix, for providing a very sensitive tool for qualitative characterization of surfaces, thin films, super-lattice etc.

The presence of molecular ions amongst the sputtered species makes this method particularly valuable in the study of molecular surfaces and molecular absorbates. The high sensitivity of SIMS to a very small amount of material implies that this technique is adaptable to microscopy offering its image possibilities. By using this possibility in static SIMS or dynamic SIMS mode of analysis, one can obtain a two dimensional (2D) surface mapping or a three dimensional (3D) reconstruction of the elemental distributions, respectively within the target matrix[4.13].

4.5.0 Experimental Set-up for Anisotropy Measurements

4.5.1 Principle of the Torque Magnetometer

The apparatus used is a sensitive Torque magnetometer with a Proportional Integrating Differentiating (P.I.D) regulator following the technique used by B. Westerstrandh et al.[4.14]. This apparatus allows measurements of the torque as a function of direction cosines of the magnetic with respect to crystallographic axes. A laser source provides a coherent light beam of constant intensity which falls symmetrically on two photo-diodes and illuminates them equally. Any deviation of the beam from the symmetric position due to the rotation of the mirror fixed on the specimen attached to this holder produces an out of balance photo-current. This photo-current is fed in to the P.I.D. regulator which produces a compensating current and sends it to the compensating coil placed in a permanent magnetic field.

To avoid any spuratic torque due to the image effect in the pole pieces, the specimen is placed in the central position between the poles of a rotatable magnet. The center of the sample is made to coincide with the axis of the rotatable magnet and this is ensured by the exact repetition of the torque value at every 180^0 rotation of the field. Thin films that was deposited on circular substrate (0.5 cm dia) provide maximum symmetry about the axis of the rotating field. Torque against angle showed reasonable reproducibility for forward and reverse rotation of the field[4.15].

4.5.2 Mathematical formulation for the torque analysis

The measured value of magnetic torque are fed into an IBM 486 PC for Fourier analysis. The Fourier coefficients are evaluated using a program written MS BASIC language designed specially for the analysis of magnetic torque data. The input data are the torque (τ) in volt and the corresponding angle (θ). The analysis also give the offset angle of the magnetic field, which may be adjusted by rotating

the magnet through the offset angle to locate the zero torque position. The evaluated Fourier coefficients are the values at the saturation field and are used to calculate anisotropy energy of the sample. This anisotropy energy is the energy difference between the easy direction of magnetization of the film and the direction perpendicular to that. In other words, this is the anisotropy energy, which is developed due to induced magnetic field (M) and other mechanical stress which the film has suffered during deposition. Using the thickness of the sample and the calibration constant of the torque magnetometer the anisotropy constants are evaluated.

Several methods may be used for the measurement of anisotropy. The most common techniques employed are the torque magnetometer, the hysteresis lopper and the ferromagnetic resonance spectrometer. In our laboratory facilities a torque magnetometer has been developed.

One of the most dependable method of measuring anisotropy is to measure the torque on a specimen as a function of the direction of the saturation magnetization relative to the easy axes (EA). The usual scheme employed in this torque measurement[4.16] consists of supporting from a vertical torsion fiber, a test specimen and an applied field and recording point by point, the angular deflections of the fiber for various directions of the field relative to the specimen orientation. It is a time consuming method and also has some disadvantages.

A continuous reading magnetometer with the conventional fiber replaced by a system which instantaneously produces a torque just equal and opposite to that produced by the test specimen and which emits an electrical signal proportional to the torque would overcome this disadvantage of the conventional torsion fiber magnetometer. Such apparatus is being widely used[4.17,4.18]. This type of torque magnetometer has been used in our measurements. The torque magnetometer for the measurement of torque works in the range 10^{-10} Nm to 5×10^{-4} Nm. The torque

compensation is achieved by feed back mechanism from a pair of photodiode (detector) into a PID regulator system which generates a current through a compensation coil located in the field of a pair of permanent magnet.

The inherent property of a magnetic material in a static magnetic field is to align itself to the minimum energy configuration. The energy variation with respect to sample orientation is represented by a torque exerted on the sample. The torque (L) exerted on sample is related to the total anisotropy energy, E_a, by

$$L = -dE_a/d\theta \qquad 4.2$$

where θ is the angle between a fixed direction in the sample and the direction of the magnetic field. Thus it is evident that by measuring the torque from a sample in a magnetic field we can gain information about the magnetic anisotropy energy of a material. For ferromagnetic substances the anisotropy constants can be deduced from Fourier analysis of the torque data as a function of the angle θ between magnetic field and a direction fixed in the sample (aligned axis in the case of magnetic thin film).

Akulov (1929) showed that E_a can be expressed in terms of a series expansion of the direction cosines of M_s (saturation magnetization) relative to the crystal axis. In a cubic crystal, let M_s is in an arbitrary direction with respect to the crystal axes α_1. α_2, α_3 be the direction cosines of the magnetization vector, then the anisotropy energy is

$$E_a = K_o + K_1 (\alpha_1^2\alpha_2^2 + \alpha_2^2 \alpha_3^2 + \alpha_3^2 \alpha_1^2) + K_2 (\alpha_1^2 \alpha_2^2 \alpha_3^2) \qquad 4.3$$

where K_o, K_1, K_2 are the anisotropy constants for zero, first order and second order respectively. The 1st term of equation (4.3) K_o is independent of α, and is isotropic and is usually ignored, because we are interested only in the change of anisotropy energy (E_a), when M_s vector rotates from one direction to another. When K_2 is zero, the direction of easy magnetization is determined by the sign of K_1. *If* K_1 is

positive, the $E_{100} < E_{110} < E_{111}$ and $<100>$ is the direction of easy magnetization. If K_1 is negative, $E_{111} < E_{110} < E_{100}$ and $<111>$ is the direction of easy magnetization. For iron K_1 is positive whereas for nickel, K_1 is negative.

The anisotropy energy expression for a hexagonal crystal with easy c-axis can be written as

$$E_a = K_o + K_1 Sin^2\theta + K_2 Sin^4\theta + \ldots\ldots\ldots\ldots \quad 4.4$$

The expression for the torque can be obtained from equation (4.2). Thus $dE_a/d\theta$ is the torque exerted by the crystal on M_s and $-dE_a/d\theta$ is the torque exerted on the crystal by M_s. Then the torque on the crystal per unit volume is $L = dE_a/d\theta$

we get from equation (4.4)

$$L = -(K_1 + K_2) Sin2\theta + (K_2/2) Sin4\theta \quad 4.5$$

From equation (4.5) K_1 and K_2 are determined from Fourier coefficient. Expression (4.5) can be written as

$L = A_2 Sin2\theta + A_4 Sin4\theta$, where $A_2 = -(K_1+K_2)$ and $A_4 = K_2/2$

therefore, $K_1 = -(A_2 + 2A_4)$ and $K_2 = 2A_4$

4.6

Thus the uniaxial anisotropy $K_u = K_1 = A_2 + 2A_4$

K_2 is being neglected because $A_2 >> A_4$

Since in the present measurements the specimens used for anisotropy measurements were in the form of thin film and were deposited in presence of an applied magnetic field The magnetic moments of the crystallites are supposed to line up along the field direction giving the specimen an uni-axial anisotropic character. If in presence of applied field all the crystallities moment succeeds having a single direction of alignment against thermal agitation the energy expression will have the form

$E_a = K_u Sin^2\theta$ and the corresponding torque expression will simply be

$$L = - K_u Sin2\theta$$

and the resultant torque curve will show a two fold symmetry. If the alignment of moments is not perfect i.e. instead of being aligned along a certain direction is confined in a cone around the field direction, the anisotropy energy expression will be quite complicated, but it can be approximated as

$E_a = K_u Sin^2\theta + K_u Sin^4\theta$ giving a torque expression of the form

$$L = -(K_u + K_u') Sin2\theta + \frac{K_u'}{2} Sin4\theta = +A_2 Sin2\theta + A_4 Sin4\theta \qquad (4.7)$$

where $A_2 = -(Ku + K_u')$ and $A_4 = K_u'/2$

The higher values of K_u means distribution of crystallites in a higher angle cone.

4.5.3 Design and working principle of torque magnetometer.

A simple form of torque compensation can be achieved by suspending the sample from a fibre with known torsional constant. When a magnetic field is applied on the sample, the sample align its direction of easy magnetization with the magnetic field. When the sample is rotated away from the easy direction, the sample resists its effort due to the magneto-crystalline anisotropy and thus exerts a torque. The torque from the sample will twist the fiber on which it is suspended. The rotation of the sample is followed by the rotation of a mirror rigidly connected with the fibre. A laser beam is focused to the mirror which on reflection then illuminates a couple of photodiodes. A small rotation of the mirror will give rise to an unbalance photo-current. This photo-current is fed in to a PID regulator which is kept in the reverse biased mode generates a compensating current and sends to the compensating coil suspended in the permanent magnetic field of the torque magnetometer head. Thus by measuring the compensation current through the coil we can measure the magneto-crystalline anisotropy energy of the sample. The

torque from the sample is proportional to the corresponding current through the coil. Thus we measure the current needed for the sample to keep its orientation.

The principal drawing of the torque magnetometer with a automatic compensation system is shown in figure 4.4. The sample is rigidly connected to a sample holder made of non magnetic material (copper) and the sample holder is also rigidly connected to the torsion fiber. At the upper side a mirror is rigidly connect with the fiber and the compensation coil. The whole assembly is freely suspended in a thin quartz fiber and the coil is located in a field produced by a pair of permanent magnets. Now if a laser beam is shined on the mirror, the reflected beam will shined a pair of photo-diode equally. By applying magnetic field parallel to the sample, the mirror will rotate due to the torque acting on the sample. The principle is to let a photo-detector detect the movement of the reflected beam via an amplifier generating a current through the compensation coil which inhibits the motion of the suspension.

The simplest type of electronic compensation system with a photo sensitive feedback have been designed (Westerstrandh et. al[4.14]). The simplest way is to let the current through the compensation coil be directly proportional to the signal from the detector. Such a feedback system is often referred as proportional regulator. If a torque acts on the sample the turning of the mirror gives rise to a deflection of the beam shining on the detector. The deflection from the center of the detector can be made small by increasing the amplifier gain. Nevertheless contribution from the rigidity of the suspension may seriously affect the measurement of small torque's. Neither the gain of the feedback could be increased too much since the system will then would become unstable. To improve the

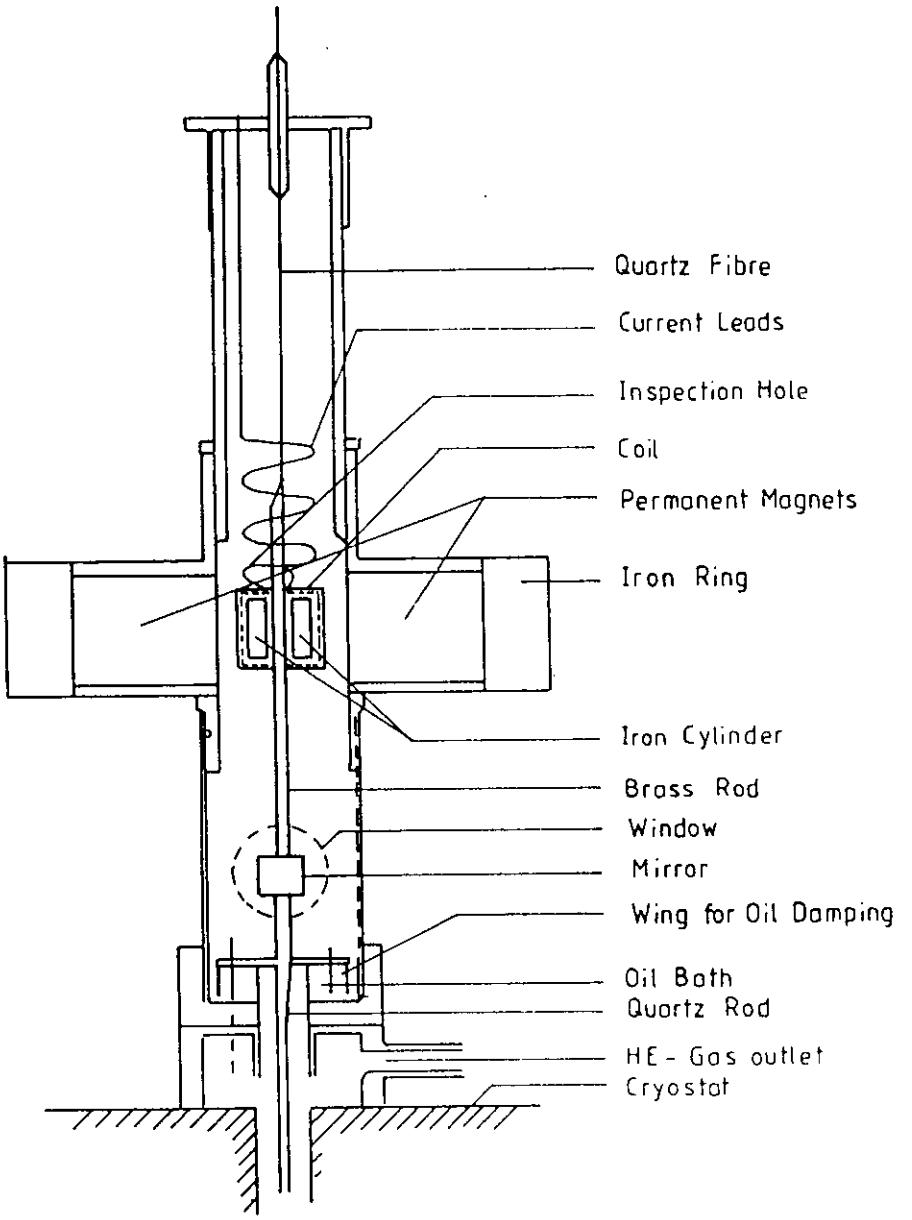

Fig. No 4.4: Crosssection of the upper part of the torque magnetometer.

stability we have used the oil damping. The viscosity of the oil damps oscillation so that we can increase the amplifier gain. To enhance the electronic damping a differential amplifier has been used in parallel with the proportional amplifier and hence improve the stability of the system. The type of compensating system can be characterized as a proportional differentiating (PD) regulator. Since the large deflection of the suspended system is a problem, the introduction of a differentiating unit allows a very high gain and a small angular deflection.

4.5.4 Experimental Details

For the measurement of magnetic anisotropy by torque magnetometer, the sample is prepared in a circular disc form. In the case of thin film substrate should be of exact circular shape on which to deposit the material of interest. The demagnetization factors of the sample is thus eliminated. To prepare thin ferromagnetic films, we cut substrates of about 0.5 cm in diameter and carefully made it perfect circular in shape. After cleaning it (etching method) the substrate is weighed by a special balance with accuracy upto 0.00001 gm. Then one circular side is covered by a tape and the other plane side is used for sample deposition, simultaneously another substrate is used, 1cm square area of which is open and the other part of the substrate is covered by a mask. The circular substrate is set on substrate holder by glued paper and the particles that are evaporating during deposition will fly through a static magnetic field ($\cong$500 O_e). After deposition we again weigh the substrate with this film and get the accurate weight of the material that is deposited onto the substrate as thin film. Then the clean face of the circular substrate is then attested to the sample holder of the torque magnetometer. The sample holder is hanged on a quartz fiber fixed with the upper part of the torque magnetometer. A small magnetic field is applied on the sample to measure the

torque that acts on it. The signal from the sample is recorded through an electronic compensation system (PID). The noise from the electronic system is eliminated by regulating the proportional gain, integrating time constant (I) and the differentiating time constant (D). Once the signal is stabilized, the magnetic field is increased in steps. In our experimental set up which ranges upto 4.3 kilo-gauss. The magnetic field is rotated in steps of 10^0 to complete a full (360^0) rotation. For every 10^0 rotation of the magnetic field, the torque is recorded. Thus the torque data is recorded for 36 angular positions of the magnetic field. These 36 points are entered in a computer program for Fourier analyses. The Fourier coefficients A_o, A_2, A_4 and δ are calculated and are plotted against (1/H), the reciprocal of the applied field. The extrapolated values of the coefficients for (1/H) = 0, are taken. In our calculation it is observed that only A_2 coefficient is dominating. The magnetic anisotropy energy that originate in ferromagnetic thin film is mainly due to the presence of induced field during deposition.

4.5.5 The Sample Suspension

The sample is mounted at the end of the quartz rod. Quartz is a suitable material for this purpose as it is diamagnetic and has low thermal conductivity. The upper end of the quartz rod is attached to a brass rod, to which the mirror and the compensation coils are fixed. The whole assembly is suspended in a quartz fiber. The quartz fiber is very suitable because of its large tensile strength and small torsional constant. Typical value of the torsional constants are $(5\sim20) \times10^{-7}$ *Nm/rad.* The elasticity of the longitudinal direction is very low, which prevents low frequency oscillation along the axis of suspension. The compensation coil have 10 layers of 100 turns of 0.06mm dia copper wire. To minimize influence

from the stiffness of copper wire, the leads of the coil have been spiraled, below the coil there is an arrangement for oil damped effective against self oscillation.

4.5.6 The High Temperature Oven

The schematic diagram of an oven that is used to heat the sample to determine the change in magnetic property with temperature is shown in figure 4.5. The most important feature in the construction of the oven is that the inner stainless steel tube extended through out the oven and a thermocouple unit is introduced from the bottom end with the thermocouple junction placed immediately below (> 1cm) the sample. The heater coil is wound directly on the inner tube. The heater consist of a *MgO* insulated chromel constantan thermocouple with a stainless cover (O.D. 1mm & length 1.3m) manufactured by OMEGA CORP. This thermocouple is flexible, and to obtain a firm contact between the heater and the inner sample tube, the thermocouple is first wound on a tube with a some what smaller diameter and the resulting spiral is after words squeezed on to the sample tube. The thermal contact between the heater and the sample tube is improved by adding some silver point. The lower ends of the heater wires are electrically connected by means of silver point, copper wires connecting an external power supply, and are soft soldered on the upper ends of the heater wires. The silver point is dried out at ordinary atmosphere by passing some current through the heater. The advantages of using chromel constantan thermocouple as a heater for this oven are that it is readily available, nonmagnetic, insulated, easily formed and gives a bi-filar winding and close thermal contact with the sample, the heater has resistance of 75Ω at room temperature (300K).

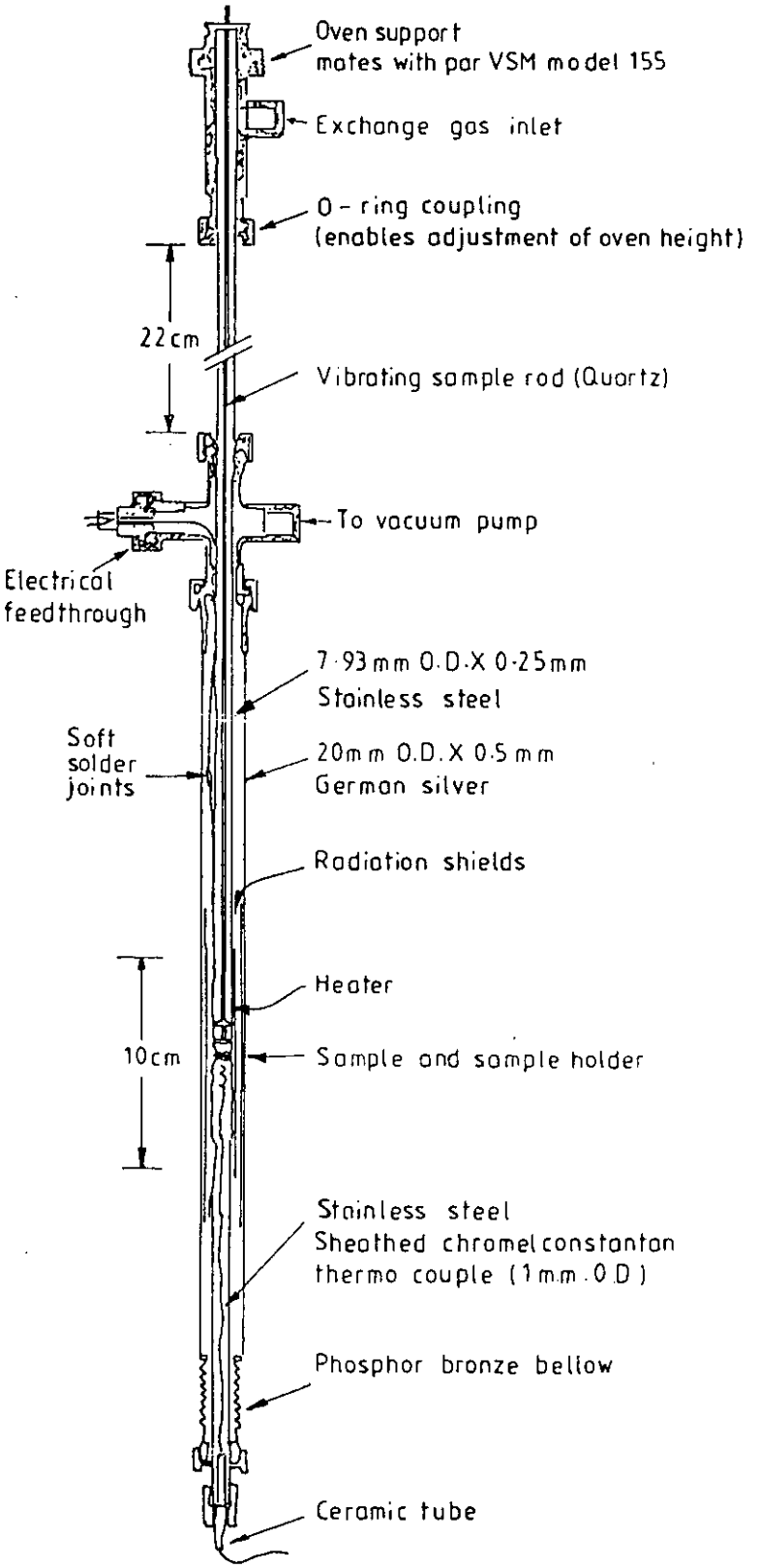

Fig. No 4.5: Schematic diagram of the high temperature oven.

Five radiation shields, consisting of 50μm stainless steel foils are located out side the heater. These are tied directly on to the heater using reinforced glass fiber threads. The outer tube via a phosphor bronze below in order to allow for the difference in length of the two tubes at higher temperatures. O-ring couplings are used through out to enable easy disassembling of the oven case of any fault.

Both the oven and the thermocouple are adjustable in height with respect to the sample. This gives a possibility to find a position of the sample in the warmest region of the oven which gives a minimum temperature gradient between the sample and the thermocouple junction. the temperature gradient $\Delta T/(T-T_o)$ over 1cm of length in the warmest part of oven is approximately 0.1% and independent of temperature.

The special characteristics of the oven are

(i) The oven can be heated from room temperature to 1143 K with in 15 minutes with a temperature difference between the thermocouple and the sample less than 1 K at the final temperature.

(ii) At constant heating or cooling rate of 5 K/min at a temperature difference of the order of 1 K is established.

(iii) Due to small thermal mass of the oven, it cools from 1150 K to 350 K in about 30 minutes which enables a fast inter-change of samples.

4.5.7 Calibration of the Torque Magnetometer

For the calibration of the torque magnetometer a single crystal disc is used. A thin nickel disc is best for this. In our laboratory, the disc is of 45mg and is oriented in such a way that the (100) crystallographic plane lies on the plane of the disc.

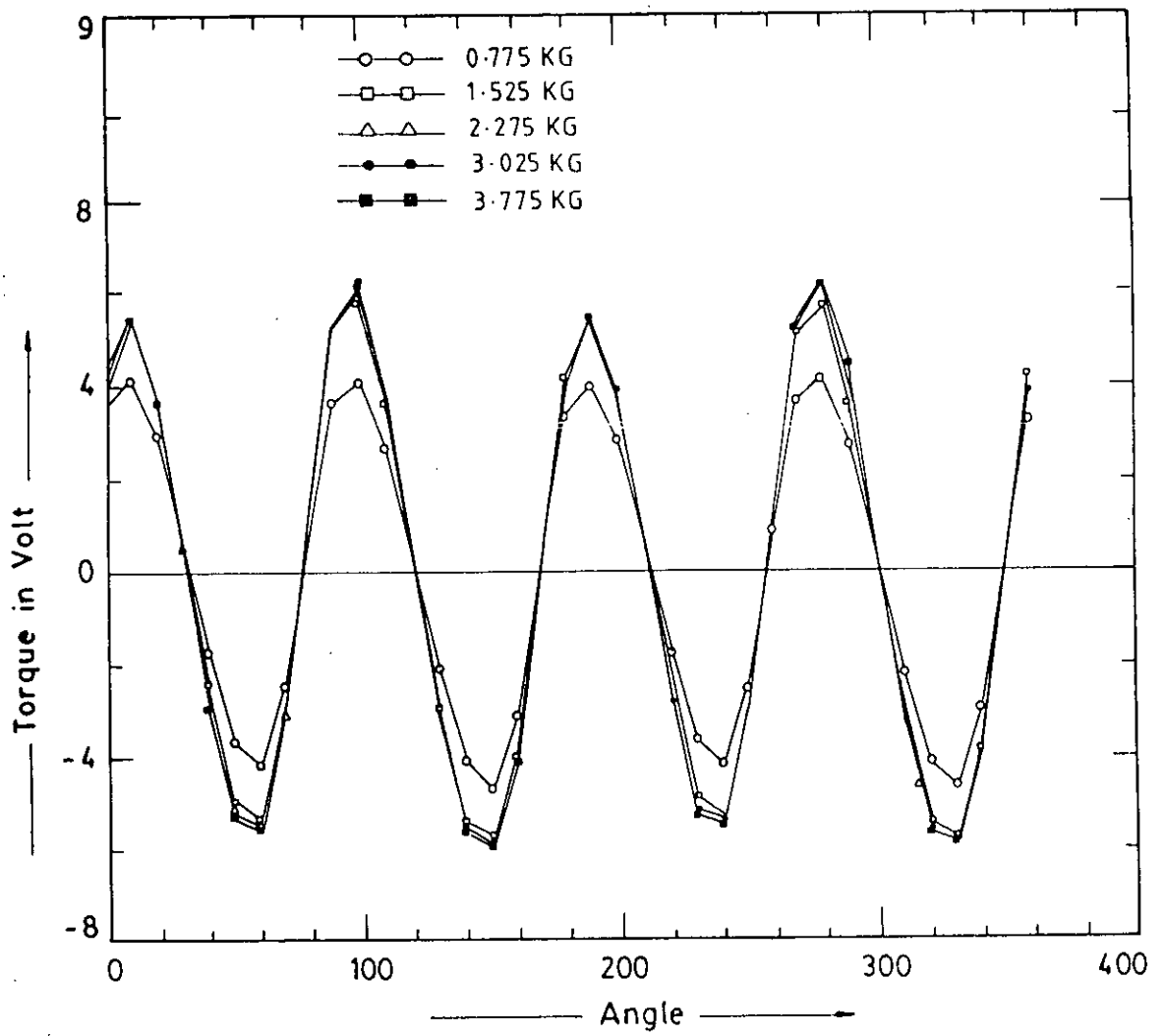

Fig. No 4.6: Torque curve for a single crystal of nickel disc in (100) plane at room temperature (25^0C).

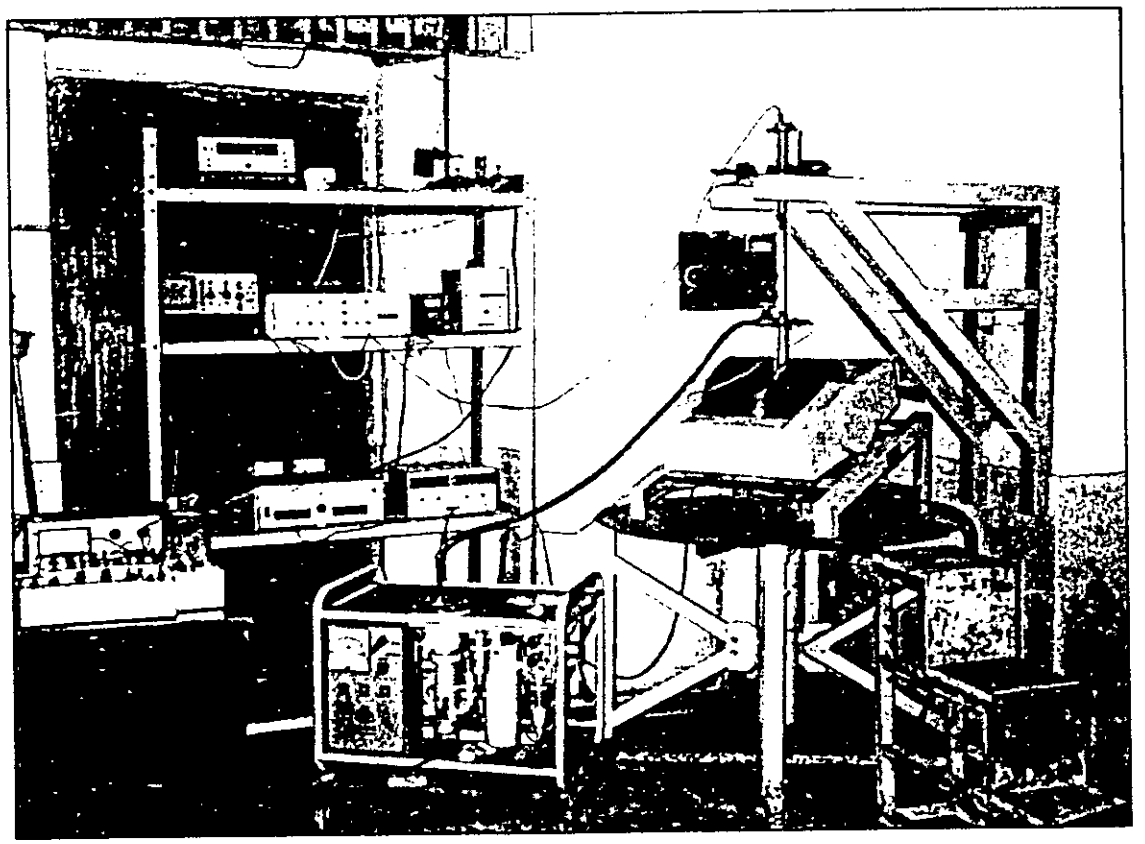

Figure- 4.7: Photograph of the Torque Magnetometer

The sample is glued to the sample holder at the lower end of quartz rod and is suspended from the quartz fiber. The sample is then placed in between the poles of an electromagnet. Three kilo gauss magnetic field which is strong enough to saturate the specimen is applied along the plane of the disc and measurement of torque is taken at every 10^{o} angular rotation for a complete rotation (360^{0}) of the magnetic field. The whole process is repeated for the variation of field strength 3.5 kilo gauss and 4.0 kilo-gauss. The measured data are entered in a computer for Fourier analysis. The Fourier coefficients are then equated with the standard equation for the torque curve. Thus from the known mass of the disc and the known values of anisotropy constants for nickel at room temperature, the calibration constant of the torque magnetometer is determined. The torque curves for as single crystal nickel disc in (100) plane are shown in figure 4.6 and the photograph of the torque measuring system is shown in figure 4.7.

4.6.0 Resistivity Measurement

4.6.1 Theory of Electrical Resistivity

The electrical resistivity ρ and its reciprocal, the conductivity $\sigma = 1/\rho$ of a material are characteristic parameter which represent the proportionality between current density vector J and the electric field E in terms of Ohm's law

$$J = \sigma E \text{ or } E = \rho J \qquad 4.8$$

Charge carrier transport involved in the measurement of ρ and σ is an irreversible thermodynamic process. The current density applied to a specimen cannot be made arbitrarily large without including Joule's heat in it, since ρ is temperature dependent so Joule's heat play a vital role in the measurement of ρ. The errors introduced by electro-thermal and thermo-electric effects in the measurement of ρ and σ of metals can be eliminated by performing measurements under isothermal

condition, by commutating the polarity of the current applied to a specimen and averaging algebraically the potential difference measured on it, by using small current (dc) in order to minimize Joule's heat. To determine the resistivity of a thin film various techniques have been developed by many workers. One of the simplest but largely acceptable method is Vander Pauw's four probe technique. A brief details of which is given in the following section.

4.6.2 Vander Pauw's Technique

To measure the electrical resistivity (ρ) and its reciprocal conductivity (σ) of thin solid films many techniques were developed. One of them is square four probe technique. Vander Pauw's method is one type of square four probe technique and an excellent method to measure the resistivity (ρ) of thin film. A brief account of this method is given below

Four contacts at the corners of Vander Pauw's specimen A, B, C and D in cyclic order are made. If current I_{AB} entering the specimen through the contact A and leaving it through the contact B produces a potential difference ($V_D \sim V_C$) between the contacts D and C repectively, then $R_{AB, CD}$ is difined as

$$R_{AB,CD} = (V_D - V_C)/I_{AB}$$

Similarly $R_{BC,DA} = (V_A - V_D)/I_{BC}$; $R_{CD,AB} = (V_B - V_A)/I_{CD}$

and $R_{DA,BC} = (V_C - V_B)/I_{DA}$

By applying some mathematical treatment, the resistivity of the material in the form of thin film is

$$\rho = 2.666 \times \delta \times (R_{AB,CD} + R_{BC,DA}) \qquad 4.9$$

where ρ is the resistivity and δ is the thickness of the film.

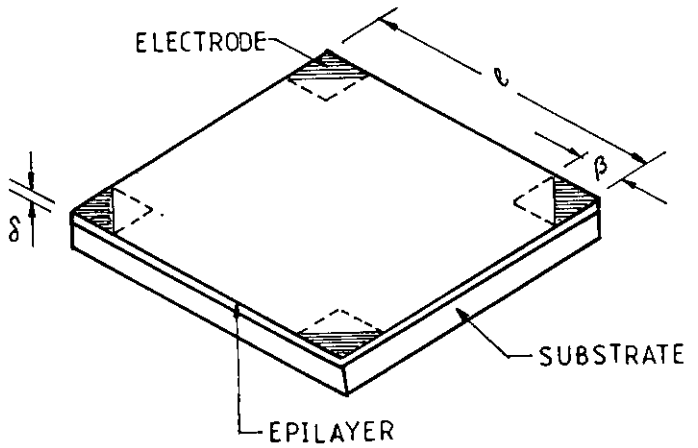

Fig. No 4.8a Vander Pauw's specimen; corner contacts made to an epitaxial layer of thickness, δ, on a square substrate; triangular or square contacts with side dimension, β, are shown on a square specimen of side dimension *l*.

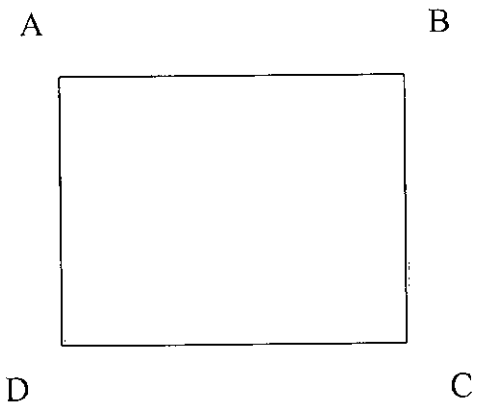

Fig. 4.8b : Vander Pauw's specimen

Equation (4.9) is adequate for determining the sheet resistivity, $\rho_s = \rho/\delta$ of a essentially infinite conducting sheet of infinitesimal thickness in comparison with the inter probe spacing 's'. Smits[4.19] has employed the method with inclusion of some correction factor.

4.6.3 Experimental setup

Magnetic thin films are prepared by the techniques stated in section 2.5. In this case no external magnetic field was applied during deposition. The vacuum was maintained at high level, the ambient pressure being 2.5×10^{-5} Torr just before the deposition. Both the metals nickel and cobalt in powder form were used for the deposition. The two powders are of nearly the same density i.e. 8.9gm/c.c. and is purity 99.95%, their evaporation temperatures 1530^0C and 1535^0C respectively (at 10^{-4} Torr). Details of which are given in sec. 2.2. After deposition the films were taken out of the bell jar and their thickness were carefully determined. The mask used was of area $1cm^2$, the lead attachment were done carefully by indium metal described in sec 2.10. The film was then placed on the substrate holder and the connections were made with the four terminals in the form of screw situated at the base of the vacuum chamber(bell-jar). The outer terminals of the screw were connected to the multi-meter and a constant current source. A heating system was also developed to heat the sample. A heater was placed on the substrate holder on which films with their substrate were placed and clipped, a thermocouple junction was placed just in contact with the substrates. All connections were made through the screws that are at the base of the vacuum system.

4.7.0 Experimental set-up for Magnetization Measurements.

4.7.1 The Principle of Vibrating Sample Magnetometer.

All magnetization measurements have been made on EG and G Princeton Applied Research Co. make vibrating sample magnetometer (VSM)[4.21~4.22]. The principle of VSM. is as follows: when the sample of a magnetic material is placed in a uniform magnetic field, a dipole moment proportional to the product of the sample susceptibility times the applied field is induced in the sample. If the sample is made to undergo a sinusoidal motion, an electrical signal is induced in suitably located stationary pick-up coils. This signal which is at the vibrating frequency, is proportional to the magnetic moment, vibration amplitude and vibration frequency. In order to obtain the reading of the moment only, a capacitor is made to generate another signal for comparison which varies in its moment, vibration amplitudes and vibration frequency in the same manner as does the signal from the pick-up coil. These two signals are applied to the two inputs of a differential amplifier, and because the differential amplifier passes only difference between the two signals, the effect of vibration amplitude and frequency changes are cancelled. Thus only the moment determines the amplitude of the signal at the output of the differential amplifier. This signal is in turn applied to a Lock-in amplifier, where it is compared with the reference signal which is at its internal oscillator frequency and is also applied to the transducer which oscillates the sample rod. Thus the output of the Lock-in amplifier is proportional to the magnetic moment of the sample only avoiding any noise of frequency other that of the signal. The Lock-in amplifier yields an accuracy of 0.05% of full scale. The absolute accuracy of this system is better than 2% and reproducibility is better than 1%. Least measurable moment is 5×10^{-4}cmu.

Variable magnetic field is achieved with a Newport Electromagnet Type 177 with 17.7cm diameter pole pieces. The magnet is mounted on a graduated rotating base. The standard model is modified to provided an adjustable pole gap in order that the highest possible field strength is available. The field can be varied from 0 to 9KG. The field is measured directly by using Hall probe.

4.7.2 Mechanical Design of the V.S.M.

The various mechanical parts of the vibrating sample magnetometer are shown in detail in the figure 4.9. It was installed in MMD of AECD, Dhaka Center. The base B of the V.S.M. is a circular brass plate of 8mm thickness and 250mm diameter. A brass tube T of 25mm outer diameter and 0.5mm thickness runs normally through the base such that the axis of the tube and the center of the plate coincide. The base and the tube are joined together by soft solder. The tube extends 60mm upward and 24mm downward from the base. There is a vacuum port on the lower part of the tube 120mm below.

Electrical connections from the audio amplifier to the speaker and from the reference coil system to the phase-shifter are taken via the Perspex feed-through. By connecting the vacuum port of the tube T to a vacuum pump the sample environment can be changed. The speaker SP is fitted 25mm above the tube T with the help of four brass stands. The lower ends of stands are screwed to the base plate while the rim of the speaker is screwed on the tops of the stands. The speaker has a circular hole of 10mm diameter along the axis of it. An aluminium disc having female threads in it is fitted to the paper cone with araldite. The aluminium connector having male threads on it and attached to the drive rod assembly fits in the aluminium disc and thus the drive rod assembly is coupled to the speaker.

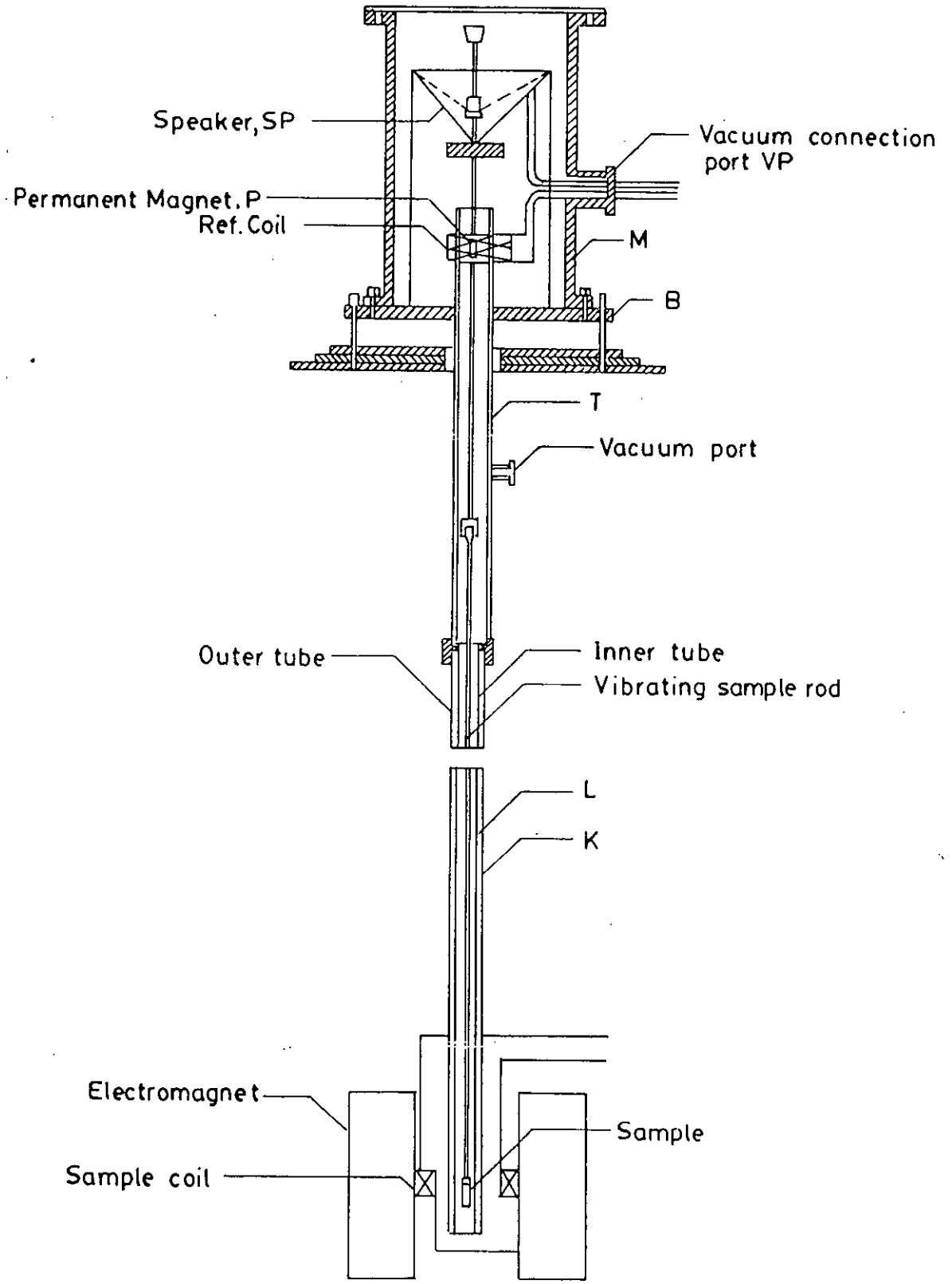

Fig. No 4.9: Mechanical construction of the vibrating sample magnetometer.

The drive rod assembly consists of two detachable parts which are joined together by means of aluminium threaded connectors. Each part is a thin Pyrex glass tubing of 4mm diameter. The upper part has a small permanent magnet P situated 100mm below the aluminium connector attached to it. At the lower end of the drive rod assembly a Perspex sample holder having quite thin wall can be fitted tightly with the sample in it. A few Perspex spears are also attached to the driver rod throughout its length. The spacers guide the vibration of the sample only in the vertical direction and stops sidewise vibration or motion. The total length of the drive rod assembly is 920mm up to base. The lower end of the tube T is joined to a brass extension tube L by a threaded coupling and an O'ring seal. Another thin tube K made of German silver and of 8mm inner diameter runs through the extension tube L from the compiling point C to about 50mm below the sample position. Above the base there is a hollow brass cylinder M of 180mm length and 130mm inner diameter, having 40mm wide collars at its both ends. The lower collar seats on an O'ring seal which is situated in a circular groove in the base plate. On the upper collar, there rests an aluminium top N with an O'ring seal. The brass cylinder M has a side port VP. This is again a brass tube of 41mm diameter and 43mm length. The port has a collar at the end away from the cylinder. A Perspex vacuum feed through is fitted at its end with O'ring seal. This port is connected to the cylinder by soft solder.

The base plate of the V.S.M. rests on three leveling screws above a brass frame which in turn rests on an iron angle bridge. The bridge is rigidly fitted to the side wall of the room. The brass frame is provided with arrangements with the help of which it can be moved in two perpendicular directions in the horizontal plane.

The leveling screws are used to make the drive rod vertical and to put the sample at the center of the pole-gap between the pickup coils. The sample can also be moved up and down by the leveling screws.

4.7.3 Electronic Circuits of the V.S.M.

The function of the associated electronic circuits are:

(i) To permit accurate calibration of the signal output obtained from the detection coils.

(ii) To produce a convenient AC output signal which is directly related to the input and which can be recorded.

(iii) To produce sufficient amplification for high sensitivity operation

The block diagram of the electronic circuit used for the V.S.M. consists of a mechanical vibrator, a sine wave generator, an audio amplifier, a ratio transformer, a phase-shifter, a Lock-in amplifier, a pick-up coil system, a reference coil system and an electromagnet as shown in figure 4.10.

The sample magnetized by the electromagnet generates an emf. in the pick-up coils PC. The strength of this signal is proportional to the magnetization of the sample. The vibrating permanent magnet also generates an emf. of fixed amplitude in the surrounding reference coils. This reference signal is stepped down with the help of a ratio transformer so that its amplitude is equal to that the sample signal. The two signals are then brought in phase and put to the Lock-in amplifier.

The Lock-in amplifier works as a null detector. The ratio transformer reading is to be calibrated using spherical shape sample S of 99.99% pure nickel.

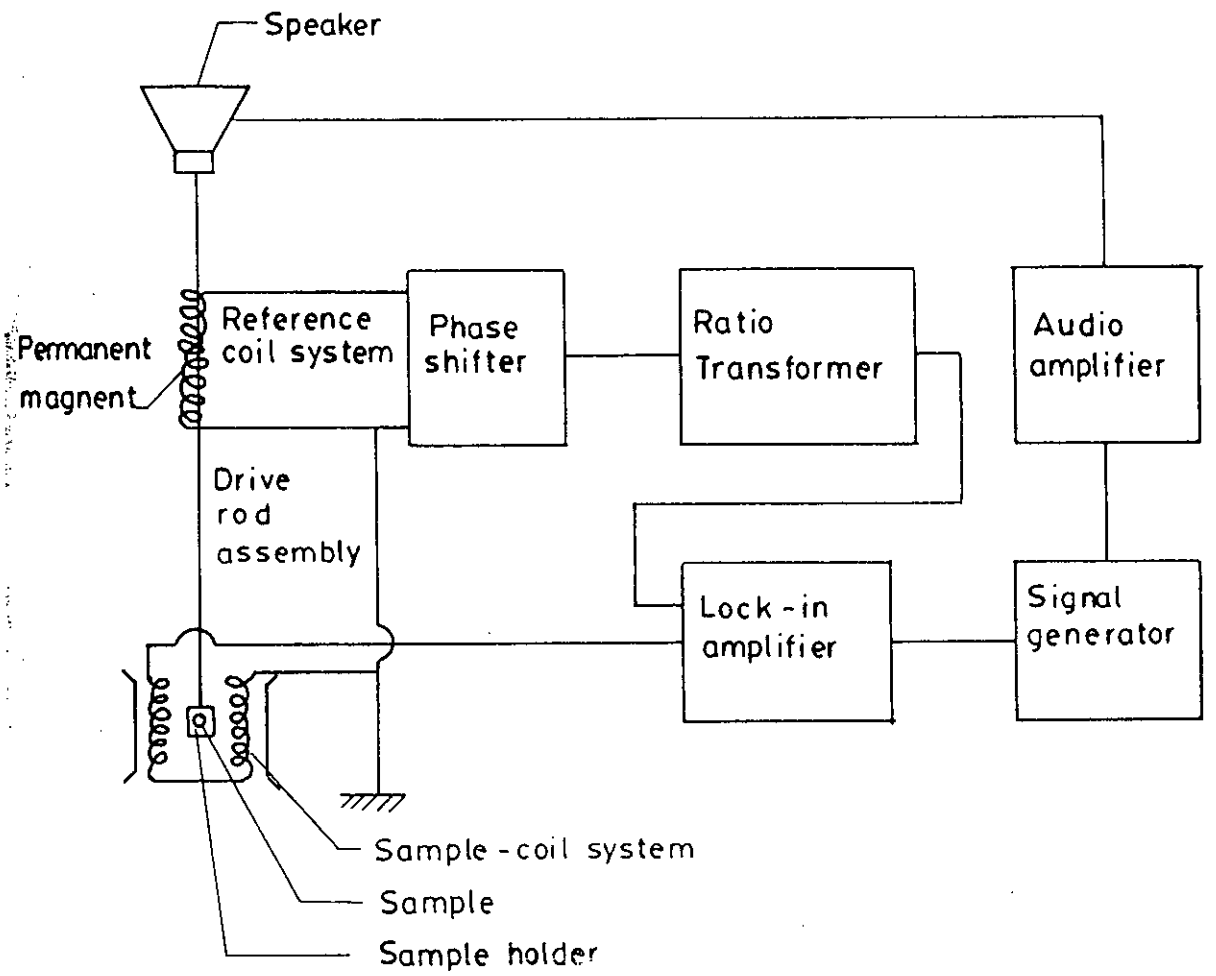

Fig. No 4.10: Schematic diagram of electronic system in the vibrating sample magnetometer.

4.7.3.1 Sensitivity limits

Limits of sensitivity are determined by signal to noise ratio at the input circuit, where noise is defined as any signal not arising from the magnetic moment of the sample. The major sources of noise are the Johnson noise of the wire used for the pick-up coils, and the magnetic responses of the sample holder, which superimposes undesired signals in phase with the wanted signal. Use of a minimum mass of weakly diamagnetic materials for a sample holder, carefully checked to contain no ferromagnetic impurities, is essential to minimize this coherent noise contribution. Corrections for the small magnetic contribution of the sample holder can then be made by measurements with the sample removed. This correction is much less then the equivalent case with a moving coil system.

We used a standard sample for calibration was spherical shaped specimens of mass 0.0584 gm of pure nickel (99.99%). The different field susceptibility $\Delta x \cong 5\times10^{-10}$ could be observed after synchronous phase detection with band width $\cong 2 \times 10^{-2}$ c/s. The other tests used was small current at 81Hz or an alternating current 81Hz passed through the coil which remained stationary.

4.7.3.2 Stability tests differential measurements

With only the Lock-in amplifier and the oscilloscope as a null detector, it was found that the 0.0584gm Ni-sample signal could be balanced reproducibly. Such reproducibility indicated that the long time drifts caused by the combined effects of vibration, amplitude changes and frequency changes a bridge sample position and other effects were negligible. Chosen synchronous phase detector added differential changes about one-tenth the size that could be recorded reproducibly.

4.7.3.3 Vibration amplitude

The pick-to-pick vibration amplitude has been varied from less than 0.1 mm upto 1.0 mm in order to examine errors caused by amplitude changes. Such tests show that the measured magnetic moment varied by less that ±0.5% over these range of amplitude, although at higher variation of amplitudes, because of the larger signals involved.

4.7.3.4 Image effects

Image effects were also examined with a small vibrating coil carrying a dc current. The image effect was no greater than ±1% for fields upto 5KG produced in an air gap of 3.6cm. Undoubtedly, there is an image induced in the magnet poles. It appears, however, that when the sample is vibrated, the effective image vibration is reduced by eddy current shielding.

4.7.3.5 Vibration frequency

The vibration frequency is not critical. High frequency operation is limited by the driving mechanism and capacitive shunting in the detection coils. Frequencies of 100Hz or less permit the use of inexpensive components and minimize eddy current shielding by the vacuum chamber. The measurements are completely independent of eddy currents in the surrounding parts, if measurements and calibration are made at the same temperature. The thickness of conducting parts has been minimized, so that the temperature dependence of penetration depth is less than 1%.

4.7.3.6 Vibration problems

Mechanical coupling between the vibrating system and the fixed detection coils must be avoided. Although the coils are arranged for minimum sensitivity to

external vibration, a noticeable background signal is obtained when the vacuum chamber contacts the detection coils. Such mechanical effects are difficult to eliminate electronically, because the spurious background signal has the same frequency as the sample signal and maintains a constant phase differences with respect to the sample signal. Usually the magnetometer and detection coils are both supported by the magnetic coupling, so that some mechanical coupling may be noticed as highest sensitivity.

4.7.4 Calibration of the V.S.M.

There are usually two methods of calibration of a vibrating sample magnetometer

(i) by using a standard sample and

(ii) by using a coil of small size whose moment can be calculated from the magnitude of the d c current through it.

We have calibrated the V.S.M. using a 0.0584gm spherical sample of 99.99% pure nickel. The sample was made spherical with the help of a sample shaping device. The saturation magnetic moment of the sample has been calculated using the available data. The ratio transformer reading is obtained by actual measurement from the relation

$$M = KK' \qquad 4.9$$

where M is magnetic moment, K' is saturation ratio transformer reading and K is V.S.M. calibration constant. But

$$M = m\sigma \qquad 4.10$$

where σ is the specific magnetization and m is the mass of the sample. From equation (4.9) and equation (4.10) calibration constant is given by

$$K = \frac{m\sigma}{K'} \qquad 4.11$$

The accuracy of this calibration, however, depends on the reliability of the standard nickel sample;the accuracy of the ratio transformer and the gain of amplifier. The equipment has been operated repeatedly with the same standard sample and stability has been found to be within 1 part in 100.

The absolute accuracy of the instrument depends on the knowledge of the magnetic properties of the calibration standard and reproducibility of sample position. When the substitution method of calibration is used, the major error ±1% is introduced by the estimation of standard nickel sample. The relative accuracy of this instrument depends on accurate calibration of the precision resistor divider net work.

The total error here can be kept less than 0.5%. A typical calibration curve of magnetic field Vs ratio transformer reading is shown in figure 4.11.

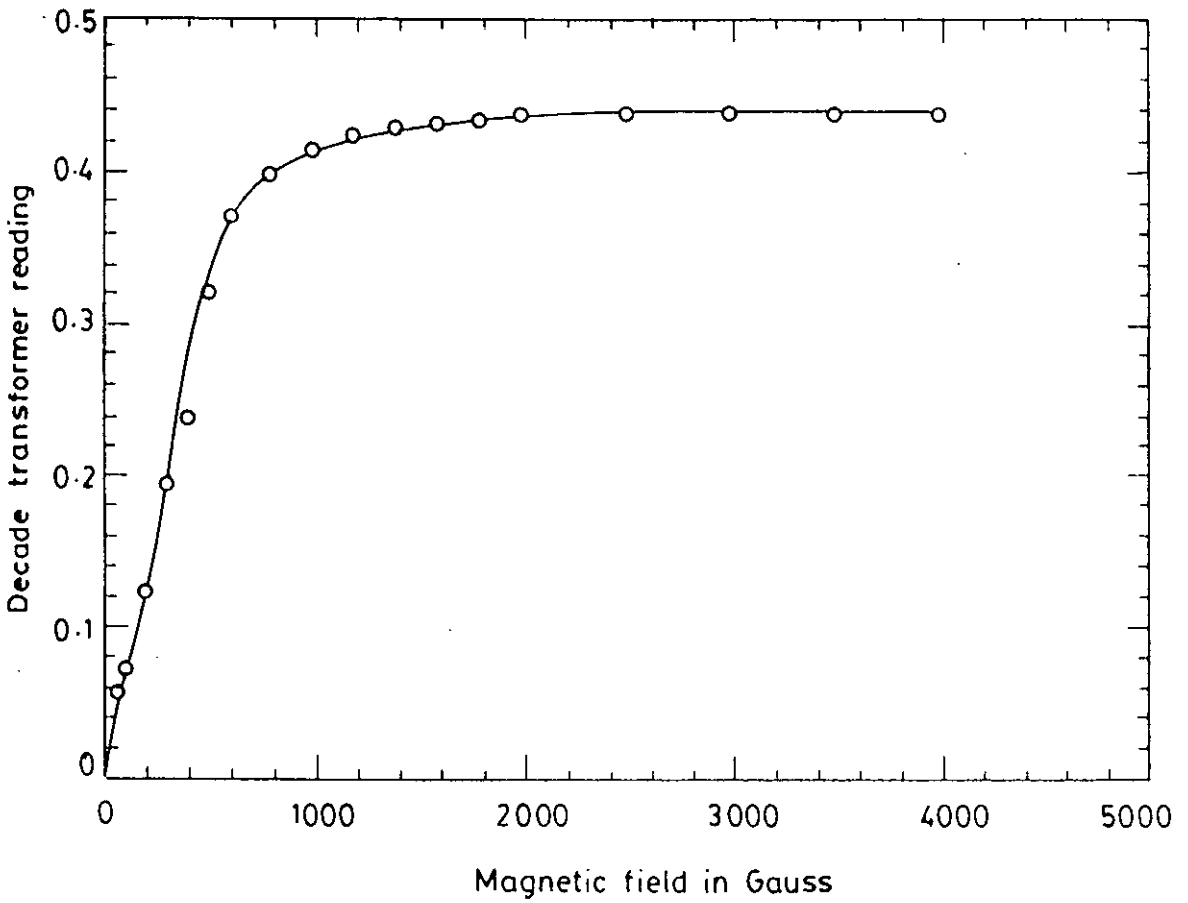

Fig. No 4.11: Calibration curve of magnetic field vs, decade transformer readings (VSM).

4.7.4.1 Calibration Data

(i) Reference signal with phase shifter and decade transformer in connection:

$$V_{erf_1} = \frac{1}{0.01} \times \frac{10\mu V}{20} \times 19$$
$$= 9.5\mu V \times 100 = 0.95mV$$

(ii) Reference signal with decade transformer in connection:

$$V_{erf_2} = \frac{1}{0.01} \times 10\mu V = 1.1mV$$

(iii) Reference signal with direct connection:

$$V_{ref_3} = 13 \times 0.1mV = 1.3mV$$

Saturation decade transformer reading for pure Ni at 20^0C is given as $K^{/} = 0.4386$.

Specific magnetization for pure Ni at 20^0C is given by $\sigma_s = 54.75^{Am^2}/Kg$

Mass of the pure Ni-sample m = 0.0584×10^{-3}Kg

Magnetic moment M = mσ = 3.1975×10^{-3}Am^2

and hence V.S.M. calibration constant is found as

$$K = \frac{m\sigma}{K^{/}} = 7.29 \times 10^{-3} Am^2$$

CHAPTER 5
RESULTS AND DISCUSSION

5.1 XRD
5.2 SEM
5.3 SIMS
5.4.0 Induced Anisotropy Energy (K_u)
5.4.1 Temperature Dependence of K_u
5.4.2 Determination of T_c from (K_u vs. T)
5.5.0 Resistivity Measurements
5.5.1 Temperature Dependence of Resistivity
5.5.2 Determination of T_c from Resistivity Anomaly
5.6 Magnetization (Saturation)

5.1 XRD

The X-ray diffraction pattern of $Ni_{95}co_5$ thin film was taken with very slow angular rotation of 0.004^0 per sec, from 8^0 to 140^0 over nine hours. **Fek$_\alpha$** radiation are used in this case and a hump around 25^0 is observe (figure 5.1a). By analyzing this with the help of a standard computational program I radial distribution function (RDF) verses interatomic distance have been plotted (r) figure 5.1b. From radial distribution function the following information are obtained:

(a) The sample has face centred cubic (fcc) lattice with cobalt atoms replacing nickel atoms.

(b) From the analysis the first peak at 1.4Å is a spurious peak. The second peak at 2.6Å corresponds to nickel-nickel nearest neighbors. and the third peak 3.6Å corresponds to nickel-nickel second nearest neighbors

(c) From figure 5.1(b): cluster size has maximum value of about 10Å

5.2 SEM

The scanning electron micro-graphs of as deposited $Ni_{100-x}Co_x$ thin films of different samples are presented in figure 5.2.1(a) to 5.2.3(d). The micro-graph shows a smooth uniform surfaces and these also show that there are clusters of irregular size and shapes. The cluster size of one of the samples was determined as described in (sec 5.1). The magnification of the micro-graphs ranges from 750 to 4000 and the accelerating voltage was 25 KV. The results show that the films of $Ni_{100-x}Co_x$ are not generally amorphous in nature. The micro-graphs also show that the grain boundaries are irregular in shape, which are haphazardly dispersed across the film surface.

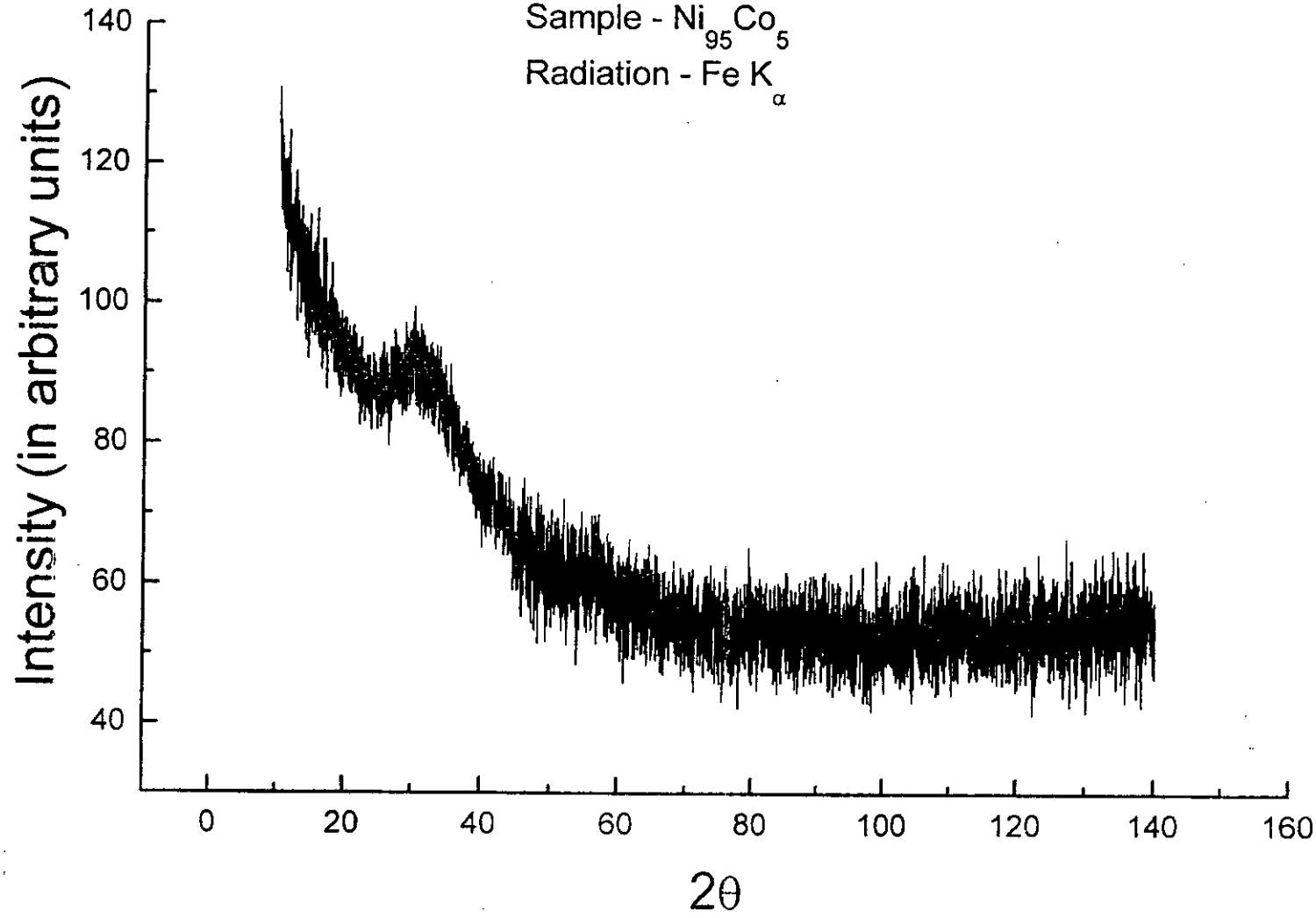

Fig. No 5.1(a): Intensity vs 2θ graph of $Ni_{95}Co_5$ thin film with very slow angular rotation (0.004^0 per sec)

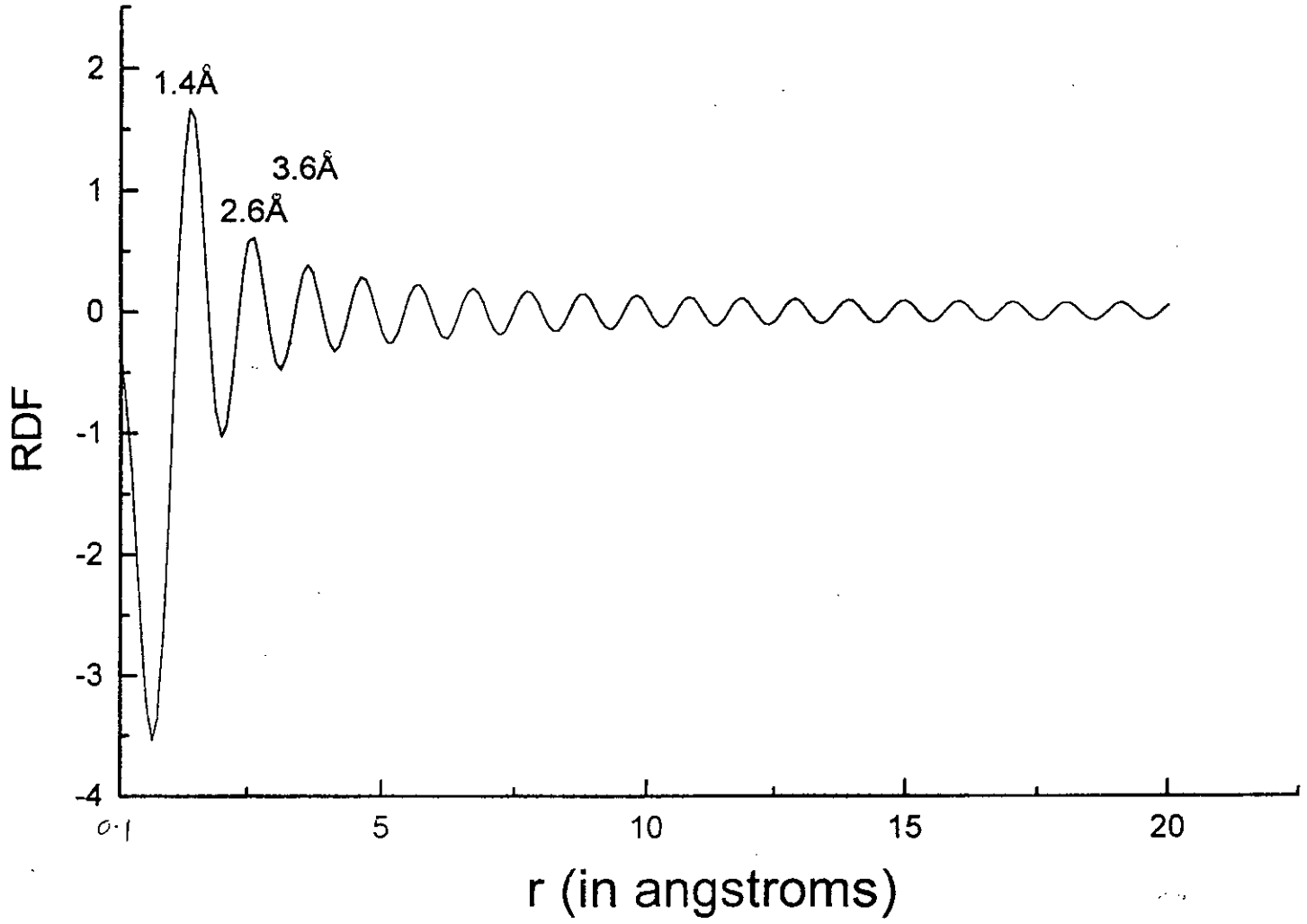

Fig. No 5.1(b): Radial distribution function (RDF) vs, inter-atomic distance (r) in angstroms Å.

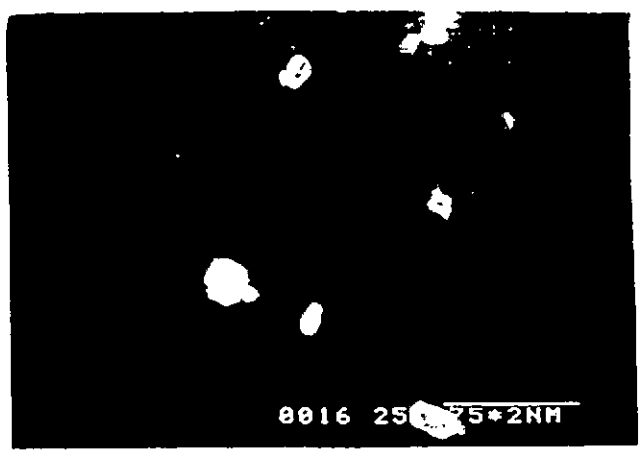

(a) 1000

(b) 2000

(c) 3000

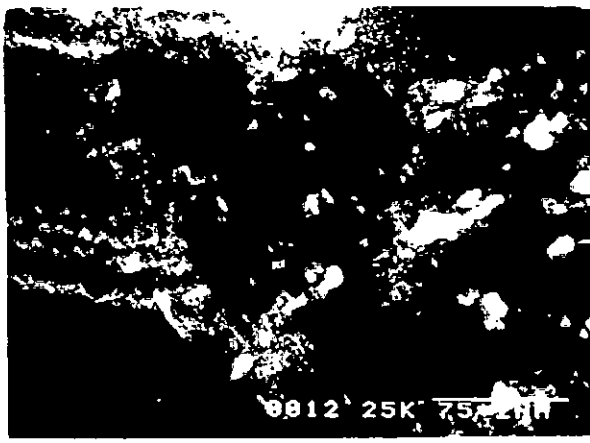

(d) 4000

Fig. No 5.2.1: Scanning electron micro graphs of $Ni_{90}Co_{10}$ at different magnifications (a) 1000, (b) 2000, (c) 3000 and (d) 4000

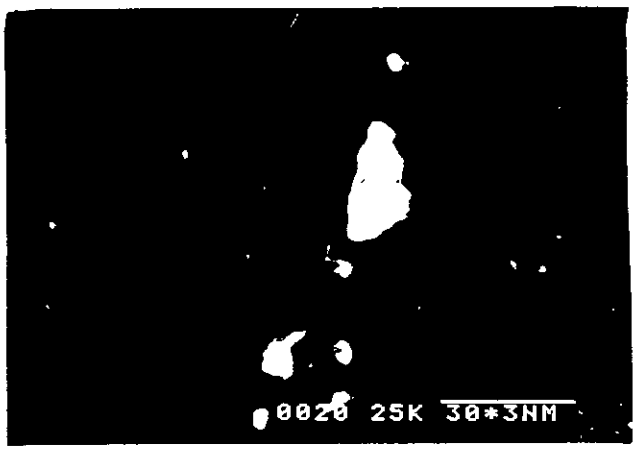

(a) 1000

(b) 2000

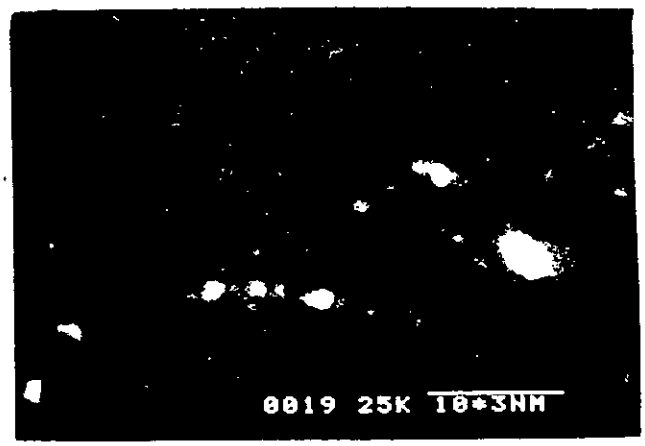

(c) 3000

(d) 4000

Fig. No 5.2.2: Scanning electron micro graphs of $Ni_{85}Co_{15}$ at different magnifications (a) 1000, (b) 2000, (c) 3000 and (d) 4000

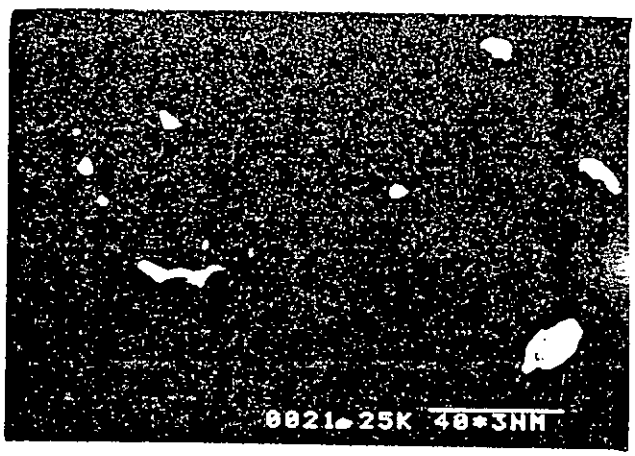

(a) 1000

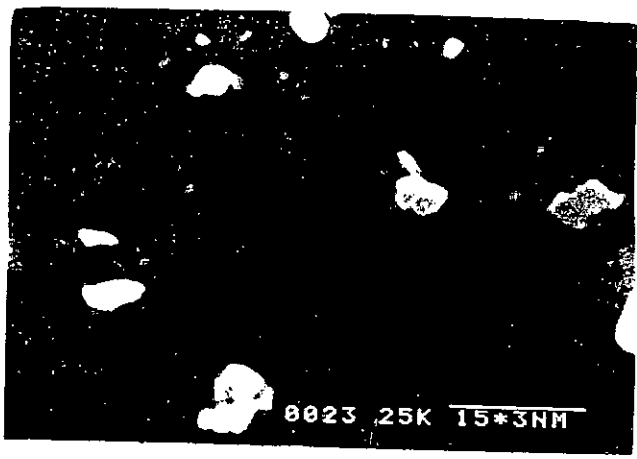

(b) 2000

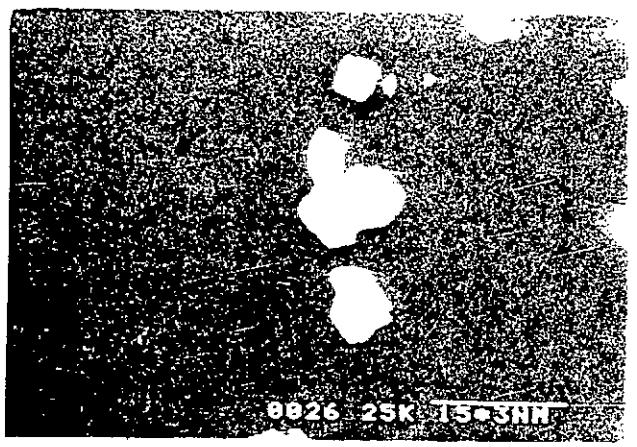

(c) 3000

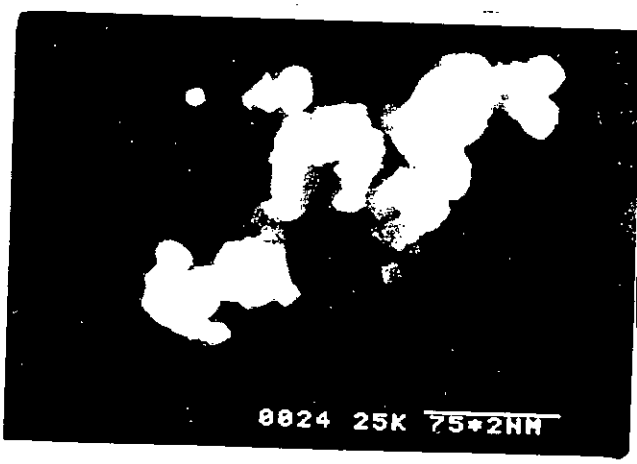

(d) 4000

Fig. No 5.2.3: Scanning electron micro graphs of $Ni_{80}Co_{20}$ at different magnifications (a) 750, (b) 2000, (c) 3000 and (d) 4000

5.3 SIMS

For SIMS analysis, I used the facilities of Surface Physics Division, Saha Institute of Nuclear Physics (SIMP), Kolkata, India. They have installed a high quality SIMS apparatus (Hyden Analytic Limited, UK) for both dynamic and static SIMS application. I have studied one of my sample ($Ni_{95}Co_5$) to observe the composition and surface morphology. The results show that the composition (Ni and Co) looks very much homogeneous over the entire thickness of the film, since the film was grown on glass, there starts a problem with SIMS analysis as soon as I reached the film/substrate interfaces. Glass being a highly insulating material, surface charge buildup occurs during ion bombardment and therefore, secondary ions get distorted to a great extent. Therefore, Ni and Co signals abruptly stopped at the interface. Nevertheless it was evidenced through SIMS that the interface was quite sharp.

5.4.0 Induced Anisotropy

5.4.1 Fourier Analysis of Torque Curve

The measured values of magnetic torque are fed into an IBM 486 PC for Fourier analysis. The Fourier coefficients (A_2 and A_4) are evaluated using a program written MS BASIC language designed specially for the analysis of magnetic torque data[5.1]. The input data are the torque (τ) in volt and the corresponding angle (θ). The analysis also give the offset angle of the magnetic field, which may be adjusted by rotating the magnet through the offset angle to locate the zero torque position. The evaluated Fourier coefficients are the values at the saturation field and are used to calculate anisotropy energy of the sample. This anisotropy energy

is the energy difference between the easy direction of magnetization of the film and the direction perpendicular to that. In other words, this is the anisotropy energy which is developed due to induced magnetic field (M) and other mechanical stress which the film has suffered during deposition. Using the thickness of the sample and the calibration constant (IV = 4.19×10^{-9}J) of the torque magnetometer the anisotropy constants are evaluated.

5.4.2 Stress Induced Anisotropy of Ni-Co Films.

The apparatus used is a standard torque magnetometer which allows continuous registration of the torque as a function of the direction of the field. The laser source provides a coherent light of constant intensity, thus making the system free from light noise. To avoid any spuratic torque due to the image effect in the pole pieces, the specimens were placed in central position. The centre of the sample was made to coincide with the axis of the magnetometer and this is ensured by the exact repetition of the torque value at every 180^0 rotation of the field. Perfectly circular shaped samples were used to provide maximum symmetry about the axis of the rotating field. The films were deposited onto the substrates of perfect circular disc to avoid shape anisotropy and demagnetizing effect. Torque against angle showed perfect reproduction for forward and reverse rotation of the field and for different films of same composition.

The field dependence of the torque versus angle curves were measured for as deposited Ni-Co films with compositions $Ni_{100-x}Co_x$ [x = 5, 10, 15 and 20]. The representative torque versus angle curves with composition $Ni_{95}Co_5$ increases with increasing field as shown in figure 5.4.1(a). This is explained as due to the competing contribution from Ni and Co atoms to anisotropy energy.

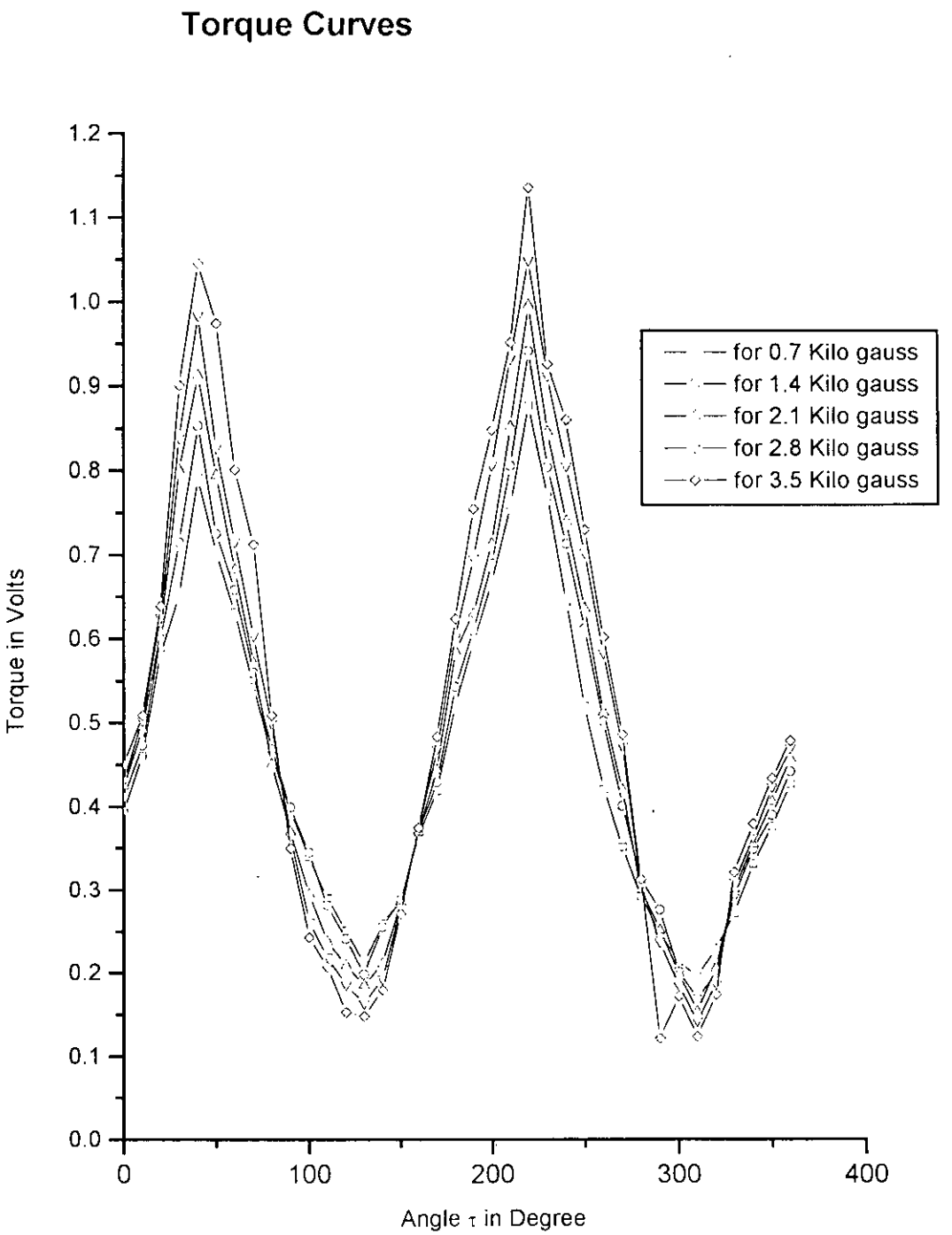

Fig. No. 5.4.1a: Torque curves $Ni_{95}Co_5$ Sample deposited in presnce of field 200 O_e

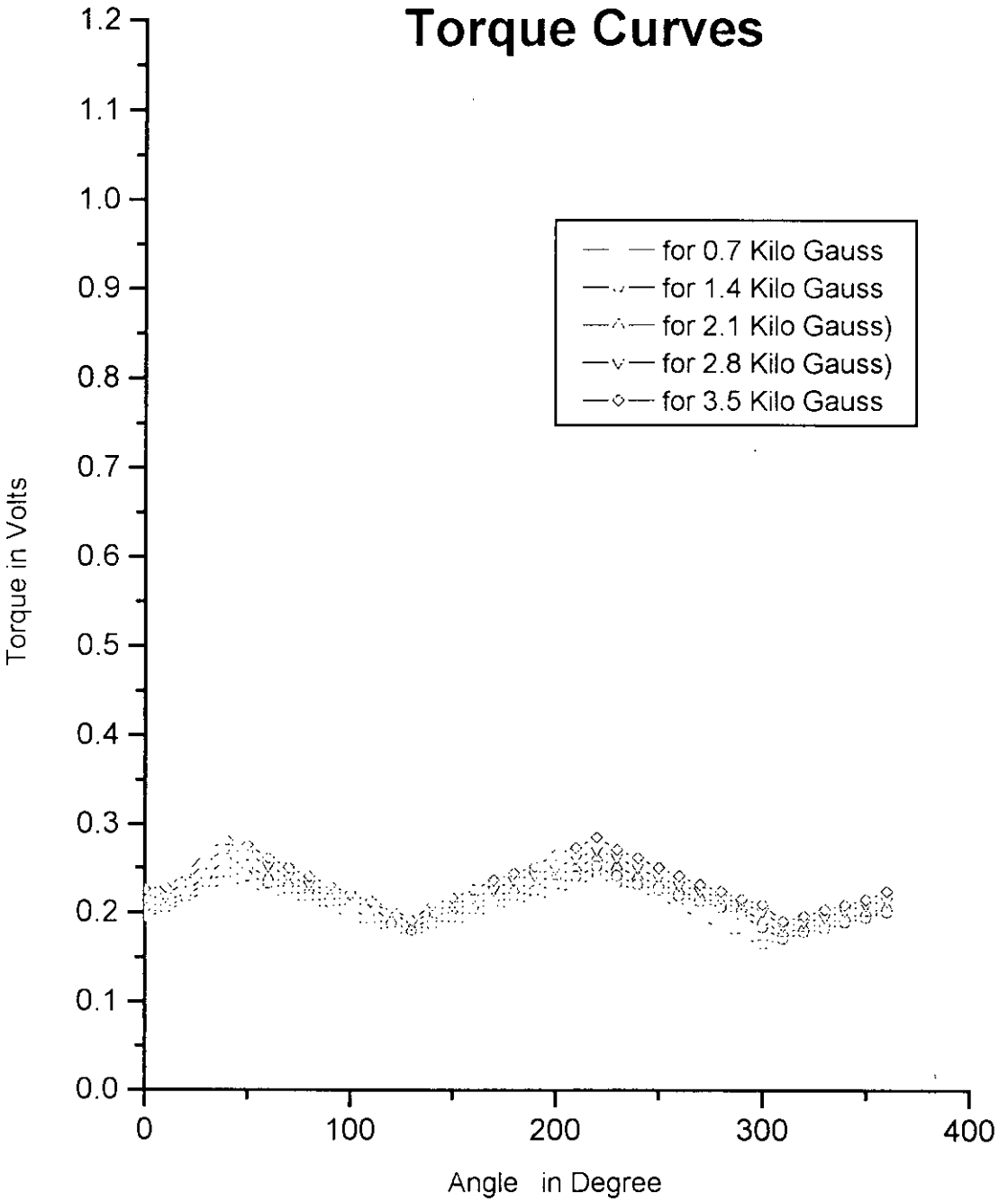

Fig. No 5.4.1b: Torque Curves $Ni_{95}Co_5$ Sample deposited without any external Field.

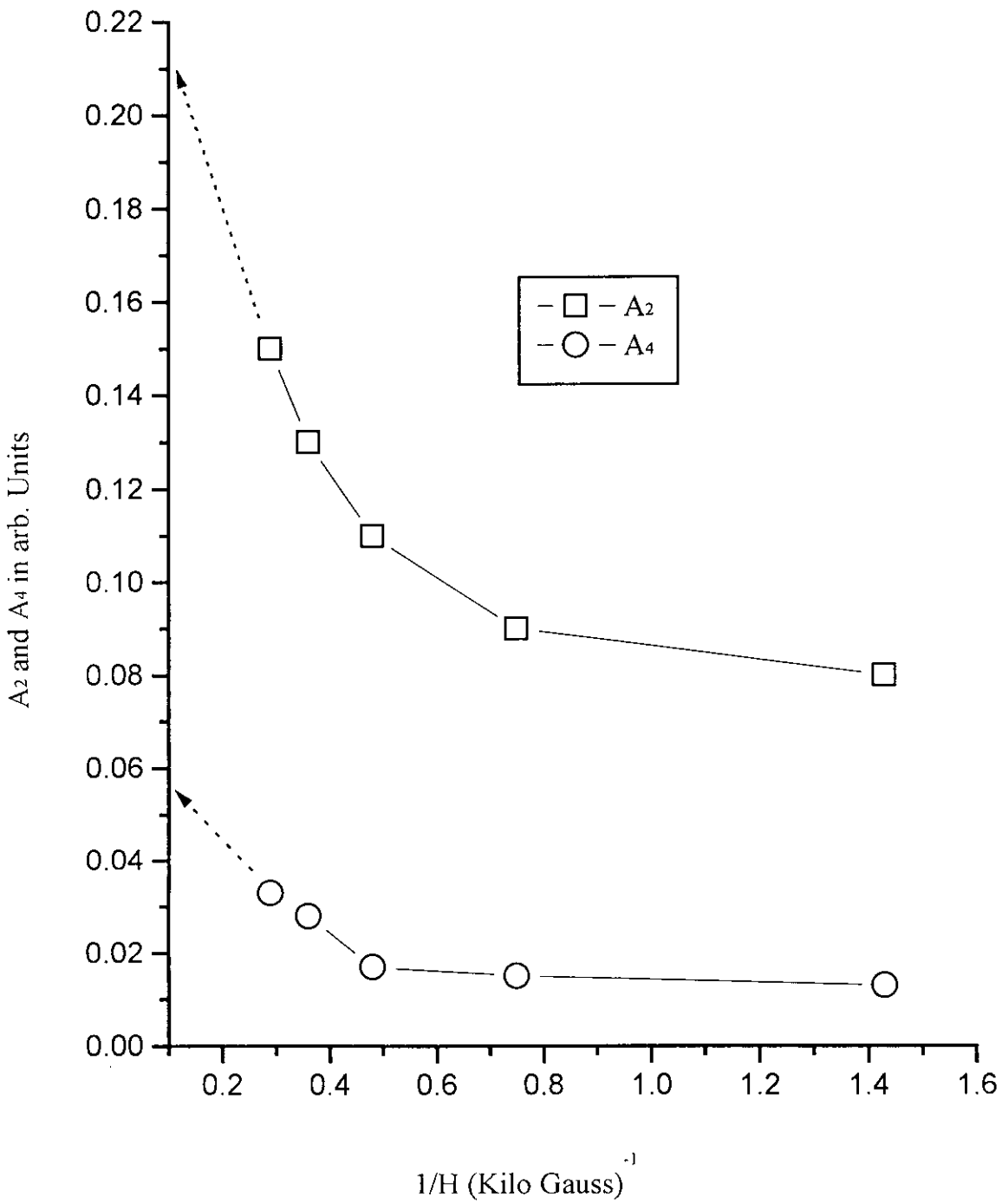

Fig.No. 4.5.2: Fourier co-efficients vs inverse Magnetic Field

We assume that the origin of magnetic anisotropy in these films is due to the presence of external magnetic field during deposition.

Different samples (thin films) of Ni-Co alloy were prepared for different compositions $Ni_{100-x}Co_x$ [x = 5, 10, 15 and 20]. Films were prepared under following conditions: (a) ambient pressure just before evaporation were 2.5×10^{-5} to 8×10^{-6} torr; (b) filament current was 8.5 amp and the filament was a *tungsten* basket; (c) evaporating time was 15 ~ 40 second; (d) measured thickness ranges from 345Å to 1880Å; (e) external field applied during deposition was 500 ***Oe*** along the substrate plane; (f) weight of the sample ranges from 0.00003 ~ 0.00017gm.

During torque measurement we applied maximum field of 4.3 kilo gauss to the sample, but even at this field the samples was not saturated. By plotting A_2 and A_4 with 1/H we got the saturation values of A_2 and A_4 from the extrapolated curves (figure 5.4.2). Two fold nature of the induced anisotropy is clear from the torque curves. We had also studied a sample ($Ni_{95}Co_5$) which was deposited without external field. It showed torque curves but its amplitude was insignificant (figure 5.4.1b). The induced anisotropy observed for the films that were deposited without field, is quite in keeping with the results of Gerahman[5.2] and Broeder[5.3], where the anisotropy arises because of oblique incidence of the evaporent atoms.

We are mostly interested in the field induced anisotropy. The induced uniaxial anisotropy however increase when the samples (thin films) are deposited in the presence of an external magnetic field. The field dependent anisotropy energy has been calculated for the four samples with composition $Ni_{80}Co_{20}$, $Ni_{85}Co_{15}$, $Ni_{90}Co_{10}$ and $Ni_{95}Co_5$, that were deposited in presence of 500 O_e field. We have

represented these samples as S_1, S_2, S_3 and S_4 respectively throughout this section. We have also deposited S_4 in the absence of any external magnetic field and calculated the anisotropy energy at room temperature. The torque curves were analyzed by using Fourier technique with evaluating the Fourier coefficient with the help of special computer program. The values of the anisotropy constant were determined by using the calibration constant of the torque magnetometer and the known mass of the sample. The anisotropy energy for both field induced and for no field are 559 J/m^3 and 58 J/m^3 respectively at room temperature. This result is most interesting in the sense that the magnitude and direction of the induced anisotropy can be controlled by manipulating the strength of the applied field and the direction of the field during deposition. The behavior of the induced anisotropy due to the presence of external magnetic field during sample preparation can be explained as follows: the external field orients the magnetic atoms during their flight through the magnetic field before they are condensed onto the substrate. The preferred orientation produce the induced anisotropy with reference to the direction of the applied magnetic field. Since the sample is not a perfect crystal, it is not possible to explain quantitatively the temperature dependence of induced anisotropy. However, a qualitative understanding of the temperature dependence of the induced anisotropy, where the anisotropy energy decreases with increase in temperature can be understood by considering the Zener[5.4] pair model. The temperature dependence anisotropy energy observed for our four samples are depicted in the tables (appendix-5.4.3a~3.d) respectively. The results are shown in figure 5.4.3 (a) to 5.4.3(d) respectively. Here it is assumed that the spins forming the pairs remain parallel, but the pairs axes are subjected to increased deviation form the magnetization direction with increasing temperature due to thermal agitation. The anisotropy energy is given by the average value of all the individual pairs of atoms.

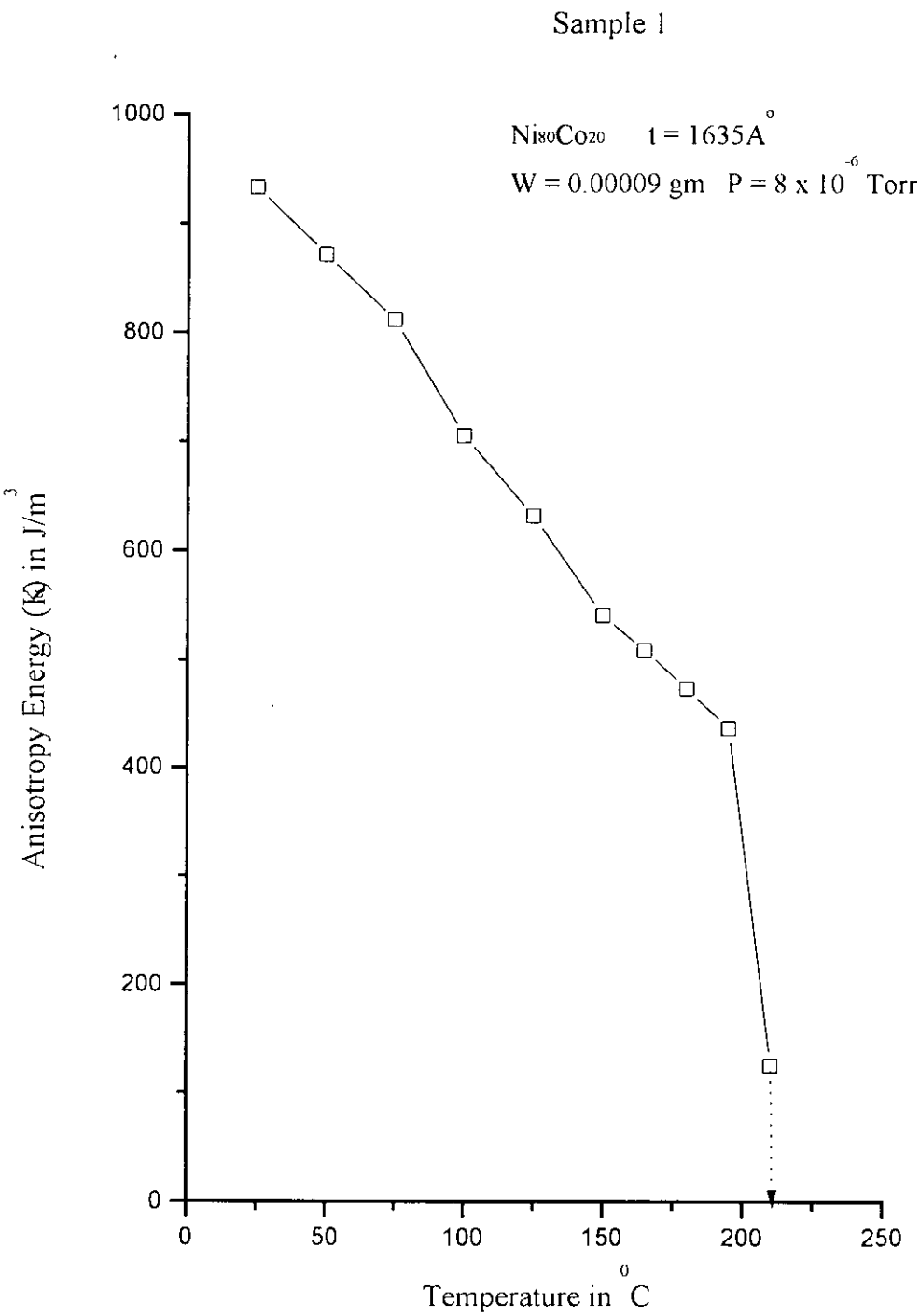

Fig. 5.4.3a: Temperature dependence in K_u

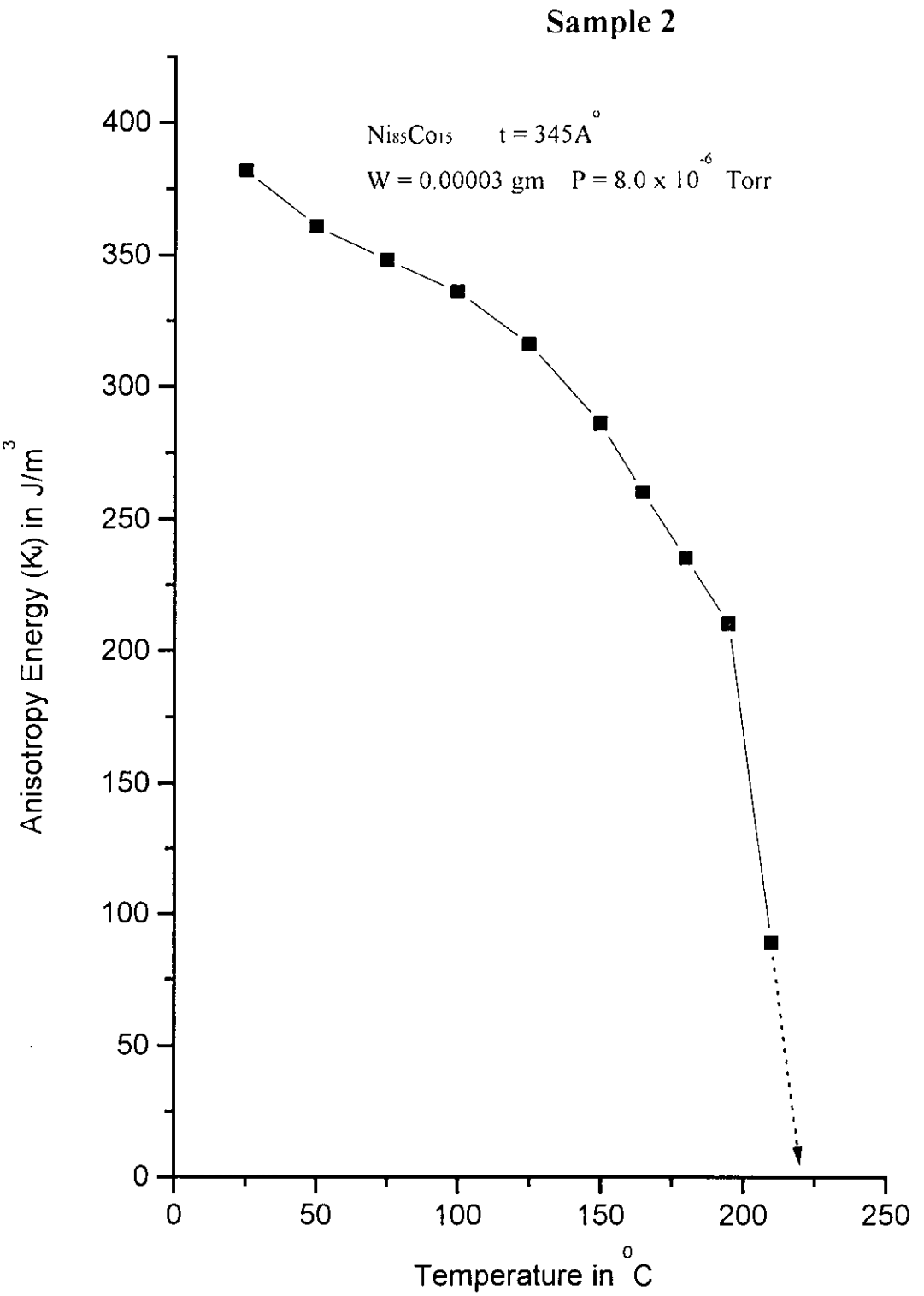

Fig. 5.4.3b: Temperature dependence in K_u

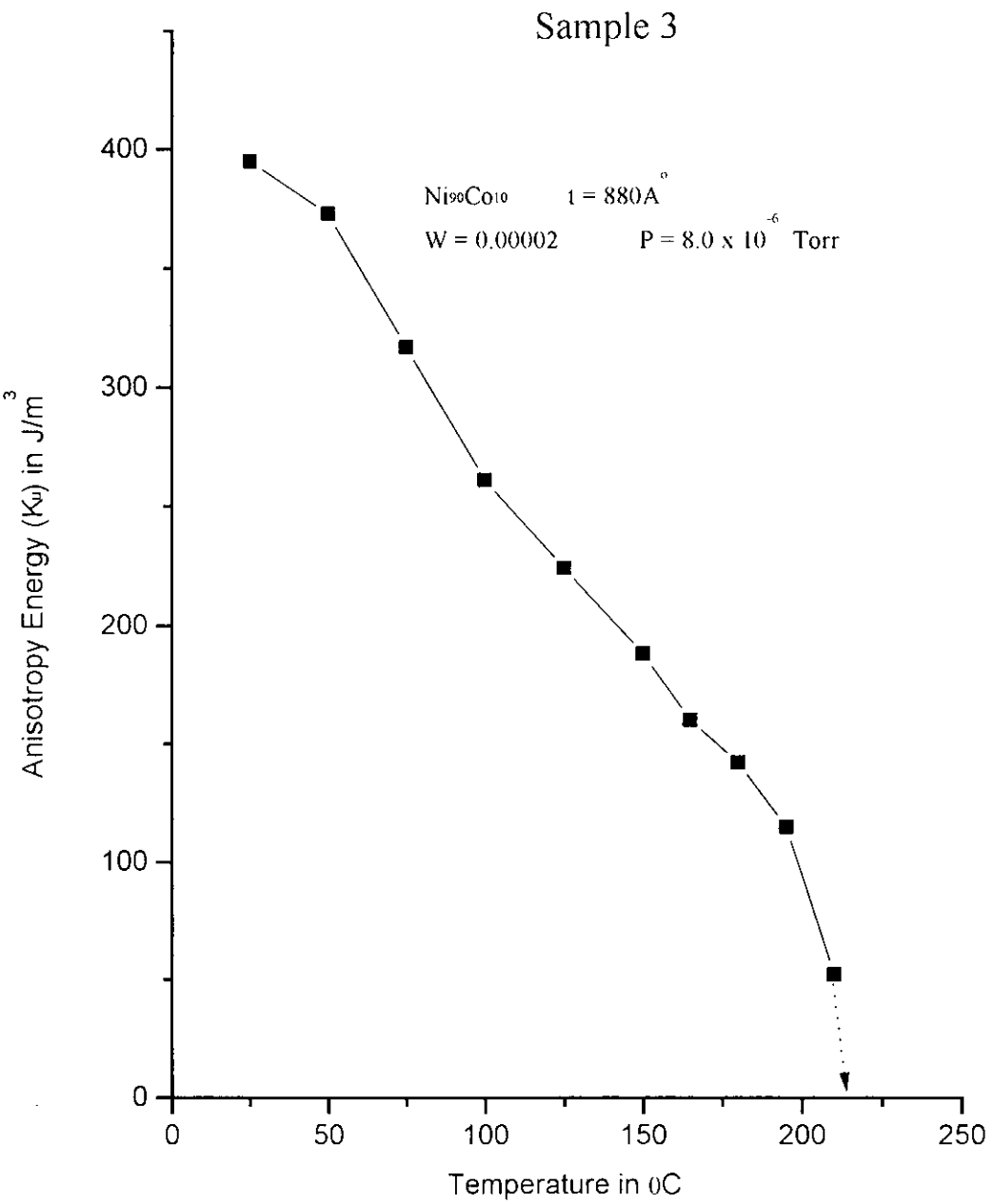

Fig. 5.4.3c: Temperature dependence of K_u

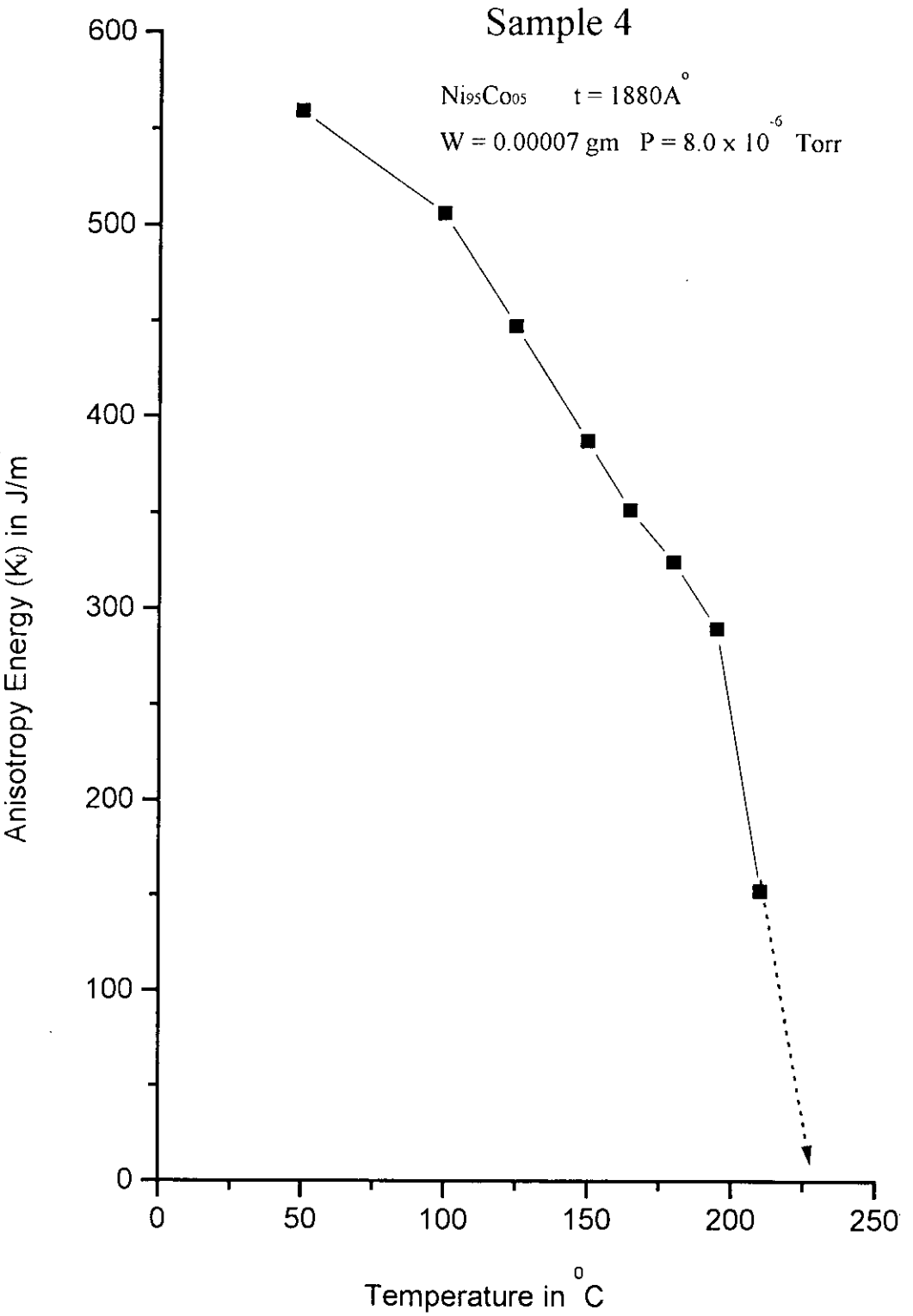

Fig. 5.4.3d: Temperature dependence of K_u

The anisotropy constants are affected by the average value of all the possible orientation of the spin pairs. The process becomes more complicated due to thermal expansion of the sample at elevated temperature as suggested by Carr[5.5].

It is observed that the value of the induced anisotropy energy in the case of thin magnetic films is much less than that corresponding to the bulk materials which decreases with temperature and tends to become zero. By extrapolating the curves $K_u \sim T$ of the samples we can attain a point where K_u - 0, and these gives the transition temperature (T_c) of the samples. For pure nickel $T_c = 358^0$C and Cobalt $T_c = 1145^0$C for the bulk samples. Whereas for thin films of our samples this value ranges from 210^0C to 230^0C depends on composition and thickness, which is less than that of bulk values.

5.4.3: Temperature Dependence of K_u

It is observed that the anisotropy energy K_u depends on composition. The temperature dependence of anisotropy constants of thin films of $Ni_{100-x}Co_x$ [x = 5, 10, 15, 20] are shown in figure 5.4.3a ~ 5.4.3d. There is almost monotonous decrease of anisotropy energy with increase of temperature, figure 5.4.3a ~ 5.4.3d. The figures also shows that K_u monotonously linearly with rise of temperature but this monotonously in change is effective upto a certain value. By extrapolating this linear curves we obtained the ferromagnetic transition temperature (T_c). For different composition of the samples we obtain the phase transition temperature which ranges $210^0 \sim 230^0$C.

Although these results are of interesting from a practical view-point they are difficult to interpret quantitatively in terms of directional order theory because of

the uncertainty as to whether equilibrium was achieved at any temperature. Directional order theory predicts decrease in K_u with increase temperature and vanishes at Curie temperature. We have extrapolated K_u to zero value to calculate T_c as shown in figure 5.4.3a ~ 5.4.3d. The results are consistent with the values of T_c as estimated the resistance anomaly in the temperature dependence of resistivity (ρ) (sec. 5.5.3). The anisotropy constants K_u calculated in J/m^3 for different samples and different temperature shown in Table (5.4.3a - 5.4.3d).

5.5.0 Transport Properties

5.5.1 Resistivity measurements

We prepared different samples of different composition i.e. $Ni_{100-x}Co_x$ [x = 5, 10, 15 and 20] for resistivity measurements. The shape of the samples was square and the size of the samples were (1 cm^2 each). After lead attachment at the four corners, the samples were placed on an electric heater which was placed below the substrate holder in the vacuum chamber. The as deposited films were placed on the heater with clips. A thermocouple (chromel-alumel) was placed on the glass substrate. A variable d.c. supply and a digital multi-meter were connected to the screws, that are connected to the four corners of the sample (film). After pumping down, the pressure inside the chamber was of the order of 10^{-5} torr, the temperature was then increased slowly upto 250^0C (for two hours) in steps of 20^0C. At every step (V_D-V_C), (V_A-V_D), (V_B-V_A), (V_C-V_B), I_{AB}, I_{BC}, I_{CD}, and I_{DA} readings were taken carefully, as described in sec. 4.6.2.

After reaching 250^0C, the temperature of the film was kept constant (three hours). The sample was then cooled slowly. After cooling the experiment was repeated. It is observed that annealed samples have lower resistivity compared to that of as

deposited films. This gave only a qualitative information about the effect of annealing.

5.5.2 Temperature dependence of Resistivity

The electrical resistivity was measured as a function of temperature (30^0~250^0C). The curves for the different samples having different composition Ni_{100-x} Co_x and of different thickness are shown in figure 5.5.2a ~ 2d.

It is observed that the resistivity increases with rise of temperature indicating normal metallic behavior. However, it is an interesting findings that the resistivity increase is not linear over the whole temperature range. From figure 5.5.2a ~ 2d it is observed that there is an anomaly in the resistivity vs temperature curves at a particular temperature and this point varies from sample to sample depending on their thickness and composition. The curves shown in figure 5.5.2a ~2d indicates the transition temperature which varies from 170^0C to 200^0C. This anomaly is attributed to the ferromagnetic to the paramagnetic transition. This result is explained by the fact that in the ferromagnetic phase the electrons are magnetically coupled by exchange interaction and thus don't contribute to the electrical conduction process. The critical temperature at which the electrons, whose spins were ordered below the Curie temperature (T_c), become thermally disordered and an anomaly in electrical resistivity results. Above T_c, the film become paramagnetic and resistivity decreases.

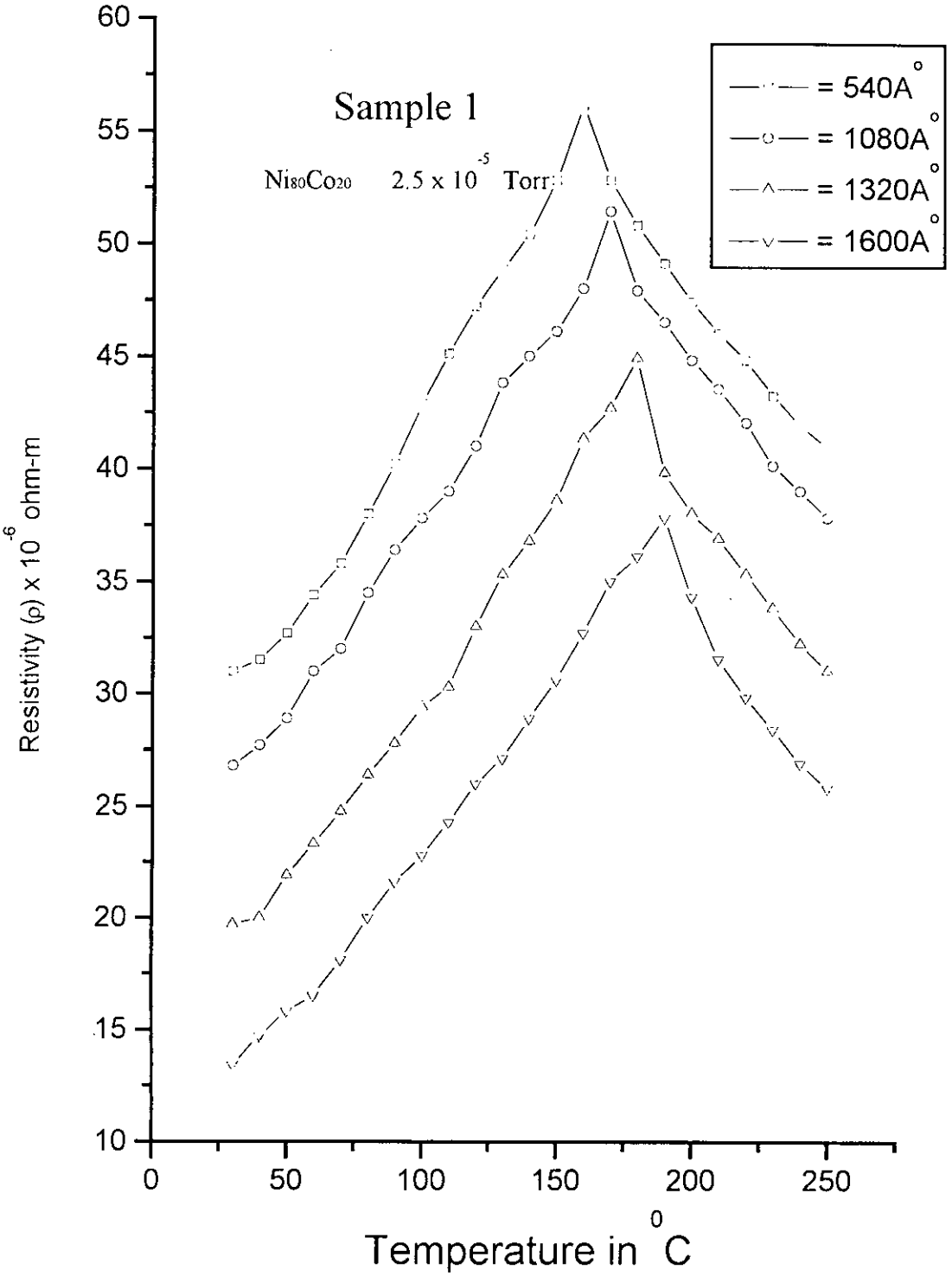

Fig. 5.5.2a: Variation of resistivity with temperature for different thickness

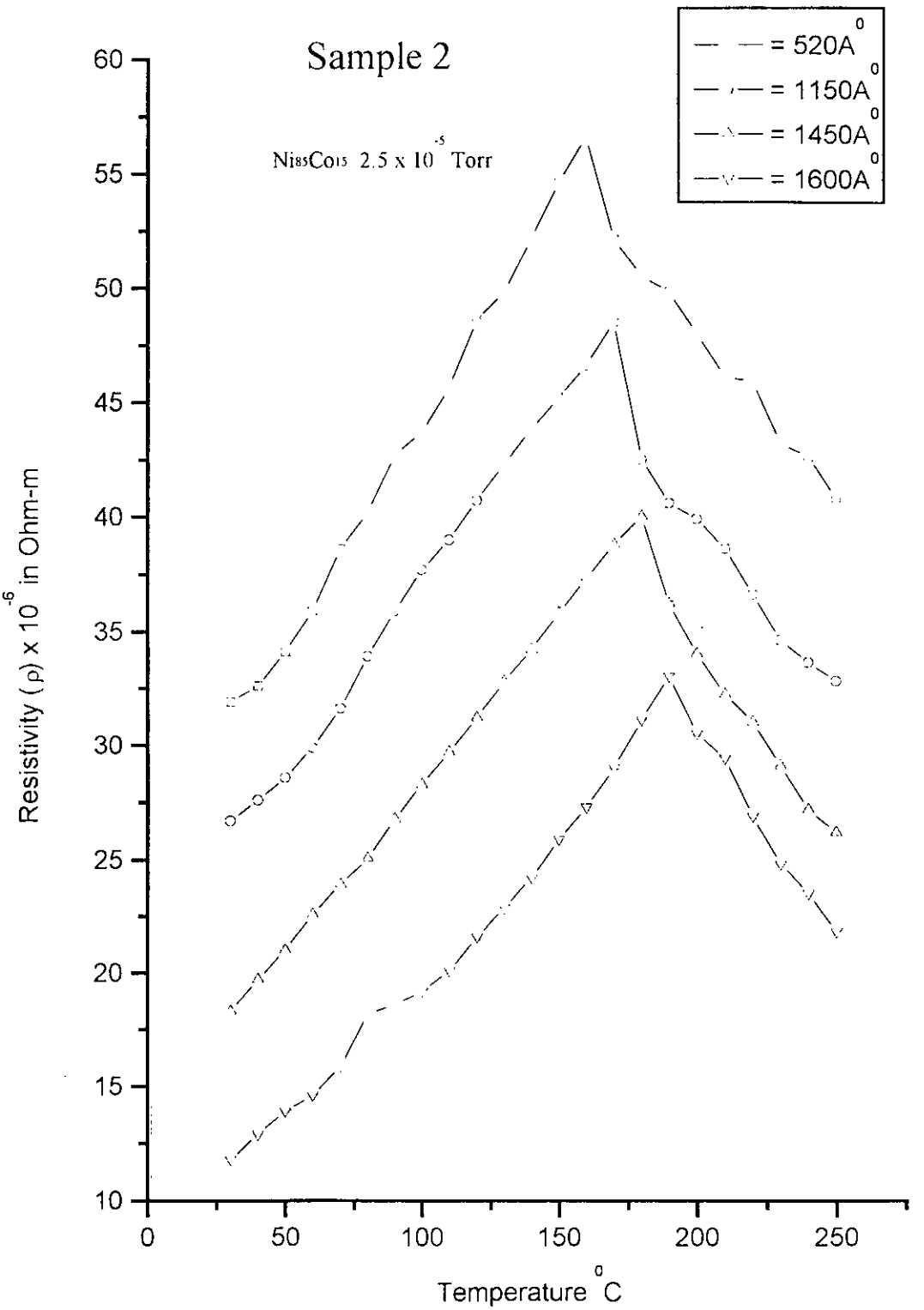

Fig. 5.5.2b: Variation of resistivity with temperature for different thickness

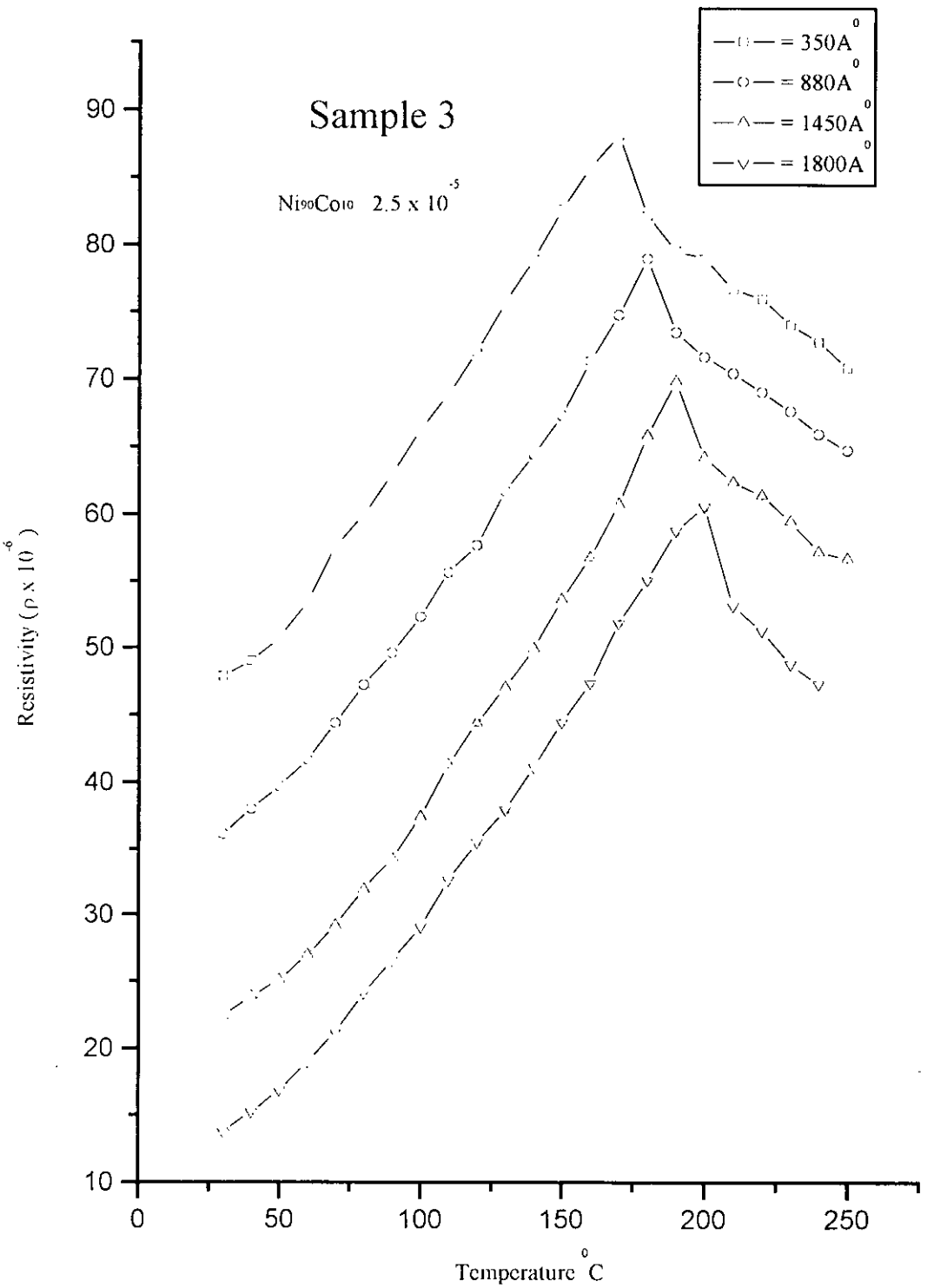

Fig. 5.5.2c: Variation of Resistivity with temperature for different thickness

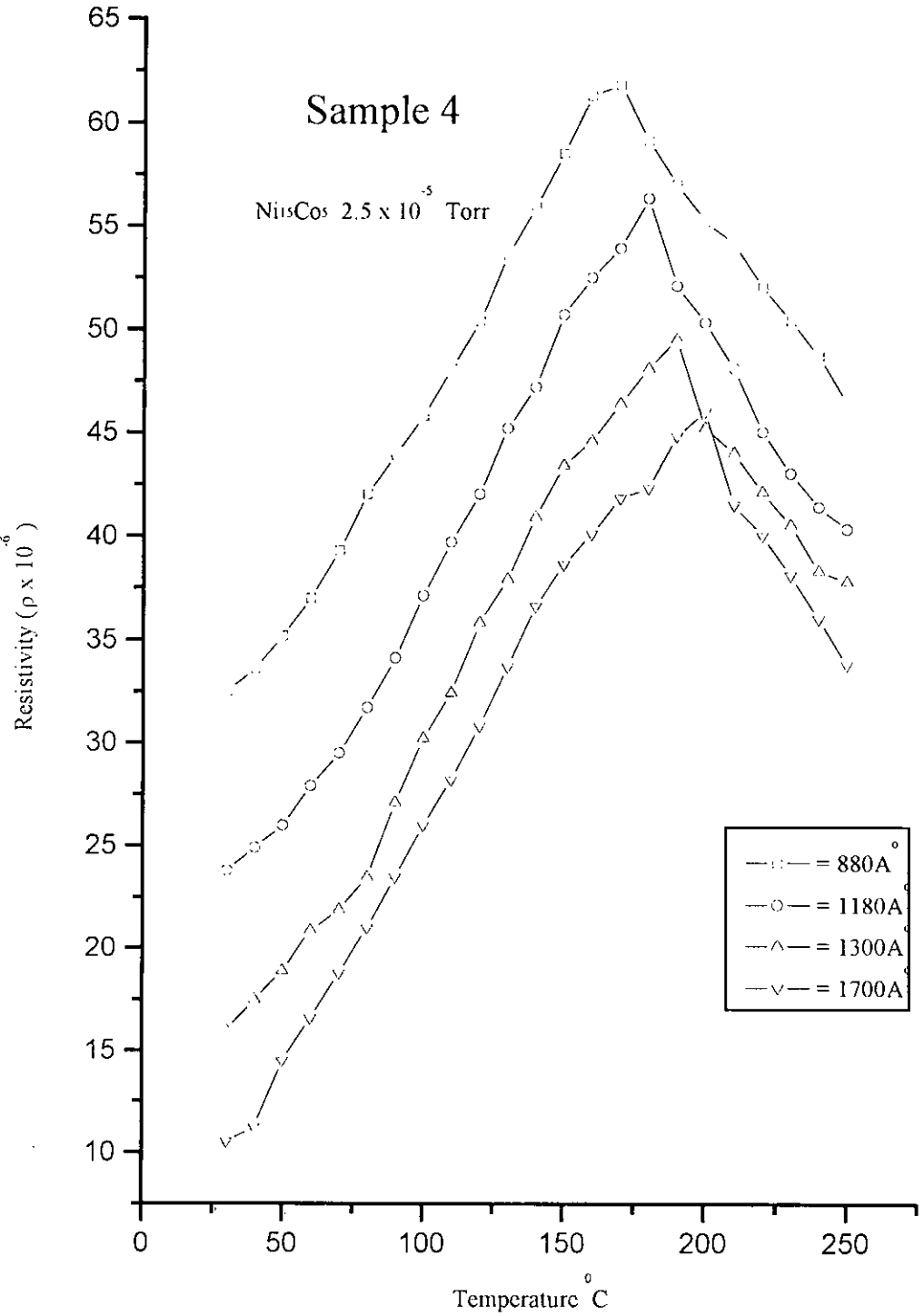

Fig. 5.5.2d: Variation of resistivity with temperature for different thickness

5.6 Specific Magnetization Measurements

The magnetization of Ni-Co thin films is measured as a function of magnetic field using a VSM[4.20]. The films were deposited onto quartz substrate of circular shape of 5 mm in diameter. Before deposition the substrate were weighed on a high sensitive electronic balance (10^{-5}) and after deposition the film was again weighed with substrate. Hence the weigh of the films were determined. Out of our four samples only one sample was of mass 10^{-4} gm and others were less than it (10^{-5} gm). The VSM used has sensitivity of magnetic moment is 5×10^{-4} e.m.u. only. Thus with this VSM we could measure only the sample $Ni_{95}Co_5$ which has thickness 1134 Å and weighed 0.00084 gm. The sample was glued to the sample holder and was mounted with the film in the outside. The magnetometer was used as a field measuring device which was not affected by the presence of sample for its low susceptibility. The lock-in action of VSM yields an accuracy of 0.05%. For the full scale the absolute accuracy of the system is better than 2%, and reproducibility is better than 1%. The proportionality constant accounting for the particular coil geometry and susceptibility is obtained by calibration with a high purity circular disc shaped nickel sample. The sample has a saturation moment of 54.75emu/gm with a saturation flux of about 4 kilo-gauss. A relative accuracy of about 1% is obtained with the double coils; the absolute accuracy depends on the alibration method.

5.6.1 Specific Magnetization at room Temperature

The specific magnetization of the sample of composition $Ni_{95}Co_5$ as deposited thin films of thickness 1134 Å and weight 0.00084 gm is measured, using a VSM

(AECD, Dhaka, Centre). The magnetization process of the sample of different field is shown in figure 5.6.1. The value of saturation magnetization of the film is 92.84 e.m.u/gm. We know that the saturation magnetization of nickel is 54.39 e.m.u./gm and that of cobalt is 161.0 e.m.u./gm at room temperature.

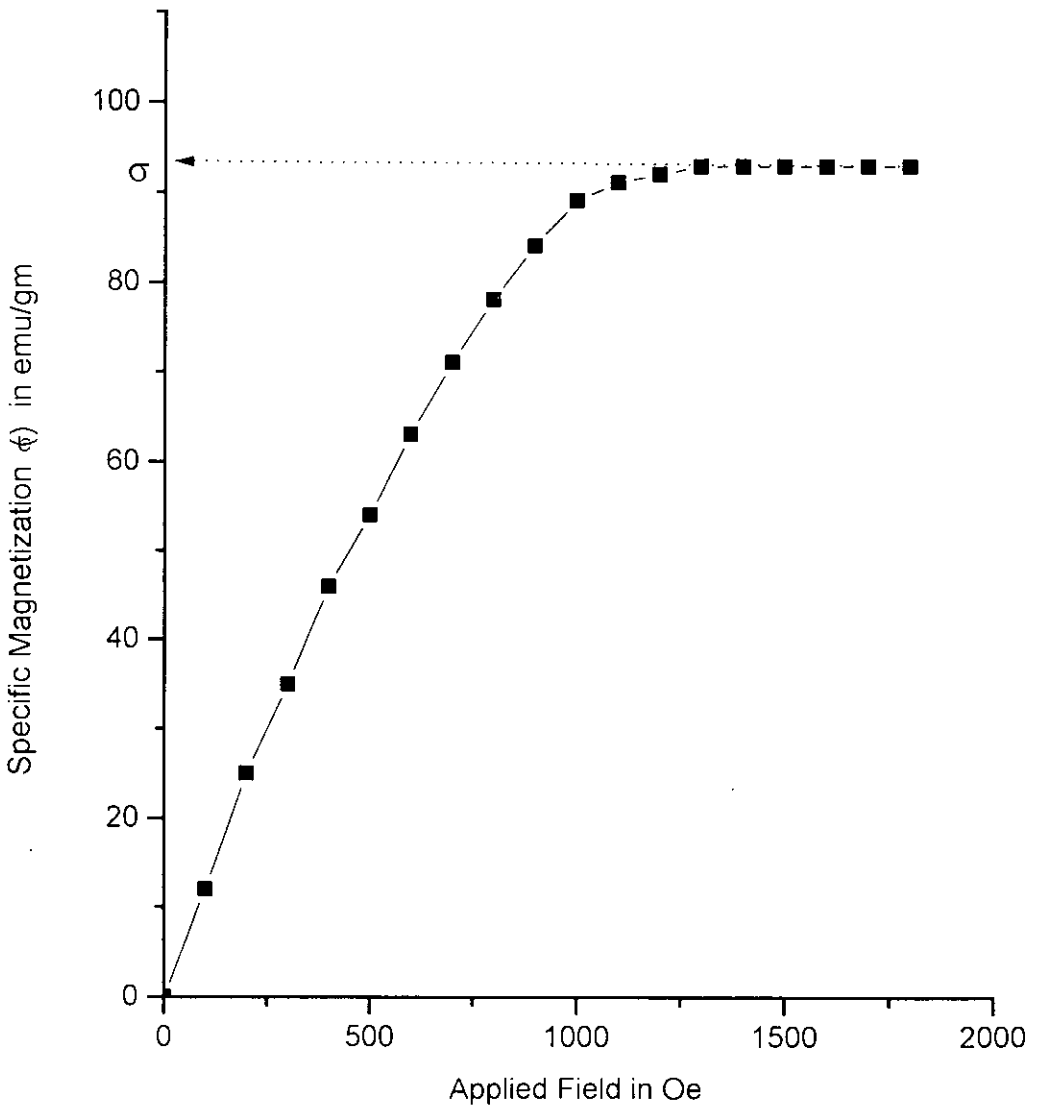

Fig. 5.6.1: Sp. magnetization vs magnetic field of thin film with composition $Ni_{95}Co_5$

CONCLUSION

Conclusion

The study of magnetic thin films is of enormous importance both for theoretical interest and for potential technological applications. Since thin films manifest their magnetic characteristics that are very susceptible to the conditions under which the samples are prepared, the preparation of the samples and their characterizations are very important. The present work thus involves the very careful preparation of magnetic thin films under high vacuum where the composition, thickness and external environment were varied. The choice of substrate, the order of the vacuum, heating current, the angle of incidence, the distance between the source and the substrate, the time span during which evaporation takes place are all very important in determining the cluster size and the nature of the arrangement of atoms within the cluster. In the special case, where an external filed is used for induce anisotropy the strength and direction of applied field is also very important. Since so many parameters are involved and there is no quantitative theoretical guidelines for the preparation of thin films, one has to take recourse to the trial and error method using some qualitative thumb rule. The preparation of the samples, therefore, is a very long drawn process and the characterization of the specimens is equally difficult and involved. We therefore used various techniques like X-ray diffraction with a very slow angular velocity which took nine hours to scan the specimen from 8^0 to 140^0. The cluster size and the crystal structure were determined by using a computer program. Scanning electron microscope is also used as a complementary technique for the same purpose. Secondary ion mass spectroscopy is used for the study of composition and homogeneity of the samples. Two of the most important magnetic characteristics of thin films

related to the theoretical understanding of magnetic ordering and technological applications are Curie temperature and magnetic anisotropy for their dependence on thickness. The theoretical controversy as to whether two dimensional lattice can be ferromagnetic cannot be sorted out in a straight forward way. Our main task, therefore, has been to find an experimental answer to this important question.

It is not possible to produce a perfect two dimensional crystal of magnetic atoms, we therefore, followed the method of approaching a two dimensional lattice by gradually reducing the thickness and looked for the dependence of Curie temperature on thickness. Although the most straight forward method would be to measure magnetization as a function of temperature to determine the magnetic phase transitions, the available magnetometers are not sensitive enough to provide such information. We, therefore, followed an alternative method of determining the Curie temperature by looking for the possible magnetic phase transition accompanied by an associated resistivity anomaly. Because the electrons which are coupled by the exchange force in the ferromagnetic state can become free in the paramagnetic state, thus showing a sudden increase in the electrical conductivity. Thin films, fortunately are convenient for this method because of their higher sheet resistance. The other method used for determining the Curie temperature was the measurement of the temperature dependence of magnetic anisotropy by torque magnetometry. The results show that the Curie temperature of magnetic thin films goes down with decreasing thickness and, within experimental error the two above mentioned methods provide consistent results. It is, therefore, concluded that in the limit of monolayer lattice, the

Curie temperature will tend to become zero, thus failing to support ferromagnetic ordering.

Although thick samples could only be studied for its magnetization by our VSM, a development of highly sensitive magnetometer with an accurately controlled oven will provide more convincing data in respect of the present observations. There is also scope for improvements in the preparation and characterization of thin films with wider variation of composition and with multilayers for more detailed study of the mechanism involved in magnetic ordering for low dimensional materials.

REFERENCES

References

Chapter - 1

1.1 "Thin Ferromagnetic films" M. J. Klain and P. S. Smith, Phys, Rev., **109**, 288 (1958)

1.2. "Magnetic thin films" Ronald F. Soohoo Harper and Row, New York 1965.

1.3. "Preparation and Magnetic anisotropy of continuous single crystal Ni-films", J. C. Anderson, 1961 Trans. 8th vacuum symposium and 2nd int. congress, Programme T press, New York, 1962, p-930.

1.4. "The Influence of Crucible Material upon the Magnetic Anisotropy of Evaporated Permalloy Films", P. Astood and M. Prutton, Brit, J. Appl. Phys **14**, 48 (1963).

1.5. "Influence of Deposition Conditions on Growth and Structure of Evaporated Films" K. H. Behrndth, Vacuum, **13**, 337 (1963).

1.6. "Remarks on the Theory of Magnetic Properties of Thin Films and Fine Particles" L. Neel, J. Phys, Radium, **17**, 250 (1956).

1.7. Micro-magetic Prediction for Magnetization Reversal in Co Ni Films". R.H. Victoria J. Appl. Phys. **62(10)**, 4220~5 (1987).

1.8. "Preparation of Thin Magnetic Films and their properties". M. S. Blois. Jr. J. Appl. Phys **26**, 975 (1955).

1.9. "Nanosecond Switching in Thin Magnetic Films" W. Dietrich and W. E. Probster, J. Appl. Phys **14**, 439 (1963).

1.10. "Effect of surface anisotropy on the spontaneous Magnetization of ferro-magnetic Thin Films". T. Ayukawa, J. Phys. Soc, Japan, **18**, 970 (1963).

1.11. "Static and Dynamic behavior of Thin Permalloy Films". D. O. Smith, J. Appl. Phys, **28**, 264 (1958).

1.12. "Local Enviroment Effects in disorder alloys". J. W. Cable, J. Appl. Phys, **49**(3), 1527 (1978).

1.13 "Order disorder temperature of Magnetic temperature". E. Figueroa, et. al. solid State Commun, **20**, 961 (1976).

1.14. "Transition Temperature of Metals". R. Malmhall et al. J. Phys. F. Met. Phys., **9**, 317 (1976).

1.15. "Anisotropy in Thin Film media Origins and Applications". William G. Hains J. Appl. Phys. **61(8)** 3497~50 (1987).

1.16. "Electron Transport in Thin Films". H. Mayer "Physik dünner schiehten: vol. **2** (1955).

1.17. "Effect of Temperature on Transport Properties in Magnetic Thin Films". N. M. Baslnara, IEEE Trans. Component, Pt-S, CP-P **(1)**; p 4 (1964).

1.18 "Electrical Conduction Mechanism in ultrathin Evaporated Metal Films". C. A. Neugebauer and M. B. Webb. J. Appl. Phys. **33**, 74 (1962).

1.19 " Symposium Electro-Megnetic properties of thim multilayers" C. Schuler, Louvain,1961, p-30.
1.20. "Power law Magnetization with Temperature". F. Bloch. Z, Physik, **24**, 295 (1952).
1.21 "General Theory of Spin-Wave Interaction". F. J. Dyson, Phys, Rev. **102** 1217 (1956).
1.22 "Spin-Wave Interaction on low Temperature". W. Opechowski, Physica, **6**, 1112 (1938).
1.23 Callen et. al., J. Phys **38** , 571 (1965)
1.24 "Allenling of Oblique Incidence". G. P. Weiss, J. Appl. Phys. **32**, 855 (1961).
1.25. "Thin Feffomagnetic Films". M. J. Klain and R. S. Smith. Phys. Rev, **81**, 378 (1951).
1.26. "Two Dimensional Magnetic Phase Transition". V. L. Pokrovsky, JMMM **200**, 515 (1999).

Chapter 2

2.1 "Thin Film Phenormena". K.l. Chopra. McGraw Hill- 1969 (Table-7)
2.2 "Thin Film Phenomena". K. L. Chopra, McGraw-Hill 1969.
2.3 "Techniques for Substrate Cleaning". G.R. Stillwell and D. B. Dove. J. Appl. Phys. **34**, 1941, (1963).
2.4 "Procedure in expenimetal Physics" J. Storng, Prentiec-Hall, Inc,. Englewood Cliffr, N.J. 1955.
2.5 " Procedure in Experimental Physics". J. Strong, Prentice-Hall, Inc, Englewood eliffs, N. J. 1965.
2.6 "A Demountable Glass Vacuum System Using Electron Bombardment in Vacuum Deposition of Ferromagnetic Films". D. M. Hart, 1958 vacuum symposium Transactions, P. 230 (1959).
2.7 "The Properties of Glass Sufrace". L. Holland, Jhon Wiley & Sons, Inc., New York, (1964).
2.8 "Physics of Thin Films". H.L Caswell, IBM., J. Res, Develop **1**, Acedamy Press, New York,(1963).
2.9 T.S. Grother , J. Phys, **34**, 580 (1963)
2.10 R.V. Telesnin , I.M. Saraeva and A..G Shiskov. Bull .Aead. Sci, USSR, Phy. **29**, 590 (1965).
2.11 "Microelectronics: Theory design and Fabrication". E. Keonjian, Mc Graw-Hill Book Co. Ny. 1963.
2.12 F. Z. Keister, R. D. Engquist, and J. M. Holley, IEEE Trans. Component Pts., CP-**11(1)**, 33 (1964).
2.13 "Measurement Techniques for Thin Films". W A. Plishkin, P- 280 Electro-chemical Society, New Yowk, (1967).
2.14 Belser, R. B. Rev. Sci. Instr. **25**, 180 (1954).

Chapter - 3

3.1 "Nucleation-Evaporation and Growth of Thin Films". B. K. Chakraborty and G. M. Pound, Acta Met. **12**, 851 (1964).

3.2 "Nucleation Structures and Macro-molecules". D. Walton, J. Chem, Phys. **37**, 2182 (1962).

3.3 "The Structure and the Transport Properties of nearly continuos Gold Films". M. S. R. Khan. Thin Solid films, **130**, 207 (1984).

3.4 "Nucleation and Growth of Thin Films". J. A. Venables, G. D. T. Spiller and M. Hanbucken Rep. Prog. Phys. **47**, 339 (1984).

3.5 E. V. Babkin, A. A. Charyev and H. O. Urinov, Thin Solid Films **150**, 11 (1987).

3.6 "Hand Book of Thin Film Technology" L.I. Maissel and R. Glang, MoGraw-Hill Book Co. 1970.

3.7 "Structure and Properties of Thin Films". G.A. Bassett, J. W. Menter and W. D. Pashley, P.11, Jhon Wiley & Sons, Inc., New York, (1959).

3.8 "Modern Developments in Electron Microscopy". D.W. Pashley, P 149. Academy Press, Inc. New York, (1964).

3.9 "Thin Films". W. D. Pashley, Americal society of Metals, Ohio, (1963).

3.10 "Thin Film Phenomena". K.L. Chopra, MeGrow-Hill Book Co. (1969).

3.11 E.G. Granquist and G.A. Niklasson, Phy. Dept. Chalmer University of Technology, Sweden, (1989).

3.12 "On the Anisotropy of Cubic Feffo-magnetic Crystals". J.H. Van Vleck, Phys. Rev. **52**, 1178 (1937).

3.13 Akulov. N., Z. Phys. **100**, 197 (1936).

3.14 Carr Jr. W.J., Phys. Rev. 197 (1958).

3.15 "Temperature Dependance of Magnetic Anisotropy Energy". Zener C., Phys. Rev. **96**, 1335 (1954).

3.16 "Theory of Ferromagnetic Anisotropy". J. H. Van Vleck, Phys. Radium, **20**, 124 (1954).

3.17 "Theory of Ferromagnetic Anisotropy". Carr. Jr. W. J., Phys, Rev. **108**, 1158 (1957).

3.18 "Temperature Dependence of Ferromagnetic Anisotropy in Cubic Crystals Keffer", F., Phys. Rev. **100**, 1692 (1955).

3.19 "Origin of Magnetic Anisotropy in Cobalt Substituted Magnetite". J.C. Slonezewski, Phys. Rev. **110**, 1341 (1958).

3.20 K. Yosida and M. Tachiki, Prog, Theor, Phys, **17**, 331 (1957).

3.21 L. Neel, Compt. Rend. J.Phys. Radium, **15**, 224 (1954).

3.22 "Measurements of the Magnetic field in a Thin Films". J,Appl. Phys.. **30**, 1619 (1959).

3.23 G.S. Mahojani, Phil, Trans, Roy, Soc. **228**, 63 (1959).

3.24 "The Magnetizatin Reversal of Thin Ni-Fe Films in Hard Direction". E. Fuchs, Z. Angraw. Phys **8**, 157 (1961).
3.25 J. R. Samble, Thin solid Films, **106** 321 (1883).
3.26 "Electrical Resistivity of Permalloy Films". A. F. Mayadas, M. Shatzkes and J.F. Janak. J. Appl. Phys, Lett. **14**, 345 (1969).
3.27 "Electrical Resistivity Model for Polycrystalline Films". A.F. Mayadas and M. shatzkes, Phys. Rev. **B 1**, 1382 (1970).
3.28 C.R. Tellier and A. J. Toeser, Thin Solid Films, **37**, 207 (1976).
3.29 "The Invar problem". Y. Namba, J. Appl. Phys, **39**, 6112 (1968).
3.30 Details of the Electronic Relaxation in $Mn_xFe_{3-x}O_4$" Y. Namba, J. Appl. Phys **9**, 1326 (1970).
3.31 H. Hoffmann and J. Vancea, Thin Solid Films, **85**, 147 (1981).
3.32 "Statistical Model for the Size Effect in Electrical Conduction". S.B. Soffer, J. Appl. Phys, **38**, 1710 (1967).
3.33 M. Watanable, J. Res. Inst, For, Catalysis, Hokkaido Univ. **26**, 107 (1978).
3.34 M. Watanable and Hiirataku, Jpn., J. Appl. Phys, **18**, 31 (1979).
3.35 J. R. Sambles, K. C. Elsome and D. J. Jarvis, Philos, Trans, Soc. London, Ser. **A 304**, 365 (1984).
3.36 J.R. Samble, K.C. Elsome and G.Sharp-Dednt, J. Phys, F, **11**, 1075 (1981).
3.37 P.Weiss, J. Phys, **6**, 667 (1907).
3.38 J.H. Van Vleck, Rev., Mod. Phys, **17**, 27 (1945).
3.39 F.Bloch, Z. Physik **74**, 295 (1932).
3.40 "Field Dependence of the Intrinsic Domain Magnetization of a Ferromagnet".T.Holstein and H. Primakoff, Phys, Rev, **58**, 1098 (1940).
3.41 "Thin Ferromagnetic Films" M. J. Klein and R. S. Smith, Phys, Rev, **81**, 378 (1951).
3.42 "Thin Ferromagnetic Films" S. J. Glass and M.J. Klein, Phys, Rev, **109**, 288 (1958).

Chapter - 4

4.1 Winer O. Wied, Ann, **31**, 629 (1887).
4.2 S. Tolansky "Multiple Beam Interferromettry of surface and films" Oxford University press 1948.
4.3 S. Tolanky "Surface Microtropology" Jhon Willy & Sons, Ny-1960.
4.4 T. M. Green and L. N. Hadley. J. Opt. Soc. Am. **45**, 228(1955).
4.5 S. J. Lines, 1961 Vacuum symposium Transaction, **52**, P. 846.
4.6 A. W. Winston, C. A. Baer, & L. R. Allen 1959, Vacuum Symposium Transaction, **49**, p. 2.
4.7 "Magnetic Anisotropy in SmCo Amorphous Films". T. Numta et.al. J. Appl. Phys, **64(10)** 5501 (1988).
4.8 Z.J.Zhou et al, J. Appl. Phys, **68(8)**, 5766 (1991).

4.9 R. Liepins and K. Sakaoku, J. Appl. Polym. Sci, **16,** 1179 (1962).
4.10 H.Biderman, Vacuum, **31**, 285 (1981).
4.11 M.R. Havens, K.G.Mayhan and W.J.Janes, J.Appl. Polym. Sci. **22**, 2799(1978).
4.12 R.Liepins et al. J.Vac. Sci. Tech. **18**, 1218 (1981).
4.13 "Secondary ion mass spectrometry for quantitative surface and in-depth analysis of materials" P. Chokraborty, Pramana (A Journal of Phys), Indian Acd. of Sci, **50(6)**, 617 (1998).
4.14 Westerstrandth a. et al, Physica Scripta, 14 5-10 (1976).
4.15 "Magnetization and Magneto-crystalline Anisotropy of Ni-Mo Single Crystal". F. A. Khan, M. A. Asgar and P. Nordblad JMMM 174,121 1997.
4.16 R. M. Bozorth, Ferromagnetism, D,. Van Nostrand Co. Inc. N. J. P 556, (1951).
4.17 R. F. Penoyer, Rev. Sci. Instr. **30**, 711 (1954).
4.18 G. T. Craft, F. J. Donahoe, and W. F. Love, Rev. Sci, Instr. **263**, 360 (1955).
4.19 S. M. Smits, Bell Syst. Tech., J. **37**, 711 (1958).
4.20 M.A. Mazid and M.A. Chowdhury, "Design and Construction of a Forner type VSM" MMD/AECD, 1 June 1986 (Bangladesh).
4.21 S. Forner, Rev., Sci, Instr. **27**, 548 (1956).

Chapter - 5

5.1 "Magnetization and Magneto-crystalline Anisotropy Measurements of Ni $MoFe_2$ P Alloys" F. A. Khan, Ph.D. Thesis, Dept. of Phys. BUET (1995).
5.2 C. D. Graham Jr. and r. M. Bozorth, Amer, Soc, Metals, P 288 (devemd 1959).
5.3 "Magnetic Interface Anisotropy in Pd/Co and Pd/Fe Multilayers". H. J. G. Draaisma, F. J. A. Broeder and W. J. M. De Jonge, JMMM **66**, 351 (1987).
5.4 "Classical theory of the temperature dependence of magnetic anisotropy energy Zener". C., Phys, Rev, **96**, 1335 (1984).
5.5 Carr. W. J. J. Appl. Phys, **29**, 436 (1962).

APPENDIX

Table 1: $Ni_{80}Co_{20}$, W= 0.00009 gm, 2.5×10^{-5}, Thickness = 1635Å, Temperature = 25^0C

θ	1 amp	2 amp	3 amp	4 amp	5 amp
0	0.718	0.482	0.865	0.263	0.611
10	0.740	0.661	1.206	0.299	0.763
20	1.025	0.875	1.477	0.466	0.903
30	1.480	1.218	1.733	0.578	1.119
40	1.594	1.572	1.930	0.548	1.185
50	1.039	1.377	1.730	0.409	1.050
60	0.623	0.833	1.532	0.381	0.578
70	0.544	0.819	1.407	0.299	0.457
80	0.536	0.717	1.321	0.221	0.151
90	0.483	0.615	1.155	0.183	0.153
100	0.127	0.332	0.876	-0.045	-0.573
110	-0.281	0.195	0.636	-0.200	-0.773
120	-0.526	-0.192	0.579	-0.250	-0.945
130	-0.526	-0.247	0.383	-0.486	-0.975
140	-0.521	0.059	0.717	-0.393	-0.923
150	-0.122	0.717	0.793	0.108	-.0866
160	0.437	0.752	0.884	0.008	-0.141
170	0.465	0.787	0.994	0.162	0.412
180	0.546	0.819	1.211	0.221	0.579
190	0.718	0.661	1.477	0.295	0.763
200	1.034	0.875	1.677	0.449	0.895
210	1.375	1.196	1.735	0.597	1.103
220	1.523	1.531	1.911	0.558	1.159
230	1.022	1.329	1.754	0.419	1.093
240	0.713	0.865	1.531	0.391	0.903
250	0.614	0.813	1.407	0.304	0.573
260	0.580	0.717	1.309	0.233	0.439
270	0.493	0.603	1.132	0.195	0.142
280	0.159	0.295	1.013	0.006	-0.198
290	-0.274	0.189	0.876	-0.231	-0.579
300	-0.496	0.153	0.537	-0.259	-0.795
310	-0.546	-0.128	0.383	-0.475	-0.983
320	-0.487	-0.263	0.509	-0.391	-0.916
330	-0.105	-0.025	0.684	-0.114	-0.881
340	0.375	0.621	0.707	0.038	-0.639
350	0.465	0.739	0.793	0.195	-0.214
360	0.564	0.823	0.874	0.294	0.412

A_o	A_2	A_4	δ	C	T
0.4310	0.828	0.079	19.546	1	26^0C
0.626	0.600	0.080	1.129	2	
1.129	0.604	0.029	-8.498	3	
-13.357	27.398	0.027	-17.482	4	
0.164	0.964	0.014	4.086	5	

1 Amp = .7 Kguss	1/H = 1.4285 = 1.43		4 Amp = 2.8 Kguss 1/H = 0.35714 = 0.36
2 Amp = 1.4 Kguss	1/H = 0.71428 = 0.75		5 Amp = 3.5 Kguss 1/H = 0.28571 = 0.29
3 Amp = 2.1 Kguss	1/H= 0.47619 = 0.48		

Table 2: $Ni_{80}Co_{20}$, W= 0.00009 gm, 2.5×10^{-5}, Thickness = 1635Å, Temperature = 50^0C

θ	1 amp	2 amp	3 amp	4 amp	5 amp
0	0.566	0.282	0.909	0.508	0.015
10	0.837	0.616	1.078	0.921	0.469
20	1.088	0.913	1.596	1.098	0.594
30	1.193	1.120	1.641	1.214	1.084
40	1.276	1.230	1.783	1.405	1.396
50	1.286	1.025	1.688	1.358	1.148
60	1.173	0.833	1.587	1.172	1.074
70	0.986	0.483	1.460	1.058	0.615
80	0.849	0.264	1.433	0.990	0.469
90	0.557	0.270	1.351	0.802	0.255
100	0.440	-0.250	0.973	0.701	0.190
110	0.119	-0.167	0.640	0.671	0.017
120	-0.075	-0.273	0.567	0.562	-0.057
130	-0.260	-0.294	0.356	0.442	-0.149
140	-0.245	-0.287	0.364	0.509	-0.027
150	-0.080	-0.011	0.375	0.579	0.012
160	0.216	0.256	0.381	0.651	0.025
170	0.480	0.264	0.528	0.790	0.098
180	0.557	0.270	0.567	0.851	0.155
190	0.837	0.616	0.893	0.925	0.465
200	1.075	0.913	0.995	1.091	0.590
210	1.188	1.120	1.238	1.206	0.998
220	1.225	1.235	1.596	1.418	1.381
230	1.295	1.052	1.785	1.361	1.152
240	1.171	0.835	1.623	1.169	1.048
250	0.987	0.498	1.574	1.043	0.629
260	0.839	0.251	1.438	0.985	0.465
270	0.548	0.173	1.351	0.815	0.219
280	0.423	-0.035	0.973	0.712	0.185
290	0.116	-0.167	0.651	0.669	0.012
300	-0.079	-0.261	0.356	0.571	-0.082
310	-0.271	-0.305	0.389	0.458	-0.153
320	-0.242	-0.251	0.431	0.513	-0.032
330	-0.077	-0.021	0.529	0.569	0.069
340	0.223	0.259	0.613	0.648	0.095
350	0.498	0.316	0.699	0.779	0.159
360	0.670	0.433	0.886	0.832	0.235

A_o	A_2	A_4	δ	C	T
0.573	0.730	0.052	-20.374	1	51^0C
0.371	0.657	0.079	-18.096	2	
1.011	0.676	0.0332	3.523	3	
0.867	0.390	0.065	-21.782	4	
0.406	0.607	0.195	21.575	2	

Table 3: $Ni_{80}Co_{20}$, W= 0.00009 gm, 2.5×10^{-5}, Thickness = 1635Å, Temperature = 75^0C

θ	1 amp	2 amp	3 amp	4 amp	5 amp
0	0.241	0.276	0.736	0.028	-0.134
10	0.616	0.412	1.215	0.405	0.118
20	0.876	0.558	1.844	0.618	0.627
30	0.905	0.867	1.975	0.434	0.150
40	1.009	0.927	2.030	0.121	1.369
50	0.843	0.772	1.980	0.908	1.099
60	0.443	0.621	1.733	0.866	0.601
70	0.324	0592	1.569	0.811	0.137
80	0.282	0.536	1.297	0.519	-0.139
90	0.241	0.463	0.861	0.272	-0.231
100	0.238	0.217	0.644	0.083	-0.254
110	-0.338	0.192	0.595	-0.053	-0.297
120	-0.518	0.053	0.447	-0.105	-0.397
130	-0.528	0.014	0.343	-0.149	-0.515
140	-0.489	0.089	0.403	-0.081	-0.390
150	-0.167	0.198	0.432	-0.064	-0.297
160	0.151	0.268	0.636	0.257	-0.242
170	0.237	0.478	0.639	0.332	-0.146
180	0.241	0.565	0.749	0.376	-0.106
190	0.594	0.412	1.213	0.412	0.107
200	0.796	0.568	1.893	0.609	0.561
210	0.885	0.794	1.996	0.913	0.998
220	0.997	0.912	2.020	1.098	1.235
230	0.832	0.813	1.970	0.935	1.054
240	0.563	0.695	1.751	0.852	0.835
250	0.443	0.611	1.543	0.795	0.521
260	0.324	0.571	1.321	0.531	0.137
270	0.282	0.522	0.965	0.265	0.213
280	0.238	0.465	0.783	0.081	-0.259
290	-0.295	0.239	0.603	-0.043	-0.381
300	-0.503	0.152	0.437	-0.121	-0.461
310	-0.543	0.032	0.312	-0.156	-0.527
320	-0.478	0.095	0.491	-0.089	-0.438
330	-0.178	0.231	0.572	-0.038	-0.297
340	0.139	0.293	0.634	0.237	-0.242
350	0.251	0.412	0.711	0.313	-0.159
360	0.325	0.563	0.857	0.391	-0.091

A_o	A_2	A_4	δ	T
0.2516111	0.6524975	0.074	15.62689	76^0C
0.4529729	0.3313414	0.023	3.141572	
1.092861	0.820582	0.015	-18.68026	
0.3795	0.5433935	0.011	11.91107	
0.122889	0.7387073	0.027	-20.08395	

Table 4: $Ni_{80}Co_{20}$, W= 0.00009 gm, 2.5×10^{-5}, Thickness = 1635Å, Temperature = 100^0C

θ	1 amp	2 amp	3 amp	4 amp	5 amp
0	0.718	2.28	0.117	0.736	0.701
10	0.839	2.44	0.609	0.992	0.936
20	0.849	2.62	0.859	1.118	1.040
30	1.075	2.86	1.006	1.416	1.113
40	1.339	3.00	1.203	1.743	1.432
50	0.845	2.88	1.039	1.215	1.105
60	0.839	2.55	0.821	0.935	1.002
70	0.807	1.96	0.622	0.842	0.963
80	0.792	1.27	0.613	0.773	0.915
90	0.766	1.07	0.481	0.749	0.763
100	0.728	0.589	0.241	0.689	0.702
110	0.701	0.474	0.034	0.578	0.624
120	0.532	0.346	-0.094	0.471	0.529
130	0.436	0.185	-0.663	0.346	0.461
140	0.522	0.264	-0.332	0.536	0.542
150	0.572	0.562	-0.092	0.672	0.611
160	0.594	0.589	0.231	0.707	0.674
170	0.709	0.813	0.316	0.745	0.703
180	0.808	0.958	0.444	0.771	0.862
190	0.831	2.01	0.602	0.899	0.931
200	0.856	2.52	0.868	0.998	1.021
210	0.998	2.72	0.995	1.319	1.102
220	1.297	2.97	1.213	1.695	1.453
230	0.840	2.81	1.006	1.315	1.117
240	0.829	2.45	0.901	1.053	1.021
250	0.795	1.86	0.703	0.912	0.953
260	0.751	1.09	0.651	0.805	0.906
270	0.680	0.98	0.518	0.761	0.751
280	0.632	0.71	0.289	0.683	0.689
290	0.581	0.48	0.015	0.581	0.621
300	0.519	0.35	-0.099	0.493	0.509
310	0.415	0.19	-0.613	0.356	0.439
320	0.511	0.27	-0.351	0.541	0.555
330	0.563	0.59	-0.112	0.685	0.608
340	0.614	0.74	0.131	0.721	0.675
350	0.751	0.89	0.315	0.769	0.725
360	0.856	1.05	0.412	0.815	0.875

A_o	A_2	A_4	δ	T
24.50	7.70	0.04754	2.54	100.5^0C
1.43	0.730	0.27	-18.61	
0.40	0.70	5.25	20.11	
0.85	0.72	0.11	-17.24	
0.83	0.34	0.04	-18.35	

Table 5: $Ni_{80}Co_{20}$, W= 0.00009 gm, 2.5×10^{-5}, Thickness = 1635Å, Temperature = 125^0C

θ	1 amp	2 amp	3 amp	4 amp	5 amp
0	0.071	0.544	0.620	1.178	1.466
10	0.148	0.877	0.680	1.328	1.609
20	0.441	0.894	0.766	1.654	1.786
30	0.848	0.913	0.790	1.914	1.974
40	1.066	1.072	1.196	1.959	2.22
50	0.838	0.952	0.930	1.820	2.14
60	0.573	0.921	0.889	1.558	1.869
70	0.412	0.852	0.856	1.357	1.641
80	0.071	0.813	0.850	1.123	1.510
90	-0.096	0.794	0.339	1.101	1.374
100	-0.675	0.751	-0.119	1.035	1.306
110	-1.547	0.633	-0.397	0.963	0.896
120	-2.21	0.591	-0.712	0.732	-0.176
130	-2.29	0.584	-0.847	0.605	-0.327
140	-2.27	0.544	-0.671	0.857	-0.038
150	-1.741	0.680	-0.643	0.913	0.277
160	-1.091	0.714	-0.553	0.972	1.280
170	-0.341	0.736	-0.171	1.114	1.335
180	0.093	0.767	0.339	1.251	1.393
190	0.198	0.867	0.621	1.326	
200	0.439	0.891	0.752	1.654	
210	0.825	0.902	0.794	1.969	
220	1.043	1.065	1.148	1.815	
230	0.812	0.947	0.925	1.541	
240	0.553	0.842	0.892	1.339	
250	0.422	0.778	0.849	1.152	
260	0.123	0.738	0.837	1.112	
270	-0.082	0.621	0.315	1.091	
280	-0.639	0.587	-0.128	1.003	
290	-1.429	0.571	-0.387	0.951	
300	-2.18	0.553	-0.701	0.735	
310	-2.35	0.512	-0.853	0.612	
320	-2.14	0.599	-0.702	0.857	
330	-1.719	0.689	-0.652	0.913	
340	-1.021	0.735	-0.553	0.977	
350	-0.412	0.767	-0.151	1.109	
360	-0.095	0.851	0.359	1.195	

A_o	A_2	A_4	δ	T
0.35	1.40	0.034	17.80	125^0C
0.76	0.99	0.037	17.37	
0.18	0.93	0.080	-21.03	
1.22	0.50	0.100	-8.41	
1.23	0.97	0.280	20.99	

Table 6: $Ni_{80}Co_{20}$, W= 0.00009 gm, 2.5×10^{-5}, Thickness = 1635Å, Temperature = 150^0C

θ	1 amp	2 amp	3 amp	4 amp	5 amp
0	0.779	2.030	2.01	1.513	1.632
10	1.281	2.100	2.18	2.97	2.34
20	1.382	2.130	2.38	3.29	2.38
30	1.468	2.180	2.57	3.36	2.41
40	1.698	2.220	2.93	3.37	2.44
50	1.550	2.080	2.52	3.31	2.30
60	1.427	1.970	2.02	2.98	2.15
70	1.291	1.659	1.622	2.32	1.93
80	1.161	1.003	1.377	1.748	1.696
90	0.910	0.988	1.056	1.643	1.443
100	0.742	0.980	0.973	1.609	1.283
110	0.566	0.976	0.952	1.078	0.906
120	0.466	0.973	0.914	0.431	0.809
130	0.434	0.963	0.862	-0.421	0.776
140	0.448	0.994	0.974	-0.233	0.884
150	0.492	1.098	1.132	0.633	0.831
160	0.595	1.268	1.259	1.246	1.072
170	0.674	1.635	1.561	1.681	1.286
180	0.775	1.773	1.882	2.32	1.531
190	1.185	2.091	2.081	2.97	3.09
200	1.371	2.150	2.38	3.28	2.31
210	1.689	2.185	2.57	3.39	2.41
220	1.542	2.219	2.95	3.45	2.45
230	1.437	2.095	2.61	3.32	2.31
240	1.271	1.957	2.01	2.97	2.19
250	1.095	1.645	1.609	2.30	1.95
260	0.921	1.039	1.359	1.759	1.675
270	0.718	0.988	1.031	1.641	1.492
280	0.519	0.980	0.995	1.593	1.283
290	0.436	0.973	0.944	1.062	0.925
300	0.409	0.951	0.856	0.425	0.813
310	0.400	0.977	0.974	-0.401	0.756
320	0.448	1.091	1.035	-0.269	0.804
330	0.499	1.254	1.148	0.617	0.951
340	0.681	1.413	1.254	1.365	1.095
350	0.715	1.691	1.561	1.695	1.426
360	0.821	1.785	1.925	2.21	1.912

A_0	A_2	A_4	δ	T
0.90	0.57	0.13	-14.86	150^0C
1.49	0.73	0.12	-21.51	
6.04	7.91	0.08	8.09	
1.83	1.63	0.26	11.86	
24.03	44.10	0.44	7.46	

Table 7: $Ni_{80}Co_{20}$, W= 0.00009 gm, 2.5×10^{-5}, Thickness = 1635Å, Temperature = 165^0C

θ	1 amp	2 amp	3 amp	4 amp	5 amp
0	-2.57	-1.154	-2.04	-1.820	-1.436
10	-2.32	-1.124	-1.722	-1.669	-1.378
20	-1.645	-1.096	-1.438	-1.503	-1.369
30	-1.425	-1.070	-1.078	-1.421	-1.344
40	-1.141	-1.066	-0.972	-1.310	-1.332
50	-1.177	-1.142	-0.926	-1.374	-1.383
60	-1.371	-1.218	-0.932	-1.441	-1.519
70	-1.605	-1.310	-1.535	-1.503	-1.640
80	-1.852	-1.330	-1.686	-1.712	-1.684
90	-1.917	-1.397	-1.896	-1.769	-1.750
100	-2.06	-1.419	-1.979	-1.897	-1.764
110	-2.57	-1.485	-2.03	-1.977	-1.779
120	-2.90	-1.537	-2.10	-2.060	-1.781
130	-2.94	-1.611	-2.16	-2.210	-1.882
140	-2.92	-1.369	-2.35	-2.180	-1.815
150	-2.90	-1.277	-2.64	-2.160	-1.780
160	-2.79	-1.206	-2.49	-2.140	-1.708
170	-2.65	-1.152	-2.41	-2.090	-1.621
180	-2.48	-1.127	-2.28	-1.950	-1.562
190	-2.32	-1.124	-2.10	-1.669	-1.378
200	-1.645	-1.096	-2.16	-1.503	-1.369
210	-1.425	-1.076	-2.35	-1.421	-1.344
220	-1.141	-1.066	-2.64	-1.310	-1.332
230	-1.177	-1.142	-2.48	-1.374	-1.383
240	-1.371	-1.218	-2.40	-1.441	-1.519
250	-1.605	-1.310	-2.28	-1.503	-1.640
260	-1.852	-1.330	-2.04	-1.712	-1.684
270	-1.917	-1.397	-1.722	-1.769	-1.751
280	-2.06	-1.419	-1.438	-1.879	-1.763
290	-2.57	-1.485	-1.078	-1.957	-1.780
300	-2.90	-1.537	-0.972	-2.095	-1.813
310	-2.94	-1.611	-0.926	-2.210	-1.882
320	-2.92	-1.369	-0.932	-2.170	-1.815
330	-2.90	-1.277	-1.153	-2.150	-1.780
340	-2.79	-1.206	-1.686	-2.120	-1.708
350	-2.65	-1.152	-1.886	-2.090	-1.612
360	-2.48	-1.127	-1.979	-1.950	-1.526

A_o	A_2	A_4	δ	T
2.16	0.27	0.09	-18.57	165^0C
1.28	0.22	0.04	-3.37	
1.80	0.16	0.20	-12.27	
-1.79	0.42	0.055	-11.84	
-38.57	0.69	0.073	-17.50	

Table 8: $Ni_{80}Co_{20}$, W= 0.00009 gm, 2.5×10^{-5}, Thickness = 1635Å, Temperature = 180^0C

θ	1 amp	2 amp	3 amp	4 amp	5 amp
0	-1.662	-1.466	1.169	1.51	1.296
10	-1.262	-0.444	2.23	1.60	1.313
20	-0.445	-0.306	2.46	1.67	1.341
30	-0.697	-0.222	2.92	1.76	1.371
40	-0.684	-0.196	2.99	1.82	1.412
50	-0.813	-0.416	2.95	1.38	1.307
60	-1.248	-0.669	2.87	1.05	1.288
70	-2.17	-1.059	2.34	0.82	1.248
80	-2.46	-2.01	2.03	0.56	1.219
90	-2.63	-2.54	1.82	0.34	1.186
100	-2.73	-3.00	1.46	0.22	1.119
110	-2.80	-3.03	1.146	0.14	1.076
120	-2.86	-3.22	0.907	0.042	0.967
130	-2.88	-3.25	0.823	0.13	0.883
140	-2.82	-3.20	0.884	0.32	1.007
150	-2.43	-2.91	0.932	0.57	1.111
160	-2.09	-2.43	0.981	0.87	1.196
170	-1.94	-1.79	1.101	1.14	1.271
180	-1.813	-1.54	1.116	1.25	1.290
190	-1.262	-0.944	2.09	1.61	1.313
200	-0.945	-0.445	2.46	1.65	1.341
210	-0.697	-0.241	2.92	1.72	1.371
220	-0.684	-0.192	2.99	1.81	1.412
230	-0.813	-0.416	2.95	1.80	1.307
240	-1.248	-0.669	2.87	1.15	1.288
250	-2.17	-1.054	2.34	0.81	1.248
260	-2.46	-2.02	2.03	0.57	1.219
270	-2.63	-2.54	1.82	0.32	1.186
280	-2.73	-3.03	1.46	0.20	1.119
290	-2.80	-3.13	1.14	0.14	1.076
300	-2.86	-3.21	0.90	0.04	0.967
310	-2.88	-3.25	0.82	0.13	0.883
320	-2.82	-3.20	0.88	0.32	1.007
330	-2.43	-2.91	0.93	0.57	1.111
340	-2.09	-2.43	0.98	0.87	1.196
350	-1.94	-1.79	1.10	1.18	1.271
360	-1.821	-1.54	1.4	1.29	1.290

A_o	A_2	A_4	δ	T
-1.96	1.083	0.22	-15.88	180^0C
-1.63	1.09	0.48	-8.69	
1.77	1.10	0.20	-17.48	
1.23	0.18	0.81	11.29	
1.20	0.29	4.58	-18.11	

Table 9: $Ni_{80}Co_{20}$, W= 0.00009 gm, 2.5×10^{-5}, Thickness = 1635Å, Temperature = 195^0C

θ	1 amp	2 amp	3 amp	4 amp	5 amp
0	1.076	1.275	0.975	1.99	1.306
10	1.143	1.754	1.121	2.05	1.96
20	1.174	1.821	1.129	2.13	2.21
30	1.198	1.844	1.313	2.21	2.54
40	1.214	1.884	1.228	2.26	3.02
50	1.016	1.828	1.036	2.09	2.25
60	0.997	1.797	0.882	1.97	2.15
70	0.925	1.718	0.741	1.681	2.11
80	0.875	1.667	0.646	1.404	1.96
90	0.857	1.628	0.541	1.371	1.533
100	0.846	1.296	0.413	1.097	1.496
110	0.829	0.946	0.359	0.720	1.090
120	0.815	0.587	0.324	0.665	0.714
130	0.807	0.532	0.333	0.632	0.563
140	0.904	0.915	0.336	1.036	0.932
150	1.021	1.046	0.426	1.265	1.252
160	1.105	1.310	0.521	1.465	1.306
170	1.175	1.458	0.793	1.646	1.388
180	1.219	1.506	1.123	1.847	1.589
190	1.413	1.759	1.121	2.05	1.96
200	1.172	1.821	1.129	2.13	2.21
210	1.198	1.844	1.313	2.21	2.54
220	1.221	1.844	1.228	2.26	3.02
230	1.011	1.797	1.036	2.09	2.25
240	0.979	1.718	0.882	1.97	2.15
250	0.915	1.667	1.741	1.681	2.11
260	0.860	1.628	1.464	1.405	1.96
270	0.821	1.296	1.541	1.371	1.533
280	0.805	0.946	0.413	1.095	1.496
290	0.795	0.836	0.359	1.720	1.090
300	0.790	0.587	0.324	0.665	0.714
310	0.775	0.532	0.333	0.632	0.563
320	0.889	0.915	0.336	0.995	0.932
330	1.005	1.046	0.426	1.256	1.252
340	1.108	1.310	0.521	1.456	1.306
350	1.118	1.458	0.793	1.664	1.388
360	1.201	1.506	1.123	1.874	1.589

A_o	A_2	A_4	δ	T
.94	0.60	0.07	-1.33	
1.39	0.57	0.04	-12.12	195^0C
0.73	0.47	0.08	1.06	
1.48	0.70	0.09	10.90	
1.64	0.84	0.09	-8.61	

Table 10: $Ni_{80}Co_{20}$, W= 0.00009 gm, 2.5×10^{-5}, Thickness = 1635Å, Temperature = 210^0C

θ	1 amp	2 amp	3 amp	4 amp	5 amp
0	1.38	1.19	1.07	1.15	0.99
10	1.60	1.40	1.10	1.60	1.820
20	2.00	2.51	1.11	2.14	2.02
30	2.25	2.78	1.14	2.97	2.12
40	2.56	3.04	1.11	2.82	2.15
50	2.40	2.49	1.08	2.67	1.98
60	2.21	2.14	1.06	2.55	1.78
70	2.06	1.86	0.93	2.40	1.62
80	1.82	1.64	0.77	2.18	1.34
90	1.71	1.43	0.62	1.79	0.92
100	1.46	1.32	0.49	1.38	0.41
110	1.12	1.15	0.39	0.98	0.32
120	0.50	0.89	0.27	0.76	0.27
130	0.39	0.70	0.19	0.90	0.251
140	0.65	0.74	0.34	1.06	0.55
150	1.06	0.91	0.54	1.09	0.72
160	1.16	1.13	0.76	1.21	0.99
170	1.25	1.29	0.98	1.32	1.51
180	1.33	1.35	1.04	1.42	1.68
190	1.60	1.40	1.10	1.60	1.82
200	2.00	2.51	1.11	2.14	2.02
210	2.25	2.78	1.14	2.97	2.12
220	2.56	3.04	1.11	2.82	2.15
230	2.40	2.49	1.08	2.67	1.98
240	2.21	2.14	1.06	2.55	1.78
250	2.06	1.86	0.93	2.40	1.62
260	1.82	1.64	0.77	2.18	1.34
270	1.71	1.43	0.62	1.79	0.92
280	1.46	1.32	0.49	1.38	0.41
290	1.12	1.15	0.39	0.968	0.32
300	0.56	0.89	0.27	0.76	0.27
310	0.39	0.70	0.19	0.90	0.25
320	0.65	0.74	0.34	1.06	0.55
330	1.06	0.91	0.54	1.09	0.72
340	1.16	1.13	0.76	1.21	0.99
350	1.25	1.29	0.98	1.32	1.51
360	1.33	1.35	1.04	1.42	1.68

A_o	A_2	A_4	δ	T
1.53	0.86	0.07	-4.79	210^0C
1.58	0.53	0.03	-14.95	
0.77	0.44	0.09	-13.87	
1.72	0.56	0.18	15.37	
1.26	0.50	0.08	-7.37	

Table 11: $Ni_{80}Co_{20}$, W= 0.00009 gm, 2.5×10^{-5}, Thickness = 1635Å, Temperature = 225^0C

θ	1 amp	2 amp	3 amp	4 amp	5 amp
0	0.637	0.470	0.499	0.218	0.448
10	0.728	0.481	0.610	0.448	0.554
20	0.733	0.512	0.725	0.534	0.645
30	0.822	0.620	0.745	0.612	0.502
40	0.912	0.712	0.741	0.892	0.905
50	0.868	0.508	0.615	0.747	0.662
60	0.850	0.487	0.512	0.664	0.558
70	0.732	0.338	0.445	0.623	0.448
80	0.664	0.272	0.435	0.355	0.358
90	0.629	0.128	0.385	0.335	0.339
100	0.555	0.275	0.374	0.325	0.316
110	0.465	0.250	0.227	0.218	0.309
120	0.460	0.246	0.194	0.196	0.299
130	0.470	0.250	0.113	0.118	0.295
140	0.473	0.302	0.220	0.155	0.454
150	0.487	0.381	0.228	0.227	0.457
160	0.446	0.421	0.372	0.385	0.505
170	0.462	0.540	0.419	0.448	0.516
180	0.551	0.664	0.551	0.634	0.542
190	0.728	0.481	0.610	0.448	0.554
200	0.733	0.512	0.725	0.534	0.645
210	0.822	0.620	0.745	0.612	0.802
220	0.912	0.712	0.741	0.892	0.905
230	0.868	0.508	0.615	0.747	0.662
240	0.850	0.487	0.512	0.664	0.558
250	0.732	0.338	0.445	0.623	0.448
260	0.664	0.272	0.435	0.355	0.358
270	0.629	0.128	0.385	0.335	0.339
280	0.555	0.275	0.374	0.325	0.316
290	0.465	0.285	0.227	0.218	0.309
300	0.460	0.296	0.194	0.199	0.295
310	0.470	0.250	0.113	0.118	0.295
320	0.473	0.302	0.220	0.154	0.454
330	0.478	0.381	0.228	0.227	0.457
340	0.446	0.421	0.372	0.385	0.505
350	0.462	0.540	0.419	0.448	0.516
360	0.551	0.664	0.551	0.634	0.542

A_o	A_2	A_4	δ	T
0.63	0.22	0.044	-19.32	225^0c
0.42	0.20	0.028	-13.67	
3.57	0.20	0.36	-17.33	
0.43	0.28	0.054	12.65	
0.50	0.2	0.091	-20.84	

Table 12: $Ni_{85}Co_{15}$, S.W = 0.00003 gm, 1.2×10^{-5} Torr, Thickness = 345Å, Temperature = 25^0C

θ	1 amp	2 amp	3 amp	4 amp	5 amp
0	- 0.356	- 0.270	- 0.335	- 0.289	- 0.344
10	-0.247	-0.243	-0.270	-0.270	-0.335
20	-0.255	-0.184	-0.263	-0.265	-0.328
30	-0.229	-0.160	-0.172	-0.242	-0.311
40	-0.211	-0.138	-0.155	-0.225	-0.189
50	-0.247	-0.144	-0.167	-0.257	-0.198
60	-0.387	-0.168	-0.186	-0.266	-0.209
70	-0.448	-0.198	-0.287	-0.289	-0.217
80	-0.360	-0.270	-0.295	-0.306	-0.233
90	-0.359	-0.312	-0.315	-0.328	-0.253
100	-0.345	-0.326	-0.335	-0.355	-0.348
110	-0.337	-0.344	-0.405	-0.373	-0.355
120	-0.280	-0.391	-0.431	-0.394	-0.391
130	-0.291	-0.470	-0.484	-0.517	-0.560
140	-0.413	-0.462	-0.387	-0.477	-0.481
150	-0.460	-0.315	-0.367	-0.394	-0.391
160	-0.497	-0.291	-0.348	-0.353	-0.372
170	-0.457	-0.271	-0.342	-0.315	-0.313
180	-0.325	-0.241	-0.331	-0.257	-0.295
190	-0.247	-0.243	-0.270	-0.270	-0.335
200	-0.255	-0.184	-0.263	-0.265	-0.328
210	-0.229	-0.160	-0.172	-0.242	-0.311
220	-0.211	-0.138	-0.155	-0.225	-0.189
230	-0.247	-0.144	-0.167	-0.257	-0.198
240	-0.387	-0.168	-0.186	-0.266	-0.209
250	-0.448	-0.198	-0.287	-0.289	-0.217
260	-0.360	-0.270	-0.295	-0.306	-0.233
270	-0.359	-0.312	-0.315	-0.328	-0.253
280	-0.345	-0.326	-0.335	-0.355	-0.348
290	-0.286	-0.344	-0.405	-0.373	-0.355
300	-0.241	-0.391	-0.431	-0.394	-0.391
310	-0.413	-0.470	-0.484	-0.517	-0.566
320	-0.460	-0.462	-0.387	-0.477	-0.481
330	-0.497	-0.316	-0.367	-0.394	-0.391
340	-0.457	-0.291	-0.348	-0.353	-0.372
350	-0.325	-0.271	-0.342	-0.315	-0.313
360	-0.247	-0.241	-0.331	-0.257	-0.295

A_o	A_2	A_4	δ	T
0.34	0.75	0.013	-2.23	
0.27	0.13	0.015	-7.41	
0.31	0.12	0.017	13.71	
0.33	0.10	0.028	21.47	
0.32	0.12	0.033	-10.22	

Table 13: $Ni_{85}Co_{15}$, S.W = 0.00003 gm, 1.2×10^{-5} Torr, Thickness = 345Å, Temperature = 50^0C

θ	1 amp	2 amp	3 amp	4 amp	5 amp
0	-0.340	-0.319	-0.240	-0.363	-0.281
10	-0.320	-0.277	-0.228	-0.304	-0.267
20	-0.280	-0.247	-0.181	-0.222	-0.161
30	-0.212	-0.242	-0.173	-0.196	-0.147
40	-0.192	-0.233	-0.149	-0.172	-0.140
50	-0.195	-0.246	-0.174	-0.186	-0.154
60	-0.202	-0.249	-0.222	-0.205	-0.263
70	-0.242	-0.291	-0.230	-0.365	-0.274
80	-0.263	-0.314	-0.271	-0.381	-0.322
90	-0.268	-0.327	-0.313	-0.393	-0.341
100	-0.288	-0.345	-0.342	-0.407	-0.349
110	-0.340	-0.355	-0.355	-0.444	-0.368
120	-0.385	-0.429	-0.387	-0.471	-0.419
130	-0.526	-0.527	-0.521	-0.575	-0.595
140	-0.427	-0.453	-0.379	-0.479	-0.431
150	-0.376	-0.384	-0.369	-0.457	-0.372
160	-0.308	-0.348	-0.340	-0.428	-0.346
170	-0.290	-0.336	-0.331	-0.376	-0.332
180	-0.280	-0.282	-0.292	-0.354	-0.313
190	-0.320	-0.277	-0.228	-0.304	-0.267
200	-0.280	-0.247	-0.181	-0.222	-0.161
210	-0.212	-0.233	-0.173	-0.196	-0.147
220	-0.192	-0.246	-0.149	-0.172	-0.140
230	-0.195	-0.249	-0.174	-0.186	-0.154
240	-0.202	-0.291	-0.222	-0.205	-0.263
250	-0.242	-0.319	-0.230	-0.365	-0.274
260	-0.263	-0.325	-0.271	-0.381	-0.322
270	-0.268	-0.347	-0.313	-0.393	-0.341
280	-0.288.	-0.358	-0.342	-0.407	-0.349
290	-0.340	-0.396	-0.355	-0.444	-0.368
300	-0.385	-0.429	-0.387	-0.471	-0.419
310	-0.525	-0.527	-0.521	-0.575	-0.595
320	-0.427	-0.453	-0.379	-0.479	-0.341
330	-0.376	-0.384	-0.365	-0.457	-0.372
340	-0.308	-0.348	-0.340	-0.428	-0.346
350	-0.290	-0.336	-0.331	-0.376	-0.332
360	-0.280	-0.282	-0.292	-0.354	-0.313

A_o	A_2	A_4	δ	T
-0.25	0.15	0.09	17.01	
-0.33	0.09	0.05	20.35	
-0.27	0.12	0.03	19.26	
-0.35	0.14	0.02	-8.13	
-0.31	0.16	0.01	2.13	

Table 14: $Ni_{85}Co_{15}$, S.W = 0.00003 gm, 1.2×10^{-5} Torr, Thickness = 345Å, Temperature = 75^0C

θ	1 amp	2 amp	3 amp	4 amp	5 amp
0	-0.303	-0.296	-0.277	-0.304	-0.275
10	-0.271	-0.266	-0.254	-0.292	-0.258
20	-0.252	-0.214	-0.181	-0.246	-0.138
30	-0.185	-0.197	-0.131	-0.208	-0.114
40	-0.184	-0.192	-0.121	-0.193	-0.112
50	-0.192	-0.194	-0.132	-0.209	-0.129
60	-0.247	-0.204	-0.139	-0.267	-0.269
70	-0.275	-0.285	-0.204	-0.296	-0.291
80	-0.317	-0.329	-0.265	-0.301	-0.313
90	-0.330	-0.343	-0.292	-0.363	-0.342
100	-0.335	-0.352	-0.330	-0.403	-0.387
110	-0.365	-0.361	-0.353	-0.431	-0.401
120	-0.416	-0.451	-0.380	-0.468	-0.443
130	-0.462	-0.563	-0.498	-0.548	-0.578
140	-0.381	-0.491	-0.395	-0.484	-0.391
150	-0.318	-0.359	-0.363	-0.463	-0.334
160	-0.302	-0.341	-0.340	-0.413	-0.304
170	-0.281	-0.332	-0.305	-0.333	-0.294
180	-0.275	-0.306	-0.279	-0.274	-0.275
190	-0.271	-0.266	-0.254	-0.292	-0.250
200	-0.252	-0.214	-0.181	-0.246	-0.138
210	-0.185	-0.197	-0.131	-0.208	-0.114
220	-0.184	-0.192	-0.121	-0.143	-0.112
230	-0.192	-0.194	-0.132	-0.209	-0.129
240	-0.247	-0.204	-0.204	-0.267	-0.269
250	-0.275	-0.285	-0.265	-0.296	-0.291
260	-0.317	-0.329	-0.292	-0.301	-0.313
270	-0.330	-0.343	-0.330	-0.363	-0.342
280	-0.335	-0.352	-0.353	-0.403	-0.387
290	-0.365	-0.361	-0.380	-0.431	-0.401
300	-0.416	-0.451	-0.498	-0.468	-0.443
310	-0.462	-0.563	-0.395	-0.548	-0.578
320	-0.381	-0.491	-0.363	-0.484	-0.391
330	-0.318	-0.359	-0.340	-0.463	-0.334
340	-0.302	-0.341	-0.305	-0.413	-0.309
350	-0.218	-0.331	-0.279	-0.333	-0.294
360	-0.275	-0.306	-0.254	-0.274	-0.275

A_o	A_2	A_4	δ	T
-0.299	0.107	0.015	-0.76	
-0.32	0.133	0.013	-20.75	
-0.36	0.165	0.017	-17.46	
-0.25	0.181	0.010	-17.448	
-0.29	0.15	0.007	-21.09	

Table 15: $Ni_{85}Co_{15}$, S.W = 0.00003 gm, 1.2×10^{-5} Torr, Thickness = 345Å, Temperature = 100^0C

θ	1 amp	2 amp	3 amp	4 amp	5 amp
0	-0.260	-0.299	-0.271	-0.302	-0.280
10	-0.255	-0.237	-0.254	-0.259	-0.261
20	-0.253	-0.205	-0.250	-0.225	-0.224
30	-0.223	-0.175	-0.237	-0.207	-0.215
40	-0.178	-0.166	-0.231	-0.198	-0.206
50	-0.227	-0.170	-0.249	-0.209	-0.221
60	-0.242	-0.206	-0.251	-0.254	-0.231
70	-0.248	-0.241	-0.269	-0.284	-0.279
80	-0.254	-0.258	-0.283	-0.296	-0.298
90	-0.291	-0.317	-0.294	-0.341	-0.302
100	-0.307	-0.358	-0.303	-0.360	-0.322
110	-0.342	-0.379	-0.365	-0.368	-0.338
120	-0.346	-0.405	-0.397	-0.401	-0.395
130	-0.384	-0.455	-0.463	-0.493	-0.512
140	-0.378	-0.435	-0.406	-0.415	-0.347
150	-0.350	-0.391	-0.348	-0.369	-0.328
160	-0.320	-0.370	-0.328	-0.366	-0.305
170	-0.271	-0.328	-0.297	-0.351	-0.301
180	-0.253	-0.308	-0.287	-0.335	-0.285
190	-0.255	-0.237	-0.254	-0.259	-0.261
200	-0.253	-0.205	-0.250	-0.225	-0.224
210	-0.223	-0.175	-0.237	-0.207	-0.215
220	-0.178	-0.166	-0.231	-0.198	-0.206
230	-0.227	-0.170	-0.249	-0.204	-0.221
240	-0.242	-0.206	-0.251	-0.254	-0.231
250	-0.248	-0.241	-0.269	-0.284	-0.279
260	-0.254	-0.258	-0.283	-0.296	-0.298
270	-0.291	-0.317	-0.294	-0.341	-0.302
280	-0.307	-0.358	-0.303	-0.360	-0.322
290	-0.346	-0.379	-0.365	-0.368	-0.338
300	-0.384	-0.405	-0.397	-0.401	-0.395
310	-0.399	-0.455	-0.463	-0.493	-0.512
320	-0.378	-0.435	-0.406	-0.415	-0.347
330	-0.350	-0.391	-0.348	-0.369	-0.328
340	-0.271	-0.370	-0.327	-0.366	-0.305
350	-0.253	-0.308	-0.297	-0.351	-0.301
360	-0.225	-0.279	-0.287	-0.335	-0.205

A_o	A_2	A_4	δ	T
-0.39	0.19	0.008	7.45	
-0.30	0.13	0.003	8.41	
-0.31	0.08	0.003	-16.62	
-0.32	0.11	0.006	2.4	
-0.30	0.016	0.015	-15.55	

Table 16: $Ni_{85}Co_{15}$, S.W = 0.00003 gm, 1.2×10^{-5} Torr, Thickness = 345Å, Temperature = 125^0C

θ	1 amp	2 amp	3 amp	4 amp	5 amp
0	-0.251	-0.295	-0.260	-0.237	-0.343
10	-0.247	-0.276	-0.239	-0.210	-0.318
20	-0.207	-0.176	-0.231	-0.187	-0.285
30	-0.168	-0.129	-0.229	-0.160	-0.257
40	-0.160	-0.128	-0.226	-0.148	-0.254
50	-0.156	-0.109	-0.228	-0.165	-0.258
60	-0.173	-0.128	-0.235	-0.169	-0.293
70	-0.234	-0.131	-0.265	-0.187	-0.331
80	-0.248	-0.161	-0.265	-0.205	-0.358
90	-0.284	-0.220	-0.291	-0.247	-0.393
100	-0.301	-0.246	-0.308	-0.306	-0.398
110	-0.333	-0.260	-0.327	-0.326	-0.423
120	-0.403	-0.328	-0.338	-0.341	-0.428
130	-0.461	-0.341	-0.340	-0.353	-0.411
140	-0.476	-0.354	-0.298	-0.284	-0.395
150	-0.465	-0.347	-0.280	-0.238	-0.392
160	-0.374	-0.320	-0.272	-0.210	-0.347
170	-0.260	-0.266	-0.261	-0.191	-0.343
180	-0.253	-0.251	-0.258	-0.188	-0.329
190	-0.247	-0.276	-0.239	-0.210	-0.318
200	-0.207	-0.176	-0.231	-0.187	-0.285
210	-0.168	-0.129	-0.229	-0.160	-0.257
220	-0.160	-0.128	-0.226	-0.148	-0.254
230	-0.156	-0.109	-0.228	-0.165	-0.258
240	-0.173	-0.128	-0.238	-0.169	-0.293
250	-0.234	-0.131	-0.255	-0.187	-0.331
260	-0.248	-0.161	-0.265	-0.205	-0.358
270	-0.284	-0.220	-0.291	-0.247	-0.393
280	-0.301	-0.260	-0.308	-0.306	-0.398
290	-0.333	-0.328	-0.327	-0.326	-0.0423
300	-0.403	-0.341	-0.338	-0.341	-0.428
310	-0.461	-0.354	-0.348	-0.353	-0.436
320	-0.476	-0.347	-0.298	-0.284	-0.411
330	-0.465	-0.320	-0.280	-0.238	-0.395
340	-0.374	-0.266	-0.272	-0.210	-0.392
350	-0.260	-0.260	-0.261	-0.191	-0.347
360	-0.253	-0.251	-0.258	-0.188	-0.329

A_o	A_2	A_4	δ	T
-0.29	0.14	0.03	16.69	
-0.24	0.11	0.009	11.23	
-0.27	0.05	0.012	7.75	
-0.23	0.08	0.013	0.81	
-0.35	0.09	0.015	-20.03	

Table 17: $Ni_{85}Co_{15}$, S.W = 0.00003 gm, 1.2×10^{-5} Torr, Thickness = 345Å, Temperature = 150^0C

θ	1 amp	2 amp	3 amp	4 amp	5 amp
0	-0.241	-0.316	-0.338	-0.324	-0.293
10	-0.224	-0.309	-0.301	-0.321	-0.281
20	-0.204	-0.300	-0.278	-0.316	-0.276
30	-0.192	-0.283	-0.272	-0.309	-0.272
40	-0.185	-0.280	-0.259	-0.290	-0.267
50	-0.198	-0.283	-0.263	-0.316	-0.276
60	-0.212	-0.300	-0.275	-0.326	-0.293
70	-0.242	-0.305	-0.289	-0.333	-0.326
80	-0.265	-0.312	-0.322	-0.350	-0.338
90	-0.299	-0.330	-0.368	-0.357	-0.360
100	-0.309	-0.341	-0.`378	-0.361	-0.367
110	-0.311	-0.369	-0.386	-0.366	-0.373
120	-0.332	-0.397	-0.410	-0.372	-0.374
130	-0.337	-0.431	-0.447	-0.376	-0.382
140	-0.314	-0.392	-0.444	-0.364	-0.380
150	-0.294	-0.372	-0.396	-0.357	-0.358
160	-0.273	-0.351	-0.379	-0.335	-0.328
170	-0.255	-0.336	-0.374	-0.317	-0.317
180	-0.247	-0.326	-0.334	-0.307	-0.308
190	-0.224	-0.309	-0.301	-0.321	-0.281
200	-0.204	-0.300	-0.278	-0.316	-0.276
210	-0.192	-0.283	-0.272	-0.309	-0.272
220	-0.185	-0.280	-0.259	-0.290	-0.267
230	-0.198	-0.283	-0.263	-0.316	-0.276
240	-0.212	-0.300	-0.275	-0.325	-0.293
250	-0.242	-0.305	-0.289	-0.333	-0.326
260	-0.265	-0.312	-0.322	-0.350	-0.338
270	-0.299	-0.330	-0.386	-0.357	-0.360
280	-0.309	-0.341	-0.378	-0.361	-0.367
290	-0.311	-0.369	-0.386	-0.366	-0.323
300	-0.332	-0.397	-0.410	-0.372	-0.379
310	-0.337	-0.431	-0.447	-0.376	-0.387
320	-0.314	-0.392	-0.444	-0.364	-0.380
330	-0.294	-0.372	-0.396	-0.357	-0.358
340	-0.273	-0.351	-0.379	-0.335	-0.328
350	-0.255	-0.336	-0.374	-0.317	-0.317
360	-0.247	-0.326	-0.334	-0.307	-0.308

A_o	A_2	A_4	δ	T
-0.26	0.070	0.007	15.68	
-0.334	0.057	0.004	-17.96	
-0.343	0.045	0.002	15.69	
-0.335	0.041	0.006	-18.03	
-0.3265	0.058	0.005	-12.89	

Table 18: $Ni_{85}Co_{15}$, S.W = 0.00003 gm, 1.2×10^{-5} Torr, Thickness = 345Å, Temperature = 165^0C

θ	1 amp	2 amp	3 amp	4 amp	5 amp
0	-0.283	-0.275	-0.168	-0.233	-0.149
10	-0.259	-0.255	-0.124	-0.146	-0.144
20	-0.250	-0.193	-0.121	-0.034	-0.145
30	-0.201	-0.185	-0.100	-0.034	-0.188
40	-0.186	-0.182	-0.093	-0.024	-0.120
50	-0.197	-0.188	-0.122	-0.044	-0.127
60	-0.205	-0.230	-0.127	-0.075	-0.183
70	-0.259	-0.271	-0.180	-0.216	-0.195
80	-0.270	-0.280	-0.201	-0.262	-0.198
90	-0.289	-0.288	-0.244	-0.269	-0.229
100	-0.313	-0.289	-0.271	-0.275	-0.254
110	-0.320	-0.296	-0.279	-0.284	-0.259
120	-0.348	-0.306	-0.287	-0.288	-0.271
130	-0.354	-0.320	-0.301	-0.294	-0.276
140	-0.323	-0.311	-0.291	-0.293	-0.261
150	-0.313	-0.302	-0.277	-0.287	-0.249
160	-0.304	-0.297	-0.263	-0.281	-0.234
170	-0.293	-0.279	-0.215	-0.286	-0.215
180	-0.281	-0.267	-0.197	-0.245	-0.201
190	-0.259	-0.255	-0.124	-0.146	-0.194
200	-0.250	-0.193	-0.121	-0.039	-0.145
210	-0.201	-0.185	-0.100	-0.034	-0.118
220	-0.186	-0.182	-0.093	-0.024	-0.120
230	-0.197	-0.188	-0.122	-0.044	-0.127
240	-0.205	-0.230	-0.127	-0.075	-0.183
250	-0.259	-0.271	-0.180	-0.216	-0.195
260	-0.270	-0.280	-0.201	-0.262	-0.198
270	-0.289	-0.288	-0.244	-0.289	-0.229
280	-0.313	-0.289	-0.271	-0.275	-0.254
290	-0.320	-0.296	-0.279	-0.284	-0.259
300	-0.348	-0.306	-0.287	-0.288	-0.275
310	-0.354	-0.320	-0.301	-0.294	-0.276
320	-0.323	-0.311	-0.291	-0.293	-0.261
330	-0.313	-0.302	-0.277	-0.287	-0.249
340	-0.304	-0.297	-0.263	-0.281	-0.239
350	-0.293	-0.279	-0.215	-0.268	-0.215
360	-0.281	-0.267	-0.197	-0.245	-0.201

A_o	A_2	A_4	δ	T (165)
-0.276	0.068	0.013	16.69	
-0.264	0.059	0.020	-11.98	
-0.204	0.098	0.012	-6.48	
-0.207	0.121	0.015	-13.09	
-0.200	0.160	0.019	15.72	

Table 19: $Ni_{85}Co_{15}$, S.W = 0.00003 gm, 1.2×10^{-5} Torr, Thickness = 345Å, Temperature = 180^0C

θ	1 amp	2 amp	3 amp	4 amp	5 amp
0	-0.126	-0.175	-0.118	-0.182	-0.163
10	-0.101	-0.121	-0.075	-0.177	-0.125
20	-0.099	-0.083	-0.062	-0.123	-0.058
30	-0.079	-0.072	-0.037	-0.119	-0.008
40	-0.085	-0.065	-0.117	-0.116	-0.004
50	-0.102	-0.076	-0.150	-0.129	-0.023
60	-0.104	-0.080	-0.189	-0.132	-0.031
70	-0.143	-0.093	-0.199	-0.157	-0.045
80	-0.162	-0.112	-0.220	-0.177	-0.078
90	-0.170	-0.135	-0.234	-0.194	-0.113
100	-0.218	-0.188	-0.237	-0.208	-0.142
110	-0.221	-0.208	-0.241	-0.220	-0.148
120	-0.235	-0.238	-0.247	-0.247	-0.223
130	-0.260	-0.247	-0.251	-0.255	-0.249
140	-0.231	-0.244	-0.238	-0.250	-0.265
150	-0.211	-0.227	-0.220	-0.224	-0.237
160	-0.163	-0.222	-0.196	-0.175	-0.181
170	-0.149	-0.206	-0.186	-0.158	-0.169
180	-0.139	-0.185	-0.135	-0.135	-0.128
190	-0.101	-0.121	-0.075	-0.177	-0.125
200	-0.099	-0.083	-0.062	-0.123	-0.058
210	-0.074	-0.072	-0.037	-0.119	-0.008
220	-0.085	-0.065	-0.117	-0.116	-0.004
230	-0.102	-0.076	-0.150	-0.129	-0.023
240	-0.104	-0.080	-0.189	-0.132	-0.031
250	-0.143	-0.093	-0.199	-0.157	-0.045
260	-0.162	-0.112	-0.220	-0.177	-0.078
270	-0.170	-0.135	-0.234	-0.194	-0.113
280	-0.218	-0.185	-0.237	-0.208	-0.142
290	-0.221	-0.208	-0.241	-0.220	-0.148
300	-0.235	-0.238	-0.247	-0.247	-0.223
310	-0.260	-0.247	-0.251	-0.255	-0.265
320	-0.231	-0.227	-0.238	-0.250	-0.237
330	-0.211	-0.222	-0.220	-0.224	-0.181
340	-0.113	-0.206	-0.196	0.175	-0.169
350	-0.149	-0.185	-0.186	-0.156	-0.128
360	-0.139	-0.121	-0.135	-0.135	-0.125

A_o	A_2	A_4	δ	T(180)
-0.152	0.094	0.008	-17.57	
-0.159	0.092	0.0063	-11.03	
-0.179	0.088	0.003	1.37	
-0.179	0.081	0.007	-10.49	
-0.119	0.106	0.005	-5.37	

Table 20: $Ni_{85}Co_{15}$, S.W = 0.00003 gm, 1.2×10^{-5} Torr, Thickness = 345Å, Temperature = 195^0C

θ	1 amp	2 amp	3 amp	4 amp	5 amp
0	-0.118	-0.098	-0.140	-0.109	-0.119
10	-0.089	-0.085	-0.082	-0.085	-0.091
20	-0.086	-0.059	-0.007	-0.055	-0.076
30	-0.073	-0.046	-0.005	-0.036	-0.072
40	-0.091	-0.041	-0.044	-0.013	-0.039
50	-0.095	-0.054	-0.099	-0.037	-0.059
60	-0.164	-0.067	-0.125	-0.057	-0.076
70	-0.168	-0.084	-0.166	-0.112	-0.085
80	-0.183	-0.115	-0.177	-0.155	-0.095
90	-0.190	-0.171	-0.181	-0.169	-0.149
100	-0.195	-0.182	-0.191	-0.179	-0.183
110	-0.210	-0.201	-0.202	-0.201	-0.199
120	-0.219	-0.206	-0.212	-0.217	-0.210
130	-0.230	-0.219	-0.224	-0.230	-0.231
140	-0.221	-0.205	-0.195	-0.211	-0.211
150	-0.213	-0.191	-0.183	-0.195	-0.134
160	-0.189	-0.178	-0.178	-0.161	-0.126
170	-0.172	-0.163	-0.167	-0.131	-0.119
180	-0.167	-0.104	-0.146	-0.107	-0.101
190	-0.089	-0.085	-0.082	-0.085	-0.091
200	-0.086	-0.059	-0.007	-0.055	-0.076
210	-0.073	-0.046	-0.005	-0.036	-0.072
220	-0.091	-0.041	-0.044	-0.013	-0.031
230	-0.095	-0.054	-0.099	-0.0.37	-0.059
240	-0.164	-0.067	-0.125	-0.057	-0.076
250	-0.168	-0.084	-0.166	-0.112	-0.085
260	-0.183	-0.115	-0.177	-0.155	-0.095
270	-0.190	-0.171	-0.181	-0.169	-0.149
280	-0.195	-0.182	-0.191	-0.179	-0.188
290	-0.210	-0.201	-0.202	-0.201	-0.199
300	-0.219	-0.206	-0.212	-0.217	-0.210
310	-0.230	-0.219	-0.224	-0.230	-0.231
320	-0.221	-0.205	-0.195	-0.211	-0.211
330	-0.213	-0.191	-0.183	-0.195	-0.034
340	-0.189	-0.178	-0.178	-0.161	-0.026
350	-0.172	-0.163	-0.167	-0.131	-0.199
360	-0.167	-0.104	-0.146	-0.107	-0.010

A_o	A_2	A_4	δ	T
-0.163	0.0695	0.0199	-0.376	
-0.131	0.0882	0.0047	-16.88	
-0.143	0.0853	0.0032	-5.22	
-0.131	0.0951	0.0092	-16.87	
-0.125	0.0774	0.0018	-2.27	

Table 21: $Ni_{85}Co_{15}$, S.W = 0.00003 gm, 1.2×10^{-5} Torr, Thickness = 345Å, Temperature = 210^0C

θ	1 amp	2 amp	3 amp	4 amp	5 amp
0	-0.065	-0.184	-0.103	-0.103	-0.880
10	-0.059	-0.110	-0.098	-0.101	-0.065
20	-0.036	-0.097	-0.054	-0.090	-0.051
30	-0.021	-0.071	-0.040	-0.077	-0.034
40	-0.016	-0.060	-0.034	-0.058	-0.020
50	-0.025	-0.082	-0.038	-0.070	-0.037
60	-0.052	-0.110	-0.066	-0.086	-0.061
70	-0.060	-0.141	-0.096	-0.121	-0.075
80	-0.066	-0.169	-0.114	-0.147	-0.106
90	-0.086	-0.198	-0.142	-0.173	-0.115
100	-0.145	-0.199	-0.161	-0.194	-0.157
110	-0.162	-0.203	-0.172	-0.239	-0.186
120	-0.197	-0.207	-0.193	-0.260	-0.203
130	-0.200	-0.231	-0.204	-0.251	-0.230
140	-0.162	-0.200	-0.176	-0.249	-0.210
150	-0.149	-0.191	-0.136	-0.237	-0.165
160	-0.089	-0.176	-0.128	-0.186	-0.125
170	-0.075	-0.171	-0.115	-0.146	-0.112
180	-0.060	-0.166	-0.112	-0.108	-0.089
190	-0.059	-0.110	-0.098	-0.101	-0.065
200	-0.036	-0.097	-0.054	-0.090	-0.051
210	-0.021	-0.071	-0.040	-0.077	-0.034
220	-0.016	-0.060	-0.034	-0.058	-0.020
230	-0.025	-0.110	-0.038	-0.070	-0.037
240	-0.052	-0.082	-0.066	-0.086	-0.061
250	-0.060	-0.141	-0.098	-0.121	-0.075
260	-0.066	-0.169	-0.114	-0.147	-0.106
270	-0.086	-0.198	-0.142	-0.173	-0.115
280	-0.145	-0.199	-0.161	-0.194	-0.157
290	-0.162	-0.203	-0.172	-0.239	-0.186
300	-0.197	-1.207	-0.193	-0.260	-0.203
310	-0.200	-1.231	-0.204	-0.251	-0.230
320	-0.162	-0.200	-0.176	-0.249	-0.210
330	-0.162	-0.191	-0.136	-0.237	-0.165
340	-0.149	-0.176	-0.128	-0.186	-0.125
350	-0.089	-0.171	-0.115	-0.146	-0.115
360	-0.075	-0.116	-0.112	-0.108	-0.086

A_o	A_2	A_4	δ	T (210)
-0.096	0.073	0.025	-13.90	
-0.154	0.069	0.017	-17.42	
-0.115	0.071	0.012	13.70	
-0.154	0.097	0.016	-12.82	
-0.217	0.097	0.015	-20.33	

Table 22: $Ni_{85}Co_{15}$, S.W = 0.00003 gm, 1.2×10^{-5} Torr, Thickness = 345Å, Temperature = 25^0C

θ	1 amp	2 amp	3 amp	4 amp	5 amp
0	-0.888	-1.104	-1.106	-1.103	-1.170
10	-0.849	-1.092	-1.103	-1.100	-1.098
20	-0.839	-1.085	-1.102	-1.099	-1.093
30	-0.826	-1.081	-1.101	-1.098	-1.092
40	-0.823	-1.074	-1.101	-1.096	-1.090
50	-0.835	-1.076	-1.102	-1.0.98	-1.091
60	-0.846	-1.078	-1.102	-1.100	-1.092
70	-0.850	-1.089	-1.105	-1.130	-1.093
80	-0.873	-1.111	-1.118	-1.149	-1.094
90	-0.904	-1.117	-1.128	-1.157	-1.151
100	-0.915	-1.118	-1.131	-1.160	-1.185
110	-0.929	-1.121	-1.135	-1.169	-1.191
120	-0.941	-1.128	-1.158	-1.183	-1.209
130	-0.946	-1.140	-1.161	-1.216	-1.217
140	-0.946	-1.129	-1.146	-1.181	-1.173
150	-0.931	-1.121	-1.136	-1.161	-1.171
160	-0.916	-1.118	-1.127	-1.159	-1.168
170	-0.905	-1.144	-1.120	-1.151	-1.165
180	-0.900	-1.111	-1.109	-1.108	-1.152
190	-0.849	-1.092	-1.103	-1.100	-1.098
200	-0.839	-1.085	-1.102	-1.099	-1.093
210	-0.826	-1.081	-1.101	-1.098	-1.092
220	-0.823	-1.074	-1.101	-1.096	-1.090
230	-0.835	-1.078	-1.102	-1.098	-1.091
240	-0.846	-1.089	-1.102	-1.100	-1.092
250	-0.850	-1.111	-1.105	-1.130	-1.093
260	-0.873	-1.117	-1.118	-1.149	-1.094
270	-0.904	-1.118	-1.128	-1.157	-1.151
280	-0.915	-1.121	-1.131	-1.160	-1.185
290	-0.929	-1.125	-1.135	-1.169	-1.191
300	-0.941	-1.128	-1.158	-1.183	-1.209
310	-0.946	-1.140	-1.161	-1.216	-1.217
320	-0.931	-1.129	-1.146	-1.181	-1.173
330	-0.916	-1.121	-1.136	-1.161	-1.171
340	-0.910	-1.118	-1.127	-1.159	-1.168
350	-0.905	-1.114	-1.120	-1.151	-1.165
360	-0.900	-1.111	-1.109	-1.108	-1.152

A_o	A_2	A_4	δ	T(86)
-0.877	0.084	0.014	-19.38	
-1.107	0.066	0.005	915.95	
-1.109	0.061	0.069	-1.435	
-1.167	0.081	0.013	-9.760	
-1.138	0.091	0.015	4.870	

Table 23: $Ni_{85}Co_{15}$, S.W = 0.00003 gm, 1.2×10^{-5} Torr, Thickness = 345Å, Temperature = 50^0C

θ	1 amp	2 amp	3 amp	4 amp	5 amp
0	-1.090	-1.106	-1.097	-1.089	-1.204
10	-1.088	-1.104	-1.095	-1.080	-1.188
20	-1.087	-1.101	-1.087	-1.054	-1.183
30	-1.086	-1.097	-1.082	-1.040	-1.183
40	-1.085	-1.095	-1.073	-1.029	-1.185
50	-1.087	-1.098	-1.094	-1.052	-1.197
60	-1.088	-1.102	-1.095	-1.068	-1.201
70	-1.093	-1.103	-1.102	-1.078	-1.233
80	-1.096	-1.105	-1.105	-1.079	-1.242
90	-1.098	-1.110	-1.119	-1.093	-1.273
100	-1.101	-1.132	-1.128	-1.122	-1.281
110	-1.112	-1.164	-1.150	-1.142	-1.284
120	-1.121	-1.184	-1.171	-1.182	-1.338
130	-1.132	-1.204	-1.029	-1.219	-1.313
140	-1.121	-1.192	-1.184	-1.175	-1.244
150	-1.113	-1.141	-1.120	-1.156	-1.239
160	-1.103	-1.125	-1.109	-1.105	-1.230
170	-1.100	-1.119	-1.102	-1.094	-1.206
180	-1.097	-1.112	-1.098	-1.091	-1.197
190	-1.088	-1.104	-1.095	-1.080	-1.188
200	-1.087	-1.101	-1.087	-1.054	-1.184
210	-1.086	-1.097	-1.082	-1.040	-1.183
220	-1.085	-1.095	-1.073	-1.029	-1.185
230	-1.087	-1.098	-1.084	-1.052	-1.197
240	-1.088	-1.102	-1.095	-1.068	-1.1201
250	-1.093	-1.103	-1.102	-1.078	-1.233
260	-1.096	-1.105	-1.105	-1.079	-1.242
270	-1.098	-1.110	-1.119	-1.093	-1.273
280	-1.101	-1.132	-1.128	-1.122	-1.281
290	-1.112	-1.164	-1.150	-1.142	-1.284
300	-1.121	-1.184	-1.171	-1.182	-1.338
310	-1.132	-1.204	-1.209	-1.219	-1.313
320	-1.122	-1.192	-1.184	-1.175	-1.244
330	-1.113	-1.141	-1.120	-1.156	-1.239
340	-1.103	-1.125	-1.109	-1.105	-1.230
350	-1.100	-1.119	-1.102	-1.094	-1.200
360	-1.097	-1.112	-1.098	-1.091	-1.197

A_o	A_2	A_4	δ	T(50)
-1.100	0.058	0.006	-20.61	
-1.127	0.043	0.019	-15.75	
-1.118	0.045	0.017	-15.30	
-1.103	0.062	0.015	-18.58	
-1.223	0.068	0.017	6.24	

Table 24: $Ni_{85}Co_{15}$, S.W = 0.00003 gm, 1.2×10^{-5} Torr, Thickness = 345Å, Temperature = 75^0C

θ	1 amp	2 amp	3 amp	4 amp	5 amp
0	-1.188	-0.829	-1.372	-1.403	-1.370
10	-1.184	-0.813	-1.369	-1.378	-1.349
20	-1.173	-0.810	-1.350	-1.333	-1.304
30	-1.165	-0.807	-1.311	-1.320	-1.289
40	-1.156	-0.777	-1.307	-1.255	-1.253
50	-1.167	-0.808	-1.321	-1.295	-1.259
60	-1.174	-0.811	-1.352	-1.331	-1.295
70	-1.182	-0.814	-1.367	-1.371	-1.305
80	-1.194	-0.832	-1.431	-1.385	-1.345
90	-1.199	-0.834	-1.513	-1.432	-1.465
100	-1.222	-0.839	-1.526	-1.606	-1.586
110	-1.228	-0.878	-1.547	-1.612	-1.608
120	-1.236	-0.890	-1.553	-1.622	-1.619
130	-1.248	-0.930	-1.560	-1.656	-1.664
140	-1.234	-0.885	-1.557	-1.615	-1.620
150	-1.225	-0.863	-1.541	-1.611	-1.610
160	-1.219	-0.838	-1.521	-1.436	-1.597
170	-1.209	-0.833	-1.470	-1.427	-1.479
180	-1.195	-0.831	-1.396	-1.389	-1.458
190	-1.184	-0.813	-1.369	-1.378	-1.349
200	-1.173	-0.810	-1.350	-1.335	-1.304
210	-1.165	-0.807	-1.311	-1.320	-1.289
220	-1.156	-0.777	-.307	-1.255	-1.253
230	-1.167	-0.808	-1.321	-0.295	-1.259
240	-1.174	-0.811	-1.352	-1.337	-1.295
250	-1.182	-0.814	-1.367	-1.371	-1.305
260	-1.194	-0.832	-1.431	-1385	-1.345
270	-1.199	-0.834	-1.513	-1.432	-1.465
280	-1.228	-0.839	-1.526	-1.606	-1.586
290	-1.228	-0.878	-1.547	-1.612	-1.608
300	-1.236	-0.890	-1.553	-1.622	-1.619
310	-1.248	-0.930	-1.560	-1.656	-1.664
320	-1.234	-0.885	-1.554	-1.615	-1.620
330	-1.225	-0.863	-1.541	-1.611	-1.610
340	-1.219	-0.838	-1.521	-1.436	-1.597
350	-1.209	-0.833	-1.470	-1.427	-1.479
360	-1.195	-0.831	-1.396	-1.389	-1.458

A_o	A_2	A_4	δ	T(75^0C)
-1.167	0.051	0.051	14.63	
-0.838	0.047	0.013	-15.83	
-1.436	0.133	0.004	12.61	
-1.449	0.175	0.032	-7.50	
-1.430	0.171	0.035	12.36	

Table 25: $Ni_{85}Co_{15}$, S.W = 0.00003 gm, 1.2×10^{-5} Torr, Thickness = 345Å, Temperature = 100^0C

θ	1 amp	2 amp	3 amp	4 amp	5 amp
0	-0.280	-0.378	-0.756	-0.757	-0.543
10	-0.279	-0.378	-0.753	-0.740	-0.504
20	-0.259	-0.376	-0.752	-0.738	-0.501
30	-0.208	-0.355	-0.751	-0.736	-0.499
40	-0.134	-0.291	-0.724	-0.729	-0.493
50	-0.143	-0.344	-0.749	-0.736	-0.494
60	-0.252	-0.360	-0.752	-0.736	-0.498
70	-0.278	-0.377	-0.754	-0.739	-0.503
80	-0.280	-0.378	-0.754	-0.742	-0.509
90	-0.283	-0.378	-0.775	-0.780	-0.543
100	-0.314	-0.393	-0.777	-0.781	-0.547
110	-0.340	-0.401	-0.796	-0.788	-0.558
120	-0.354	-0.413	-0.806	-0.806	-0.579
130	-0.371	-0.445	-0.821	-0.832	-0.588
140	-0.345	-0.418	-0.792	-0.806	-0.569
150	-0.321	-0.402	-0.774	-0.804	-0.557
160	-0.292	-0.399	-0.775	-0.782	-0.549
170	-0.283	-0.397	-0.771	-0.780	-0.546
180	-0.281	-0.385	-0.764	-0.776	-0.543
190	-0.279	-0.378	-0.753	-0.750	-0.504
200	-0.259	-0.376	-0.752	-0.738	-0.501
210	-0.208	-0.355	-0.751	-0.736	-0.499
220	-0.134	-0.291	-0.724	-0.729	-0.493
230	-0.143	-0.344	-0.749	-0.736	-0.494
240	-0.252	-0.360	-0.752	-0.736	-0.498
250	-0.278	-0.377	-0.754	-0.737	-0.503
260	-0.280	-0.378	-0.754	-0.742	-0.509
270	-0.283	-0.378	-0.775	-0.780	-0.543
280	-0.314	-0.393	-0.777	-0.781	-0.547
290	-0.340	-0.401	-0.796	-0.788	-0.558
300	-0.354	-0.413	-0.808	-0.806	-0.579
310	-0.371	-0.445	-0.821	-0.832	-0.588
320	-0.345	-0.418	-0.792	-0.806	-0.569
330	-0.321	-0.399	-0.779	-0.804	-0.557
340	-0.292	-0.397	-0.775	-0.782	-0.549
350	-0.283	-0.385	-0.771	-0.780	-0.546
360	-0.292	-0.378	-0.764	-0.780	-0.543

A_o	A_2	A_4	δ	T(100)
-0.279	0.038	0.018	18.50	
-0.382	0.039	0.005	-20.67	
-0.768	0.030	0.007	-14.29	
-0.768	0.042	0.006	-18.69	
-0.532	0.043	0.004	-6.63	

Table 26: $Ni_{85}Co_{15}$, S.W = 0.00003 gm, 1.2×10^{-5} Torr, Thickness = 345Å, Temperature = 125^0C

θ	1 amp	2 amp	3 amp	4 amp	5 amp
0	-0.762	-0.796	-0.792	-0.889	-0.557
10	-.761	-0.795	-0.792	-0.850	-0.501
20	-.760	-0.794	-0.791	-0.848	-0.496
30	-0.717	-0.791	-0.788	-0.846	-0.493
40	-0.761	-0.767	-0.761	-0.831	-0.492
50	-0.761	-0.789	-0.787	-0.844	-0.492
60	-0.762	-0.794	-0.791	-0.847	-0.495
70	-0.762	-0.795	-0.792	-0.848	-0.499
80	-0.781	-0.798	-0.794	-0.852	-0.517
90	-0.783	-0.819	-0.817	-0.896	-0.558
100	-0.805	-0.822	-0.825	-0.901	-0.562
110	-0.807	-0.826	-0.842	-0.915	-0.566
120	-0.810	-0.836	-0.857	-0.926	-0.570
130	-0.842	-0.895	-0.882	-0.966	-0.614
140	-0.819	-0.839	-0.856	-0.927	-0.586
150	-0.785	-0.835	-0.846	-0.815	-0.573
160	-0.782	-0.825	-0.826	-0.904	-0.566
170	-0.780	-0.826	-0.822	-0.898	-0.559
180	-0.762	-0.796	-0.817	-0.894	-0.549
190	-0.761	-0.795	-0.792	-0.850	-0.501
200	-0.760	-0.794	-0.791	-0.848	-0.496
210	-0.717	-0.791	-0.788	-0.846	-0.493
220	-0.761	-0.767	-0.761	-0.831	-0.492
230	-0.761	-0.789	-0.787	-0.844	-0.492
240	-0.762	-0.794	-0.791	-0.847	-0.495
250	-0.762	-0.795	-0.792	-0.848	-0.499
260	-0.781	-0.798	-0.799	-0.852	-0.517
270	-0.783	-0.819	-0.819	-0.896	-0.558
280	-0.805	-0.822	-0.825	-0.901	-0.562
290	-0.749	-0.826	-0.842	-0.915	-0.566
300	-0.810	-0.836	-0.857	-0.926	-0.570
310	-0.842	-0.895	-0.882	-0.966	-0.614
320	-0.819	-0.839	-0.856	-0.927	-0.586
330	-0.785	-0.835	-0.846	-0.915	-0.573
340	-0.782	-0.825	-0.826	-0.904	-0.566
350	-0.780	-0.820	-0.822	-0.898	-0.559
360	-0.762	-0.796	-0.817	-0.894	-0.549

A_o	A_2	A_4	δ	T(125)
-0.781	0.036	0.005	18.01	
-0.798	0.031	0.007	9.05	
-0.815	0.041	0.007	-18.18	
-0.884	0.051	0.006	-13.47	
-0.867	0.053	0.005	-10.96	

Table 27: $Ni_{85}Co_{15}$, S.W = 0.00003 gm, 1.2×10^{-5} Torr, Thickness = 345Å, Temperature = 150^0C

θ	1 amp	2 amp	3 amp	4 amp	5 amp
0	-0.571	-0.580	-0.564	-0.538	-0.541
10	-0.555	-0.574	-0.563	-0.509	-0.519
20	-0.554	-0.570	-0.562	-0.506	-0.518
30	-0.553	-0.569	-0.561	-0.504	-0.516
40	-0.529	-0.568	-0.539	-0.459	-0.516
50	-0.554	-0.569	-0.561	-0.502	-0.517
60	-0.554	-0.570	-0.562	-0.506	-0.518
70	-0.556	-0.572	-0.563	-0.508	-0.532
80	-0.574	-0.579	-0.587	-0.511	-0.554
90	-0.579	-0.588	-0.593	-0.538	-0.564
100	-0.581	-0.592	-0.595	-0.550	-0.567
110	-0.602	-0.598	-0.609	-0.552	-0.581
120	-0.619	-0.614	-0.615	-0.581	-0.588
130	-0.641	-0.681	-0.655	-0.610	-0.625
140	-0.625	-0.623	-0.611	-0.590	-0.582
150	-0.609	-0.610	-0.604	-0.564	-0.574
160	-0.601	-0.598	-0.593	-0.550	-0.565
170	-0.580	-0.591	-0.590	-0.547	-0.561
180	-0.575	-0.582	-0.584	-0.538	-0.554
190	-0.555	-0.574	-0.56.3	-0.509	-0.519
200	-0.554	-0.570	-0.562	-0.506	-0.518
210	-0.553	-0.569	-0.561	-0.504	-0.516
220	-529	-0.568	-0.539	-0.497	-0.516
230	-0.554	-0.569	-0.561	-0.502	-0.517
240	-0.554	-0.570	-0.562	-0.506	-0.518
250	-0.556	-0.572	-0.563	-0.508	-0.532
260	-0.574	-0.579	-0.587	-0.511	-0.554
270	-0.579	-0.588	-0.593	-0.538	-0.561
280	-0.581	-0.592	-0.595	-0.550	-0.567
290	-0.602	-0.598	-0.609	-0.552	-0.581
300	-0.619	-0.614	-0.615	-0.581	-0.588
310	-0.641	-0.681	-0.655	-0.610	-0.625
320	-0.625	-0.623	-0.611	-0.590	-0.582
330	-0.609	-0.610	-0.602	-0.564	-0.574
340	-0.601	-0.598	-0.593	-0.550	-0.565
350	-0.580	-0.591	-590	-0.547	-0.561
360	-0.575	-0.582	-0.584	-0.538	-0.554

A_o	A_2	A_4	δ	T
-0.580	0.039	0.008	18.83	
-0.591	0.031	0.012	-19.61	
-0.573	0.038	0.029	-21.70	
-0.537	0.045	0.006	-19.20	
-0.538	0.067	0.029	3.75	

Table 28: $Ni_{85}Co_{15}$, S.W = 0.00003 gm, 1.2×10^{-5} Torr, Thickness = 345Å, Temperature = 165^0C

θ	1 amp	2 amp	3 amp	4 amp	5 amp
0	-0.549	-0.561	-0.553	-0.553	-0.514
10	-0.547	-0.557	-0.552	-0.552	-0.511
20	-0.542	-0.553	-0.550	-0.550	-0.508
30	-0.541	-0.550	-0.548	-0.539	-0.506
40	-0.522	-0.517	-0.525	-0.519	-0.486
50	-0.542	-0.550	-0.548	-0.547	-0.507
60	-0.545	-0.552	-0.551	-0.549	-0.510
70	-0.548	-0.556	-0.553	-0.550	-0.513
80	-0.550	-0.560	-0.555	-0.554	-0.548
90	-0.571	-0.572	-0.572	-0.576	-0.554
100	-0.575	-0.593	-0.580	-0.586	-0.561
110	-0.595	-0.598	-0.598	-0.610	-0.574
120	-0.607	-0.608	-0.608	-0.618	-0.579
130	-0.637	-0.630	-0.630	-0.644	-0.608
140	-0.598	-0.606	-0.606	-0.623	-0.577
150	-0.573	-0.594	-0.594	-0.596	-0.570
160	-0.571	-0.574	-0.574	-0.586	-0.557
170	-0.568	-0.572	-0.572	-0.582	-0.554
180	-0.557	-0.564	-0.564	-0.574	-0.524
190	-0.547	-0.557	-0.557	-0.550	-0.511
200	-0.542	-0.553	-0.553	-0.539	-0.508
210	-0.541	-0.550	-0.550	-0.519	-506
220	-0.522	-0.517	-0.517	-0.547	-0.486
230	-0.542	-0.550	-0.550	-0.549	-0.507
240	-0.545	-0.552	-0.552	-0.550	-0.510
250	-0.548	-0.556	-0.556	-0.554	-0.513
260	-0.550	-0.570	-0.570	-0.576	-0.548
270	-0.571	-0.572	-0.572	-0.586	-0.554
280	-0.575	-0.593	-0.593	-0.593	-0.561
290	-0.595	-0.598	-0.598	-0.610	-0.574
300	-0.608	-0.508	-0.608	-0.618	-0.579
310	-0.637	-0.630	-0.630	-0.644	-0.608
320	-0.598	-0.606	-0.616	-0.623	-0.577
330	-0.573	-0.594	-0.596	-0.596	-0.570
340	-0.571	-0.574	-0.578	-0.586	-0.557
350	-0.568	-0.572	-0.565	-0.582	-0.554
360	-0.557	-0.564	-0.554	-0.574	-0.511

A_o	A_2	A_4	δ	T(165)
-0.566	0.036	0.009	-12.28	
-0.573	0.035	0.005	-9.93	
-0.574	0.036	0.013	-12.36	
-0.580	0.042	0.003	+10.05	
-0.541	0.045	0.002	-22.17	

Table 29: $Ni_{85}Co_{15}$, S.W = 0.00003 gm, 1.2×10^{-5} Torr, Thickness = 345Å, Temperature = 180^0C

θ	1 amp	2 amp	3 amp	4 amp	5 amp
0	-0.575	-0.567	-0.591	-0.594	-0.502
10	-0.569	-0.563	-0.563	-0.564	-0.501
20	-0.568	-0.560	-0.557	-0.563	-0.499
30	-0.565	-0.549	-0.555	-0.562	-0.498
40	-0.520	-0.518	-0.554	-0.536	-0.496
50	-0.564	-0.558	-0.555	-0.561	-0.498
60	-0.567	-0.560	-0.556	-0.562	-0.500
70	-0.569	-0.563	-0.557	-0.563	-0.510
80	-0.572	-0.565	-0.586	-0.592	-0.543
90	-0.575	-0.586	-0.595	-0.597	-0.543
100	-0.577	-0.587	-0.599	-0.602	-0.550
110	-0.601	-0.600	-0.613	-0.625	-0.573
120	-0.615	-0.623	-0.631	-0.639	-0.581
130	-0.652	-0.673	-0.667	-0.672	-0.615
140	-0.617	-0.625	-0.630	-0.627	-0.566
150	-0.602	-0.619	-0.603	-0.609	-0.548
160	-0.579	-0.589	-0.598	-0.599	-0.545
170	-0.577	-0.587	-0.595	-0.598	-0.536
180	-0.573	-0.574	-0.592	-0.596	-0.502
190	-0.569	-0.563	-0.563	-0.564	-0.501
200	-0.568	-0.560	-0.557	-0.563	-0.499
210	-0.565	-0.549	-0.555	-0.562	-0.498
220	-0.520	-0.518	-0.554	-0.536	-0.496
230	-0.564	-0.558	-0.555	-0.561	-0.498
240	-0.567	-0.560	-0.556	-0.562	-0.500
250	-0.569	-0.563	-0.557	-0.563	-0.510
260	-0.572	-0.565	-0.586	-0.592	-0.541
270	-0.575	-0.584	-0.595	-0.597	-0.546
280	-0.577	-0.587	-0.599	-0.602	-0.550
290	-0.601	-0.600	-0.613	-0.624	-0.573
300	-0.615	-0.623	-0.631	-0.639	-0.581
310	-0.652	-0.673	-0.667	-0.672	-0.615
320	-0.617	-0.625	-0.630	-0.627	-0.588
330	-0.602	-0.619	-0.602	-0.609	-0.548
340	-0.579	-0.589	-0.598	-0.599	-0.545
350	-0.5777	-0.687	-0.595	-0.598	-0.536
360	-0.573	-0.674	-0.592	-0.596	-0.502

A_o	A_2	A_4	δ	T(180)
-0.580	0.030	0.008	-20.50	
-0.583	0.036	0.007	+7.26	
-0.589	0.042	0.007	-10.998	
-0.592	0.046	0.006	-9.43	
-0.534	0.048	0.004	-15.63	

Table 30: $Ni_{85}Co_{15}$, S.W = 0.00003 gm, 1.2×10^{-5} Torr, Thickness = 345Å, Temperature = 195^0C

θ	1 amp	2 amp	3 amp	4 amp	5 amp
0	-0.536	-0.537	-0.503	-0.510	-0.547
10	-0.530	-0.532	-0.502	-0.508	-0.504
20	-0.517	-0.529	-0.500	-0.506	-0.501
30	-0.516	-0.523	-0.498	-0.505	-0.501
40	-0.485	-0.502	-497	-0.503	-0.500
50	-0.516	-0.521	-0.499	-0.504	-0.501
60	-0.517	-0.528	-0.501	-0.505	-0.501
70	-0.519	-0.530	-0.503	-0.507	-0.503
80	-0.535	-0.535	-519	-0.509	-0.512
90	-0.538	-0.547	-0.523	-0.536	-0.549
100	-0.547	-0.549	-0.527	-0.538	-0.550
110	-0.555	-0.567	-0.559	-0.548	-0.567
120	-0.573	-0.581	-0.561	-0.559	-0.585
130	-0.596	-0.609	-0.593	-0.595	-0.601
140	-0.583	-0.595	-0.563	-0.578	-0.593
150	-0.558	-0.568	-0.554	-0.553	-0.576
160	-0.549	-0.550	-0.523	-0.542	-0.554
170	-0.540	-0.548	-0.521	-0.538	-0.549
180	-0.538	-0.544	-0.508	-0.535	-0.548
190	-0.530	-0.532	-0.502	-0.508	-0.504
200	-0.517	-0.529	-0.500	-0.506	-0.501
210	-0.516	-0.523	-0.498	-0.505	-0.501
220	-0.483	-0.502	-0.497	-0.503	-0.500
230	-0.516	-0.521	-0.499	-0.504	-0.501
240	-0.516	-0.528	-0.501	-0.503	-0.501
250	-0.519	-0.530	-0.503	-0.507	-0.503
260	-0.535	-0.535	-0.519	-0.504	-0.512
270	-0.538	-0.547	-0.523	-0.536	-0.549
280	-0.548	-0.549	-0.527	-0.538	-0.550
290	-0.577	-0.567	-0.559	-0.548	-0.567
300	-0.573	-0.581	-0.561	-0.559	-0.585
310	-0.596	-0.609	-0.593	-0.595	-0.601
320	-0.583	-0.595	-0.563	-0.578	-0.594
330	-0.558	-0.568	-0.559	-0.553	-0.576
340	-0.549	-0.550	-0.523	-0.542	-0.554
350	-0.540	-0.548	-0.521	-0.538	-0.549
360	-0.538	-0.544	-0.508	-535	-0.548

A_o	A_2	A_4	δ	T(195)
-0.539	0.035	0.004	-17.54	
-0.547	0.035	0.008	-18.50	
-0.525	0.037	0.012	-18.58	
-0.532	0.035	0.008	-21.39	
-0.538	0.048	0.007	-19.06	

Table 31: $Ni_{85}Co_{15}$, S.W = 0.00003 gm, 1.2×10^{-5} Torr, Thickness = 345Å, Temperature = 210^0C

θ	1 amp	2 amp	3 amp	4 amp	5 amp
0	-0.552	-0.559	-0.554	-0.561	-0.572
10	-0.549	-0.557	-0.553	-0.549	-0.545
20	-0.548	-0.556	-0.551	-0.547	-0.542
30	-0.547	-0.556	-0.550	-0.545	-0.542
40	-0.545	-0.554	-0.531	-0.544	-0.527
50	-0.547	-0.554	-0.550	-0.544	-0.541
60	-0.548	-0.556	-0.551	-0.546	-0.542
70	-0.549	-0.557	-0.552	-0.547	-0.542
80	-0.551	-0.558	-0.554	-0.558	-0.545
90	-0.556	-0.564	-0.562	-0.505	-0.573
100	-0.560	-0.568	-0.567	-0.575	-0.577
110	-0.563	-0.571	-0.581	-0.595	-0.580
120	-0.579	-0.583	-0.600	-0.600	-0.591
130	-0.598	-0.599	-0.609	-0.602	-0.603
140	-0.577	-0.591	-0.695	-0.599	-0.601
150	-0.563	-0.573	-0.587	-0.583	-0.582
160	-0.562	-0.568	-0.574	-0.575	-0.578
170	-0.559	-0.566	-0.568	-0.565	-0.575
180	-0.556	-0.562	-0.562	-0.556	-0.564
190	-0.549	-0.557	-0.553	-0.549	-0.545
200	-0.548	-0.556	-0.551	-0.547	-0.542
210	-0.547	-0.556	-0.550	-0.545	-0.542
220	-0.545	-0.554	-0.531	-0.544	-0.527
230	-0.547	-0.554	-0.550	-0.545	-0.541
240	-0.548	-0.556	-0.551	-0.546	-0.542
250	-0.549	-0.557	-0.552	-0.547	-0.542
260	-0.551	-0.558	-0.554	-0.548	-0.545
270	-0.556	-0.564	-0.562	-0.565	-0.573
280	-0.560	-0.568	-0.567	-0.575	-0.577
290	-0.563	-0.571	-0.581	-0.595	-0.580
300	-0.579	-0.583	-0.600	-0.600	-0.591
310	-0.598	-0.595	-0.609	-0.602	-0.603
320	-0.577	-0.591	-0.595	-0.599	-0.601
330	-0.563	-0.573	-0.587	-0.583	-0.582
340	-0.562	-0.568	-0.574	-0.575	-0.578
350	-0.559	-0.566	-0.568	-0.565	-0.575
360	-0.556	-0.562	-0.562	-0.556	-0.564

A_o	A_2	A_4	δ	T(210)
-0.559	0.017	0.006	-17.57	
-0.566	0.016	0.006	-19.45	
-0.550	0.023	0.003	5.49	
-0.576	0.026	0.004	-12.80	
-0.555	0.033	0.004	-3.58	

Table 32: $Ni_{.95}Co_5$, S.W = 0.00017 gm, 1.2×10^{-5} Torr, Thickness = 1880Å, Temperature = 50^0C

θ	1 amp	2 amp	3 amp	4 amp	5 amp
0	-0.864	-0.994	-0.970	-0.763	-0.908
10	-0.817	-0.963	-0.937	-0.732	-0.832
20	-0.575	-0.744	-0.931	-0.714	-0.777
30	-0.529	-0.508	-0.476	-0.505	-0.571
40	-0.308	-0.415	-0.368	-0.356	-0.454
50	-0.560	-0.502	-0.441	-0.449	-0.627
60	-0.750	-0.645	-0.534	-0.672	-0.712
70	-0.990	-0.806	-0.932	-0.720	-0.839
80	-1.036	-0.956	-0.939	-0.739	-0.889
90	-1.093	-1.010	-1.342	-0.802	-0.935
100	-1.099	-1.162	-1.355	-1.051	-1.041
110	-1.101	-1.311	-1.369	-1.508	-1.575
120	-1.107	-1.395	-1.376	-1.561	-1.604
130	-1.107	-1.541	-1.385	-1.579	-1.632
140	-1.105	-1.450	-1.370	-1.575	-1.621
150	-1.098	-1.330	-1.362	-1.533	-1.589
160	-1.031	-1.302	-1.350	-1.480	-1.565
170	-1.017	-1.047	-1.023	-0.901	-1.185
180	-0.976	-0.970	-0.976	-0.801	-0.959
190	-0.817	-0.963	-0.937	-0.732	-0.832
200	-0.575	-0.074	-0.931	-0.714	-0.777
210	-0.529	-0.508	-0.476	-0.505	-0.571
220	-0.308	-0.415	-0.368	-0.356	-0.451
230	-0.560	-0.502	-0.441	-0.449	-0.627
240	-0.750	-0.645	-0.534	-0.672	-0.712
250	-0.990	-0.806	-0.932	-0.720	-0.839
260	-1.036	-0.956	-0.939	-0.739	-0.889
270	-1.093	-1.010	-1.342	-0.802	-0.935
280	-1.099	-1.162	-1.355	-1.051	-1.041
290	-1.101	-1.311	-1.369	-1.508	-1.575
300	-1.107	-1.395	-1.376	-1.561	-1.604
310	-1.107	-1.541	-1.385	-1.579	-1.632
320	-1.105	-1.450	-1.370	-1.575	-1.621
330	-1.098	-1.330	-1.362	-1.533	-1.589
340	-1.031	-1.302	-1.350	-1.480	-1.565
350	-1.017	-1.040	-1.029	-0.901	-1.185
360	-0.976	-0.970	-0.976	-0.801	-0.959

A_o	A_2	A_4	δ	T (50)
-0.903	0.307	0.141	-14.18	
-0.963	0.347	0.133	-20.02	
-0.998	0.427	0.170	-16.67	
-0.971	0.591	0.080	20.60	
-1.077	0.551	0.076	15.16	

Table 33: $Ni_{.95}Co_5$, S.W = 0.00017 gm, 1.2×10^{-5} Torr, Thickness = 1880Å, Temperature = 100^0C

θ	1 amp	2 amp	3 amp	4 amp	5 amp
0	-1.055	-1.041	-1.051	-1.162	-0.616
10	-0.976	-0.827	-0.922	-1.033	-0.606
20	-0.763	-0.720	-0.863	-0.989	-0.467
30	-0.449	-0.658	-0.602	-0.694	-0.450
40	-0.437	-0.403	-0.408	-0.418	-0.415
50	-0.636	-0.443	-0.477	-0.501	-0.598
60	-0.961	-0.707	-0.907	-0.976	-0.614
70	-0.997	-0.826	-0.959	-0.982	-0.634
80	-1.017	-0.837	-1.050	-1.035	-0.673
90	-1.218	-1.012	-1.438	-1.175	-0.706
100	-1.478	-1.016	-1.494	-1.195	-0.748
110	-1.499	-1.020	-1.559	-1.234	-0.821
120	-1.515	-1.028	-1.586	-1.278	-1.471
130	-1.730	-1.183	-1.819	-1.438	-1.500
140	-1.535	-1.023	-13626	-1.332	-0.856
150	-1.506	-1.017	-1.583	-1.266	-0.772
160	-1.489	-1.013	-1.521	-1.210	-0.737
170	-1.467	-0.928	-1.413	-1.175	-0.673
180	-1.030	-0.873	-1.113	-1.109	-0.646
190	-0.976	-0.827	-0.922	-1.033	-0.606
200	-0.763	-0.720	-0.863	-0.989	-0.467
210	-0.449	-0.658	-0.602	-0.694	-0.450
220	-0.437	-0.403	-0.408	-0.418	-0.415
230	-0.630	-0.443	-0.477	-0.501	-0.598
240	-0.961	-0.707	-0.907	-0.976	-0.614
250	-0.997	-0.826	-0.959	-0.982	-0.634
260	-1.017	-0.837	-1.050	-1.035	-0.673
270	-1.218	-1.012	-1.438	-1.175	-0.706
280	-1.478	-1.016	-1.494	-1.195	-0.748
290	-1.499	-1.020	-1.559	-1.234	-0.821
300	-4.515	-1.028	-1.586	-1.278	-1.471
310	-1.730	-1.183	-1.819	-1.438	-1.500
320	-1.535	-1.023	-1.626	-1.332	-0.856
330	-1.506	-1.017	-1.583	-1.266	-0.772
340	-1.489	-1.013	-1.521	-1.210	-0.737
350	-1.467	-0.928	-1.413	-1.175	-0.673
360	-1.030	-0.873	-1.113	-1.109	-0.646

A_o	A_2	A_4	δ	T (100)
-1.151	0.526	0.099	-1017	
-0.865	0.266	0.089	-21.09	
-1.156	0.218	0.084	-16.95	
-1.059	0.333	0.102	-19.61	
-0.747	0.322	0.120	-14.41	

Table 34: $Ni_{.95}Co_5$, S.W = 0.00017 gm, 1.2×10^{-5} Torr, Thickness = 1880Å, Temperature = 150^0C

θ	1 amp	2 amp	3 amp	4 amp	5 amp
0	-0.646	-0.767	-0.626	-0.585	-0.442
10	-0.529	-0.737	-0.596	-0.508	-0.366
20	-0.451	-0.684	-0.437	-0.438	-0.090
30	-0.439	-0.536	-0.324	-0.410	-0.076
40	-0.368	-0.405	-0.396	-0.174	-0.168
50	-0.449	-0.433	-0.517	-0.297	-0.249
60	-0.512	-0.502	-0.580	-0.430	-0.431
70	-0.609	-0.735	-0.595	-0.447	-0.490
80	-0.649	-0.798	-0.644	-0.512	-0.632
90	-0.667	-0.842	-0.693	-0.608	-0.685
100	-0.736	-0.856	-0.701	-0.673	-0.712
110	-0.844	-0.980	-0.711	-0.731	-0.739
120	-0.884	-1.023	-0.742	-0.809	-0.803
130	-1.327	-1.109	-0.786	-1.235	-1.198
140	-0.931	-1.091	-0.722	-0.953	-0.753
150	-0.861	-0.947	-0.704	-0.740	-0.714
160	-0.827	-0.908	-0.694	-0.728	-0.702
170	-0.703	-0.850	-0.681	-0.649	-0.662
180	-0.660	-0.804	-0.656	-0.620	-0.619
190	-0.529	-0.737	-0.596	-0.508	-0.366
200	-0.451	-0.684	-0.437	-0.438	-0.090
210	-0.439	-0.536	-0.324	-0.410	-0.076
220	-0.368	-0.405	-0.396	-0.174	-0.168
230	-0.449	-0.433	-0.517	-0.297	-0.249
240	-0.512	-0.502	-0.580	-0.430	-0.431
250	-0.609	-0.735	-0.595	-0.447	-0.496
260	-0.649	-0.798	-0.644	-0.512	-0.632
270	-0.667	-0.842	-0.693	-0.608	-0.685
280	-0.736	-0.856	-0.701	-0.673	-0.712
290	-0.844	-0.980	-0.711	-0.731	-0.739
300	-0.884	-1.023	-0.742	-0.809	-0.809
310	-1.327	-1.109	-0.786	-1.235	-1.198
320	-0.931	-1.091	-0.722	-0.953	-0.753
330	-0.861	-0.947	-0.704	-0.740	-0.714
340	-0.827	-0.908	-0.694	-0.728	-0.702
350	-0.703	-0.850	-0.681	-0.649	-0.662
360	-0.660	-0.802	-0.656	-0.620	-0.619

A_o	A_2	A_4	δ	T(150)
-0.691	0.291	0.050	18.42	
-0.790	0.280	0.037	19.17	
-0.620	0.257	0.035	-10.18	
0.608	0.0309	0.033	-17.36	
0.556	0.361	0.061	-3.09	

Table 35: $Ni_{.95}Co_5$, S.W = 0.00017 gm, 1.2×10^{-5} Torr, Thickness = 1880Å, Temperature = 165^0C

θ	1 amp	2 amp	3 amp	4 amp	5 amp
0	-0.703	-0.654	0.332	0.241	0.157
10	-634	-0.506	0.360	0.382	0.354
20	-0.552	-0.488	0.370	0.555	0.408
30	-0.412	-0.456	0.718	0.683	0.641
40	-0.496	-0.378	0.791	0.686	0.663
50	-0.657	-0.422	0.587	0.680	0.582
60	-0695	-0.497	0.375	0.515	0.388
70	-0.703	-0.681	0.267	0.455	+0.343
80	-0.736	-0.706	0.197	0.441	0.299
90	-0.759	-0.774	0.127	-0.196	0.261
100	-0.793	-0.801	-0.050	-0.244	0.218
110	-0.821	-0.826	-0.121	-0.412	0.108
120	-0.854	-0.896	-0.274	-0.484	0.093
130	-1.083	-0.951	-0.584	-0.658	0.190
140	-0.839	-0.872	-0.257	-0.415	0.078
150	-0.771	-0.796	-0.161	-0.229	0.180
160	-0.704	-0.744	0.045	-0.218	0.206
170	-0.674	-0.696	0.031	-0.198	0.259
180	-0.657	-0.647	0.241	-0.115	0.288
190	-0.634	-0.506	0.360	0.382	0.354
200	-0.552	-0.488	0.670	0.555	0.408
210	-0.412	-0.456	0.718	0.683	0.641
220	-0.496	-0.378	0.791	0.686	0.663
230	-0.657	-0.422	0.587	0.680	0.582
240	-0.695	-0.497	0.375	0.515	0.388
250	-0.703	-0.681	0.267	0.455	0.343
260	-0.736	-0.706	0.197	0.441	0.299
270	-0.759	-0.774	0.127	-0.196	0.261
280	-0.793	-0.801	-0.050	-0.244	0.218
290	-0.821	-0.826	-0.121	-0.412	0.108
300	-0.854	-0.896	-0.278	-0.484	0.093
310	-1.083	-0.951	-0.584	-0.658	0.190
320	-0.839	-0.872	-0.257	-0.415	0.078
330	-0.771	-0.796	-0.161	-0.229	0.180
340	-0.704	-0.744	-0.045	-0.218	0.206
350	-0.674	-0.696	-0.031	-0.198	0.254
360	-0.567	-0.647	-0.241	-0.115	0.288

A_o	A_2	A_4	δ	T(165)
-0.715	0.177	0.025	10.98	
-0.674	0.136	0.024	-15.08	
0.161	0.205	0.060	3.39	
-0.085	0.110	0.072	3.99	
0.284	0.263	0.021	-18.17	

Table 36: $Ni_{.95}Co_5$, S.W = 0.00017 gm, 1.2×10^{-5} Torr, Thickness = 1880Å, Temperature = 180^0C

θ	1 amp	2 amp	3 amp	4 amp	5 amp
0	0.551	0.144	0.496	0.231	0.455
10	0.649	0.389	0.502	0.253	0.582
20	0.668	0.555	0.709	0.380	0.690
30	0.706	0.641	0.774	0.415	0.741
40	0.885	0.667	0.853	0.914	0.981
50	0.783	0.649	0.723	0.479	0.902
60	0.719	0.584	0.534	0.398	0.753
70	0.698	0.253	0.512	0.320	0.639
80	0.644	0.136	0.459	0.231	0.456
90	0.632	0.130	0.345	0.225	0.334
100	0.628	0.070	0.292	0.212	0.300
110	0.485	-0.128	0.264	0.131	0.251
120	0.385	-0.212	0.184	0.113	0.240
130	0.021	-0.285	0.114	-0.206	-0.107
140	0.101	-0.213	0.282	0.080	0.187
150	0.425	0.049	0.325	0.126	0.234
160	0.465	0.105	0.349	0.210	0.301
170	0.507	0.135	0.456	0.226	0.319
180	0.535	0.143	0.465	0.230	0.447
190	0.649	0.389	0.502	0.253	0.582
200	0.668	0.555	0.709	0.380	0.690
210	0.706	0.641	0.774	0.415	0.741
220	0.885	0.667	0.853	0.914	0.981
230	0.783	0.649	0.723	0.479	0.902
240	0.719	0.584	0.534	0.398	0.753
250	0.698	0.253	0.459	0.320	0.635
260	0.644	0.136	0.397	0.231	0.456
270	0.632	0.136	0.292	0.225	0.334
280	0.628	0.070	0.264	0.212	0.300
290	0.485	0.128	0.184	0.131	0.251
300	0.385	0.212	0.151	0.113	0.240
310	0.021	0.285	0.114	-0.206	-0.107
320	0.101	0.213	0.282	0.080	0.187
330	0.425	0.099	0.325	0.126	0.234
340	0.465	0.105	0.349	0.210	0.301
350	0.507	0.135	0.456	0.226	0.319
360	0.535	0.143	0.465	0.230	0.447

A_o	A_2	A_4	δ	T(180)
0.55	0.26	0.06	-21.83	
0.18	0.22	0.04	-15.62	
0.43	0.28	0.05	-18.04	
0.26	0.34	0.04	-20.45	
0.45	0.37	0.05	21.74	

Table 37: $Ni_{.95}Co_5$, S.W = 0.00017 gm, 1.2×10^{-5} Torr, Thickness = 1880Å, Temperature = 195^0C

θ	1 amp	2 amp	3 amp	4 amp	5 amp
0	0.024	0.322	-0.405	-0.366	0.414
10	0.031	0.331	-0.265	-0.347	0.436
20	0.652	0.379	-0.192	-0.253	0.450
30	0.774	0.645	-0.040	-0.105	0.490
40	0.778	0.826	-0.172	-0.056	0.513
50	0.695	0.584	-0.023	-0.160	0.792
60	0.274	0.340	-0.052	-0.184	0.747
70	0.027	0.322	-0.251	-0.313	0.438
80	-0.006	0.304	-0.345	-0.365	0.429
90	-0.052	0.196	-0.465	-0.394	0.408
100	-0.095	0.186	-0.573	-0.412	0.359
110	-0.102	0.141	-0.596	-0.708	0.244
120	-0.179	0.016	-0.631	-0.771	0.163
130	-0.200	-0.075	-0.837	-0.872	0.004
140	-0.180	0.116	-0.619	-0.869	0.025
150	-0.101	0.176	-0.584	-0.730	0.232
160	-0.069	0.195	-0.569	-0.629	0.291
170	-0.017	0.240	-0.477	-0.396	0.401
180	-0.005	0.304	-0.420	-0.367	0.410
190	0.031	0.331	-0.265	-0.347	0.436
200	0.652	0.379	-0.192	-0.253	0.450
210	0.774	0.645	-0.040	-0.106	0.490
220	0.778	0.826	-0.172	-0.056	0.513
230	0.695	0.584	-0.023	-0.160	0.792
240	0.274	0.340	-0.052	-0.184	0.747
250	0.027	0.322	-0.251	-0.313	0.438
260	-0.006	0.304	-0.345	-0.365	0.429
270	-0.052	0.196	-0.465	-0.394	0.408
280	-0.095	0.186	-0.573	-0.412	0.359
290	-0.102	0.141	-0.596	-0.708	0.244
300	-0.179	0.016	-0.631	-0.771	0.163
310	-0.200	-0.075	-0.837	-0.872	0.004
320	-0.180	-0.116	-0.619	-0.869	0.025
330	-0.101	-0.176	-0.584	-0.730	0.232
340	-0.069	-0.195	-0.569	-0.629	0.291
350	-0.017	-0.240	-0.477	-0.396	0.401
360	-0.005	-0.306	-0.420	-0.367	0.410

A_o	A_2	A_4	δ	T(195)
0.12	0.41	0.06	-14.66	
0.29	0.27	0.06	-17.25	
0.38	0.34	0.05	19.60	
0.44	0.38	0.05	21.10	
0.38	0.45	0.02	-12.14	

Table 38: $Ni_{.95}Co_5$, S.W = 0.00017 gm, 1.2×10^{-5} Torr, Thickness = 1880Å, Temperature = 210^0C

θ	1 amp	2 amp	3 amp	4 amp	5 amp
0	0.362	0.340	0.859	0.273	0.154
10	0.570	0.348	0.967	0.305	0.175
20	0.519	0.408	0.978	0.448	0.250
30	0.682	0.862	0.984	0.555	0.774
40	0.760	0.948	0.989	0.821	0.803
50	0.754	0.470	0.983	0.602	0.740
60	0.617	0.396	0.976	0.552	0.282
70	0.513	0.342	0.972	0.351	0.186
80	0.475	0.325	0.579	0.281	0.164
90	0.415	0.307	0.430	0.176	0.135
100	0.283	0.294	0.133	0.122	0.082
110	0.166	0.279	0.037	0.045	0.055
120	0.131	0.154	0.011	0.009	0.031
130	0.098	0.095	0.004	0.005	0.026
140	0.084	0.169	0.027	0.043	0.052
150	0.149	0.270	0.053	0.052	0.075
160	0.174	0.299	0.363	0.100	0.127
170	0.213	0.315	0.556	0.151	0.148
180	0.303	0.333	0.757	0.198	0.156
190	0.510	0.348	0.967	0.305	0.175
200	0.519	0.408	0.978	0.448	0.250
210	0.682	0.862	0.984	0.555	0.774
220	0.760	0.948	0.989	0.821	0.803
230	0.754	0.470	0.983	0.602	0.740
240	0.617	0.396	0.976	0.552	0.282
250	0.513	0.342	0.972	0.351	0.186
260	0.475	0.325	0.579	0.281	0.164
270	0.283	0.307	0.430	0.176	0.135
280	0.166	0.294	0.133	0.122	0.082
290	0.131	0.179	0.037	0.045	0.055
300	0.098	0.154	0.011	0.009	0.031
310	0.084	0.095	0.004	0.005	0.026
320	0.149	0.169	0.027	0.043	0.052
330	0.174	0.270	0.053	0.052	0.075
340	0.213	0.299	0.363	0.100	0.127
350	0.303	0.315	0.556	0.151	0.148
360	0.415	0.333	0.757	0.198	0.156

A_o	A_2	A_4	δ	T(210)
0.377	0.310	0.04	21.38	
0.360	0.240	0.08	-14.79	
0.540	0.260	0.06	-11.08	
0.280	0.300	0.07	17.69	
0.240	0.380	0.05	-18.82	

Table 39: $Ni_{.95}Co_5$, S.W = 0.00015 gm, 1.2×10^{-5} Torr, Thickness = 1580Å, Temperature = 25^0C (H = 250 O_e)

θ	1 amp	2 amp	3 amp	4 amp	5 amp
0	0.395	0.411	0.425	0.432	0.451
10	0.461	0.473	0.492	0.502	0.509
20	0.582	0.599	0.608	0.625	0.639
30	0.651	0.715	0.801	0.838	0.901
40	0.792	0.853	0.912	0.983	1.045
50	0.701	0.725	0.795	0.827	0.974
60	0.631	0.658	0.682	0.715	0.801
70	0.543	0.559	0.571	0.603	0.712
80	0.461	0.468	0.451	0.499	0.509
90	0.395	0.399	0.370	0.365	0.350
100	0.340	0.345	0.295	0.261	0.243
110	0.290	0.281	0.238	0.219	0.207
120	0.251	0.241	0.209	0.185	0.153
130	0.211	0.198	0.185	0.163	0.148
140	0.259	0.255	0.211	0.193	0.179
150	0.287	0.288	0.285	0.279	0.271
160	0.365	0.369	0.370	0.372	0.375
170	0.419	0.429	0.444	0.468	0.483
180	0.521	0.542	0.585	0.601	0.623
190	0.595	0.609	0.629	0.695	0.754
200	0.665	0.689	0.713	0.805	0.848
210	0.759	0.805	0.852	0.931	0.951
220	0.876	0.941	0.995	1.048	1.135
230	0.768	0.803	0.846	0.911	0.925
240	0.643	0.712	0.739	0.804	0.859
250	0.519	0.611	0.635	0.701	0.729
260	0.420	0.501	0.512	0.582	0.601
270	0.351	0.400	0.419	0.471	0.845
280	0.291	0.312	0.300	0.305	0.313
290	0.247	0.275	0.251	0.236	0.121
300	0.213	0.201	0.199	0.184	0.171
310	0.195	0.168	0.153	0.141	0.123
320	0.229	0.199	0.205	0.186	0.173
330	0.271	0.293	0.301	0.309	0.321
340	0.331	0.348	0.354	0.362	0.379
350	0.376	0.389	0.405	0.422	0.433
360	0.426	0.441	0.457	0.469	478

Table 40: $Ni_{.95}Co_5$, S.W = 0.00007 gm, 1.2×10^{-5} Torr, Thickness = 1150Å, Temperature = 25^0C(H = 0 O_e)

θ	1 amp	2 amp	3 amp	4 amp	5 amp
0	0.195	0.198	0.206	0.215	0.226
10	0.201	0.205	0.211	0.218	0.229
20	0.212	0.217	0.222	0.235	0.242
30	0.224	0.234	0.242	0.256	0.269
40	0.235	0.245	0.259	0.272	0.281
50	0.230	0.241	0.252	0.265	0.276
60	0.222	0.233	0.240	0.252	0.261
70	0.217	0.226	0.233	0.241	0.251
80	0.211	0.218	0.226	0.232	0.241
90	0.205	0.212	0.219	0.225	0.231
100	0.194	0.206	0.213	0.220	0.221
110	0.185	0.193	0.207	0.212	0.213
120	0.181	0.188	0.191	0.201	0.206
130	0.175	0.181	0.182	0.188	0.192
140	0.182	0.187	0.195	0.202	0.209
150	0.186	0.196	0.204	0.209	0.217
160	0.195	0.205	0.210	0.217	0.226
170	0.204	0.211	0.218	0.226	0.237
180	0.210	0.219	0.226	0.237	0.245
190	0.216	0.225	0.235	0.243	0.252
200	0.220	0.232	0.242	0.250	0.265
210	0.232	0.241	0.251	0.261	0.273
220	0.240	0.252	0.262	0.270	0.285
230	0.234	0.242	0.252	0.262	0.271
240	0.225	0.232	0.241	0.251	0.262
250	0.218	0.226	0.232	0.240	0.251
260	0.206	0.219	0.225	0.231	0.242
270	0.195	0.213	0.218	0.225	0.232
280	0.182	0.207	0.212	0.217	0.224
290	0.173	0.198	0.206	0.211	0.216
300	0.165	0.184	0.191	0.202	0.210
310	0.172	0.171	0.178	0.186	0.191
320	0.179	0.179	0.184	0.190	0.197
330	0.183	0.183	0.189	0.196	0.204
340	0.189	0.190	0.195	0.203	0.209
350	0.196	0.195	0.201	0.209	0.215
360	0.205	0.201	0.207	0.214	0.224

Sample 1

Table 5.4.3a: Composition $Ni_{80}Co_{20}$

Temperature in ^0C	Anisotropy energy in J/m^3
25	933
50	871
75	812
100	705
125	631
150	540
165	508
180	473
195	436
210	125

Sample 2

Table 5.4.3b: Composition $Ni_{85}Co_{15}$

Temperature in ^0C	Anisotropy energy in J/m^3
25	382
50	361
75	348
100	336
125	316
150	286
165	260
180	235
195	210
210	89

Sample 3

Table 5.4.3c: Composition $Ni_{90}Co_{10}$

Temperature in ^0C	Anisotropy energy in J/m^3
25	395
50	373
75	317
100	261
125	224
150	188
165	160
180	142
195	115
210	52

Sample 4

Table 5.4.3d: Composition $Ni_{95}Co_{05}$

Temperature in ^0C	Anisotropy energy in J/m^3
50	559
100	506
125	447
150	387
165	351
180	324
195	289
210	152

Sample 1

Table 5.5.2a: Composition $Ni_{80}Co_{20}$

Temp. in deg. C	t = 540Å	t = 1080 Å	t = 1320 Å	t = 1600 Å
30	31.0	26.8	19.7	13.4
40	31.5	27.7	20	14.7
50	32.7	28.9	21.9	15.8
60	34.4	31.0	23.3	16.5
70	35.8	32	24.8	18.1
80	38.0	34.5	26.4	20.0
90	40.2	36.4	27.8	21.6
100	42.9	37.8	29.4	22.8
110	45.1	39.0	30.3	24.3
120	47.2	41.0	33.0	26.0
130	48.9	43.8	35.3	27.1
140	50.4	45.0	36.8	28.9
150	52.8	46.1	38.6	30.6
160	56.1	48.0	41.3	32.7
170	52.8	51.4	42.7	35.0
180	50.8	47.9	44.9	36.1
190	49.1	46.5	39.8	37.8
200	47.4	44.8	38.0	34.3
210	46.0	43.5	36.9	31.5
220	44.8	42.0	35.3	29.8
230	43.2	40.1	33.8	28.4
240	41.9	39.0	32.2	26.9
250	40.9	37.8	31.0	25.8

Sample 2

Table 5.5.2b: Composition $Ni_{85}Co_{15}$

Temp. in deg. C	t = 520Å	t = 1150 Å	t = 1450 Å	t = 1600 Å
30	31.9	26.7	18.3	11.8
40	32.6	27.6	19.7	12.9
50	34.1	28.6	21.0	13.9
60	35.9	29.9	22.6	14.6
70	38.6	31.6	23.9	15.9
80	40.2	33.9	25.1	18.2
90	42.7	35.9	26.8	18.6
100	43.7	37.7	28.3	19.2
110	45.6	39.0	29.7	20.1
120	48.6	40.7	31.2	21.6
130	49.8	42.3	32.8	22.9
140	52.1	43.8	34.2	24.2
150	54.6	45.2	35.8	25.9
160	56.6	46.6	37.3	27.3
170	52.1	48.5	38.8	29.0
180	50.5	42.5	40.0	31.1
190	49.8	40.6	36.2	33.0
200	48.0	39.9	34	30.5
210	46.1	38.6	32.2	29.4
220	45.9	36.6	31.0	26.9
230	43.2	34.6	29.1	24.8
240	42.6	33.6	27.2	23.5
250	40.8	32.8	26.2	21.8

Sample 3

Table 5.5.2c: Composition $Ni_{90}Co_{10}$

Temp. in deg. C	t = 350Å	t = 880 Å	t = 1450 Å	t = 1800 Å
30	47.9	36.1	22.4	13.8
40	49.0	38.0	23.9	15.2
50	50.7	39.7	25.1	16.8
60	53.5	41.7	27.0	19.0
70	57.6	44.4	29.2	21.2
80	59.9	47.2	31.9	24.1
90	63.0	49.6	34.3	26.6
100	66.3	52.3	37.4	29.1
110	68.9	55.6	41.3	32.6
120	72.0	57.6	44.4	35.5
130	75.7	61.7	47.0	37.9
140	78.9	64.4	49.9	41.1
150	82.6	67.3	53.6	44.4
160	85.7	71.3	56.7	47.3
170	88.1	74.7	60.7	51.8
180	82.1	78.9	65.8	55.0
190	79.5	73.4	69.8	58.7
200	78.9	71.6	64.2	60.5
210	76.6	70.4	62.3	53.1
220	75.9	69.0	61.3	51.2
230	74.0	67.6	59.4	48.7
240	72.7	65.9	57.1	47.2
250	70.8	64.7	56.6	46.1

Sample 4

Table 5.5.2d: Composition $Ni_{95}Co_{05}$

Temp. in deg. C	t = 880Å	t = 1180 Å	t = 1300 Å	t = 1700 Å
30	32.5	23.8	16	10.5
40	33.6	24.9	17.5	11.2
50	35.2	26.0	18.9	14.5
60	37.0	27.9	20.9	16.6
70	39.3	29.5	21.9	18.8
80	42.0	31.7	23.5	21.0
90	43.9	34.1	27.1	23.5
100	45.8	37.1	30.2	26.0
110	48.1	39.7	32.4	28.2
120	50.4	42.0	35.8	30.8
130	53.6	45.2	37.9	33.7
140	55.9	47.2	40.9	36.6
150	58.5	50.7	43.4	38.6
160	61.3	52.5	44.6	40.1
170	61.8	53.9	46.4	41.8
180	59.1	56.3	48.1	42.3
190	57.0	52.1	49.5	44.8
200	55.2	50.3	45.2	46.0
210	54.1	48.1	44.0	41.5
220	52.0	45.0	42.1	40.0
230	50.4	43.0	40.5	38.1
240	48.7	41.4	38.3	36.0
250	46.4	40.3	37.8	33.8

Table 5.6.1: Specific Magnetization

Field in O_e	Magnetization σ in emu/gm
0	0
100	12
200	25
300	35
400	46
500	54
600	63
700	71
800	78
900	84
1000	89
1100	91
1200	92
1300	92.84
1400	92.84
1500	92.84
1600	92.84
1700	92.84
1800	92.84

লাইব্রেরী, ঢাকা
97638
27/5/03